ROBUST CONTROL APPROACH FOR MULTIVARIABLE SYSTEMS UNDER DELAYS, PARAMETRIC UNCERTAINTY AND EXTERNAL DISTURBANCES

Ing. JOSE JORGE CARREÑO ZAGARRA
MAGISTER EN INGENIERÍA ELECTRÓNICA

UNIVERSIDAD INDUSTRIAL DE SANTANDER
FACULTAD DE INGENIERÍAS FISICOMECÁNICAS
ESCUELA DE INGENIERÍAS ELÉCTRICA, ELECTRÓNICA Y DE TELECOMUNICACIONES
BUCARAMANGA
2020

ROBUST CONTROL APPROACH FOR MULTIVARIABLE SYSTEMS UNDER DELAYS, PARAMETRIC UNCERTAINTY AND EXTERNAL DISTURBANCES

Informe final del trabajo de investigación para optar al título de

DOCTOR EN INGENIERÍA
ÁREA INGENIERÍA ELECTRÓNICA

DIRECTOR:
Ing. RODOLFO VILLAMIZAR MEJÍA
Doctor en Tecnologías de la Información

UNIVERSIDAD INDUSTRIAL DE SANTANDER
FACULTAD DE INGENIERÍAS FISICOMECÁNICAS
ESCUELA DE INGENIERÍAS ELÉCTRICA, ELECTRÓNICA Y DE TELECOMUNICACIONES
BUCARAMANGA
2020

DEDICATORIA

Este trabajo va dedicado al Señor, el Dador de los Sueños. Él ha llenado mi vida de pasión para no detenerme y soñar en grande. En medio de mis debilidades Su Gracia me ha sostenido.

A mi paciente y trabajadora esposa, Diana, quien es consciente de que cuando se escribe una tesis las personas más cercanas al autor también sufren. Su amor, su comenprensión y sus oraciones me infunden aliento.

AGRADECIMIENTOS

Tengo una deuda de gratitud muy grande con muchísimas personas. El trabajo de investigación de tesis doctoral me ha permitido conocer personas maravillosas. De antemano, agradezco al profesor Rodolfo Villamizar por su apoyo durante todos estos años de investigación. Sus consejos, revisiones y aportes han sido fundamentales para la ejecución de esta tesis. Ha sido mi mentor en el área de control automático durante más de 10 años y siempre estaré agradecido por ello.

Agradezco a los doctores Jose Luis Guzmán y Jose Carlos Moreno, quienes sin conocerme me dieron un amable recibimiento en la Universidad de Almería con el fin de que yo realizara mi estancia de investigación. La calidez y amabilidad de los andaluces se refleja en sus vidas. (Andalucía es una tierra mágica que espero volver a visitar). Gracias a su apoyo pude realizar validaciones experimentales que fueron necesarias para la culminación de la tesis. Sus aportes y consejos siempre fueron muy acertados y gran parte de los resultados se debe a ellos. Muchas gracias a todos los compañeros de grupo de investigación de Automática, Robótica y Mecatrónica de la UAL, especialmente a Martha Barceló por ayudarme con los experimentos en el fotobiorreactor.

Agradezco al doctor Po Wen Chen por recibirme durante mi corta estancia en la Universidad de Stuttgart. Allí tuve la fortuna de conocer al doctor David Schlipf, a quien siempre recordaré por su sencillez, amabilidad y conocimientos avanzados en el control turbinas eólicas. Su apoyo fue fundamental para lograr las valicaciones numéricas en el modelo de turbina eólica. Agradezco también a los compañeros de grupo de Energía Eólica de Sttutgart (SWE), siempre muy amables en los descansos, a pesar de mi falta de dominio del idioma.

También estoy muy agradecido por la atención del Dr. Emérito Hebertt Sira-Ramirez durante mi estancia en el CINVESTAV de México. Con él pude aprender los conceptos de la teoría de rechazo activo de perturbaciones que son la base de mi tesis doctoral. Durante la estancia en México agradezco mucho el apoyo de mi gran y doctor Mario Ramírez por su atención, amistad y sus fructíferos consejos en el área de ADRC. De la misma manera agradezco a mi compañero y doctor Eric William Zurita por su amabilidad y consejos en el área siempre. ¡Fueron grandes anfitriones!

Agradezco a COLCIENCIAS por financiar la totalidad de este proyecto por medio de la convocatoria 567 de Doctorados Nacionales. También agradezco a la Vicerrectoría de Investigación, a la Decanatura de la Facultad de Ingenierías Fisicomecánicas y la Escuela de Ingenierías Eléctrica, Electrónica y de Telecomunicaciones de

la Universidad Industrial de Santander por financiar todas las ponencias internacionales realizadas durante la tesis.

Agradezco la amistad y apoyo de muchos compeñeros de posgrado, entre ellos los ingenieros Wilman Pineda, Cristhiam Higuera, Hernando Rángel, Cristian Jiménez, Ricardo Dominguez, Gabriel Malagón, Jairo Blanco, Carlos Fajardo, Iván Serna, Jorge Cruz, Yulieth Jimenez y Paola Rondón. También agradezco a todos los estudiantes de posgrado y pregrado que trabajaron conmigo, entre ellos David Padilla, Leonel Calderón, Laura Tulcán, Jose Alberto Bermúdez, Miguel Ardila, Yasser Greyeb, Gabriel Zárate y Esteban López.

Agradezco también a todos mis amigos y hermanos en la fe. A mis pastores Juan Carlos Rojas y Karina Araujo, por sus sabios consejos y respaldo todo el tiempo. A la amistad durante muchos años y respaldo de mis amigos Jose Camilo Mendez, Claudia Quintero, Tatiana Saurith y Abel Pinzón.

De manera muy especial agradezco a mis hermanos Ricardo, Mafe, Camila y Bertha, por animarme, inspirarme y ayudarme siempre cuando los necesito. Ellos son más que amigos. A mis padres Silverio y Eloisa por su esfuerzo durante años. Sus corazones son los que más se llenan de felicidad con cada logro que alcanzamos, y eso alienta. ¡Que Dios les dé larga vida para que cosechen lo que con esfuerzo sembraron!

¡Muchas Gracias a todos!

Jose J. Carreño Zagarra

CONTENT

Pag.

1 INTRODUCTION **13**
1.1 Problem Definition and Motivation 13
1.2 Objectives and scope of the research 14
1.2.1 General objective 14
1.2.2 Specific objectives 14
1.3 Organization of the dissertation 15
1.4 Academic Production 15

2 LITERATURE REVIEW **20**
2.1 Open problems in control systems 20
2.1.1 Dead time 20
2.1.2 Uncertainty systems 28
2.1.3 Disturbance rejection 33

3 THEORETICAL FRAMEWORK **35**
3.1 Quantitative Feedback Theory 35
3.1.1 Basic concepts of QFT 36
3.2 Active Disturbance Rejection Control 47
3.2.1 PID control limitations 48
3.2.2 Differential flatness 50
3.2.3 Extended state observers 52
3.2.4 Generalities on GPI observers 54

4 ROBUST CONTROL APPROACH **61**
4.1 Introduction 61
4.2 Feedforward Controller Design 62
4.2.1 Disturbance rejection of linear systems 64
4.2.2 Disturbance rejection of time-delay systems 66
4.3 Robust feedback controller 69
4.3.1 Quantitative robust controller 72
4.3.2 Robust 2-DoF PI controller 76
4.4 Feedforward and feedback controllers integrated design 79

5 NUMERICAL VALIDATION **87**
5.1 Numerical Case 1: One-Stage Refrigeration Cycle 87
5.1.1 Process model 88

5.1.2 Feedforward control design 90
5.1.3 Feedback control design 92
5.1.4 Numerical validation and analysis 93
5.1.5 Conclusions 95
5.2 Numerical Case 2: Offshore Wind Turbine 97
5.2.1 Wind turbine modeling 97
5.2.2 Feedforward-feedback control design 98
5.2.3 Numerical results and discussions 104
5.2.4 Conclusions 105
5.3 Numerical Case 3: Glucose Control in Type 1 Diabetes Mellitus Patients 106
5.3.1 Mathematical model of gluco-regulatory system 106
5.3.2 Feedforward control design 108
5.3.3 Feedback control design 109
5.3.4 Numerical validations and analysis 112
5.3.5 Conclusions 114

6 EXPERIMENTAL VALIDATION 116
6.1 Experimental Case: Raceway Photobioreactor 116
6.2 Microalgal bioreactor: Operating principle 117
6.3 Dynamic model of photobioreactor 117
6.4 GPI observer design 120
6.5 Feedback controller design 121
6.6 Experimental results and discussions 123
6.7 Conclusions 129

7 CONCLUSIONS 131

A CODES PROGRAM 132
A.1 One-state Refrigeration Cycle 132
A.2 Offshore Wind Turbine 133
A.3 Glucose Control in Type 1 Diabetes 133
A.4 Raceway Photobioreactor 133

BIBLIOGRAPHY 138

LIST OF FIGURES

Pag.

Figura 1 Delay in a feedback system 20
Figura 2 Step response of a time delayed system 21
Figura 3 Feedback control scheme 23
Figura 4 Control system based on the Smith predictor 24
Figura 5 Outline of model predictive control 28
Figura 6 General structure of predictor MPC 29
Figura 7 Control system with uncertainty in the plant model. 29
Figura 8 Modelling of uncertain systems 31
Figura 9 Standard $M - \Delta$ configuration 33
Figura 10 QFT control system design: *closing the gap* [44]. 37
Figura 11 The single-loop feedback system 38
Figura 12 Templates for solar plant 39
Figura 13 Stability specification in the Nichols chart: $\delta_1 = 1.4$ 41
Figura 14 Sensitivity or plant output disturbance rejection specification 42
Figura 15 Step response for plant output disturbance 42
Figura 16 System time-domain tracking performance specifications. 43
Figura 17 Bounds of two specifications: stability and tracking references . . . 45
Figura 18 Loop-shaping for solar plant 46
Figura 19 Prefilter $F(j\omega)$ for reference tracking specifications for solar plant . 47
Figura 20 Stability analysis for solar plant 48
Figura 21 PID control topology 49
Figura 22 A two tank system 56
Figura 23 Output trajectory tracking for ADRC controlled two tank system . . 57
Figura 24 Block diagram in Simulink 58
Figura 25 Disturbance observer based control scheme 62
Figura 26 Blocks diagram of disturbance observer 63
Figura 27 Predictive Disturbance Observer for Time-Delay systems 68
Figura 28 Equivalent Structure of the Smith Predictor 69
Figura 29 Clegg Integrator (CI) 74
Figura 30 Comparison of linear controller and reset system. 75
Figura 31 Two-degrees-of-freedom closed-loop control system 77
Figura 32 Control of linear perturbed SISO system combining LADRC and QFT 81
Figura 33 Inverted pendulum on a cart 83
Figura 34 Control of inverted pendulum 86

Figura 35 Vapour compression system [11] 88
Figura 36 Block diagram of one-cycle refrigeration control system 93
Figura 37 Robustness Specifications Analysis. Stability: (a) $G_{11}(s)$, (d) $G_{22}(s)$; Disturbance rejection: (b) $G_{11}(s)$, (e) $G_{22}(s)$; Reference tracking: (c) $G_{11}(s)$, (f) $G_{22}(s)$. Specification (dashed line) and worst case within the uncertain plants at each frequency (solid line). 94
Figura 38 Comparison of the descentralized PID controller with the ADCR-PID controller: (a) Input variables; (b) Output variables. 96
Figura 39 A typical conversion system for wind energy 98
Figura 40 *Feedback-Feedforward* control approach for offshore wind turbine 99
Figura 41 Reaction to an EOG at 13m/s (left) and 25m/s (right) in the case of perfect wind preview using the 5MW reference wind turbine. Simulated with reduced SLOW model: Baseline controller (blue), Non-linear GPI (green) and Non-linear GPI with reset (red). 104
Figura 42 Schematic representation of Bergman's minimal model 107
Figura 43 Block diagram of the robust control approach for closed-loop Artificial Pancreas 110
Figura 44 QFT-bounds and $K(s)$ design-loop-shaping 111
Figura 45 Prefilter for reference tracking specification. 112
Figura 46 Nonlinear dynamic control structure 113
Figura 47 Stability analysis, frequency domain: δ_U specification (dashed line), and worst case of $KP_{eq}/(1 + KP_{eq})$ within the uncertain plants at each frequency (solid line). 113
Figura 48 Proposed predictive.observer-based control using UVA/Padova simulator 114
Figura 49 Closed-loop responses for all the *in silico* adults (complete UVA/Padova simulator) to protocol#1 and to protocol#2. 115
Figura 50 Raceway Photobioreactor 118
Figura 51 Model validation examples 121
Figura 52 Two-degrees-of-freedom closed-loop control system 122
Figura 53 Control system of pH 123
Figura 54 Experimental results of the robust LADRC for seven days 125
Figura 55 Robust LADRC details for first and sixth day 126
Figura 56 A comparative between PI+FF and LADRC 127
Figura 57 Bode plot of the Plant $P(s)$ and equivalent plant with observer $P_{eq}(s)$ 129
Figura 58 Block diagram of the refrigeration cycle 132
Figura 59 Block diagram of the controller 136
Figura 60 Block diagram of wind turbine control 136
Figura 61 Block diagram of glucose system 137
Figura 62 Block diagram of Raceway fotobioreactor 137

TABLES LIST

Pag.

Tabla 1 Individual's contribution 16
Tabla 2 Modelling of unstructured uncertain systems 30
Tabla 3 Single loop specifications (without loosing generality, $H(s) = 1$) . . . 40
Tabla 4 Quadratic inequalities 44
Tabla 5 Description of control sub-objectives 70
Tabla 6 Input variable ranges 91
Tabla 7 Performance specifications 93
Tabla 8 Parameters of filters and controller 93
Tabla 9 Robust tuning coefficients 124
Tabla 10 Performance indexes for feedforward PI controller and LADRC scheme for a sunny day and a cloudy day. 128

RESUMEN

TÍTULO: Robust Control approach for Multivariable Systems under Delays, Parametric Uncertainty and External Disturbances*

AUTOR: Jose Jorge Carreño Zagarra**

PALABRAS CLAVE: Control Robusto, Rechazo Activo de Perturbaciones, Observadores GPI, Sistemas Inciertos, Sistemas con Retardo.

DESCRIPCIÓN:

Esta disertación propone un nuevo esquema de control para sistemas multivariables con o sin retardos de tiempos, perturbaciones externas e incertidumbre paramétrica. La metodología de diseño combina el enfoque de control robusto para sistemas inciertos y el uso de observadores de alta ganancia para la estimación y atenuación de perturbaciones en línea. En la etapa de control *feedback* se propone el uso de controladores QFT, controladores PI robustos de 2 grados de libertad y controladores reset, con el fin de lograr especificaciones robustas de rendimiento y estabilidad en presencia de incertidumbre en los parámetros del modelo de planta. En la etapa de control *feedforward* se plantea el diseño de observadores GPI ya que debido a su característica de reconstrucción de variables de fase y estimación de un número finito de derivadas de la perturbación proporcionan propiedades de mitigación o rechazo de perturbaciones, seguimiento de trayectoria, rendimiento robusto y estabilización de salida.

El esquema de control propuesto fue validado con éxito en un fotobiorreactor experimental disponible en la Universidad de Almería (España), en donde se obtuvo una mejora significativa en la precisión de la regulación del pH del cultivo de microalgas y, en consecuencia, una influencia positiva en la producción de biomasa. También se realizaron validaciones numéricas en modelos multivariables no lineales, que incluye un proceso de refrigeración de un ciclo, un modelo de turbina eólica marina disponible en la Universidad de Stuttgart (Alemania) y el modelo UVA/Pádova de la Universidad de Virginia (EEUU) para la regulación de glucosa en pacientes con diabetes Mellitus tipo 1. En todos los casos se verifica que el esquema de control propuesto presenta estabilidad y desempeño robusto a pesar de las perturbaciones externas, incertidumbre paramétrica y retardos de tiempo.

* Trabajo de investigación doctoral.

** Facultad de Ingenierías Fisicomecánicas. Escuela de Ingenierías Eléctrica, Electrónica y de Telecomunicaciones. Doctorado en Ingeniería. Director: Ing. Rodolfo Villamizar Mejia.

ABSTRACT

TITLE: Robust Control approach for Multivariable Systems under Delays, Parametric Uncertainty and External Disturbances*

AUTHOR: Jose Jorge Carreño Zagarra**

KEYWORDS: Robust Control, Active Disturbance Rejection Control, GPI Observers, Uncertain Systems, Time-delay Systems.

DESCRIPTION:

This dissertation proposes a new control scheme for multivariate systems with or without time delays, external disturbances, and parametric uncertainty. The design methodology combines the robust control approach for uncertain systems and high-gain observers used to estimate and attenuate online disturbances. In the *feedback* control stage, the use of QFT controllers, robust PI controllers with 2 degrees of freedom, and reset controllers are proposed to achieve robust performance and stability specifications in the presence of uncertainty in the plant model parameters. In the *feedforward* control stage, the design of observers is proposed since due to their characteristic of reconstruction of phase variables and estimation of a finite number of derivatives of the disturbance, they provide properties of mitigation or rejection of disturbances, trajectory tracking, performance robust and stabilizing output.

The proposed control scheme was successfully validated in an experimental photobioreactor available at the University of Almería (Spain). A significant improvement in the precision of the microalgae culture's pH regulation is obtained; consequently, a positive influence in biomass production. Numerical validations are also performed on non-linear multivariable models, including a one-cycle cooling process, an offshore wind turbine model available at the University of Stuttgart (Germany), and the UVA / Pádova model from the University of Virginia (USA) for glucose regulation in patients with type 1 Diabetes Mellitus. In all cases, it is verified that the proposed control scheme presents stability and robust performance despite external disturbances, parametric uncertainty, and time delays.

* Trabajo de investigación doctoral.

** Facultad de Ingenierías Fisicomecánicas. Escuela de Ingenierías Eléctrica, Electrónica y de Telecomunicaciones. Doctorado en Ingeniería. Director: Ing. Rodolfo Villamizar Mejia.

1. INTRODUCTION

1.1. Problem Definition and Motivation

Historically, the process industry has recognized the vital job of automatic control on the proper functioning of the production processes. Although the preferred control strategy in most applications is PID (Proportional-Integral-Derivative) control, several features are not explicitly considered in the design of these classic controllers, such as delays, unmeasurable variables, parameter uncertainty, time-variant systems, nonlinearities, constraints, and multivariable interactions. Many developments of modern control theory are designed to contend with these features; however, the industry has been conservative in applying these approaches. This fact has led many critics to say that there is a gap between theory and control practice.

Control systems frequently work in the presence of time delays, mainly due to the time it takes to obtain the necessary information for decision-making and execution. From the classical control perspective, the presence of delays reduces the phase margin of the systems and which can eventually destabilize the closed-loop response. However, the rational introduction of a delay may help achieve stability in unstable systems [118], which has been a motivation to take advantage of this type of dynamic systems [29, 49, 75, 77, 118]. Typical systems with delays are chemical processes, communication, transport, power, tele-operation and bio-systems.

On the other hand, there are always modeling errors due to the difficulty of accurately modeling a complicated process. There are many causes of this discrepancy, collectively referred to as model uncertainties in the systems theory literature [51]. The development of methods to address model uncertainty is a big challenge, and many control strategies are available today to tackle it. Sometimes, in an attempt to take into account all relevant dynamics and reduce the modeling error, there could be developments of increasingly sophisticated models. However, this maneuver can lead to models that are too difficult for mathematical analysis and controller's design.

External disturbances cause another common problem in the control systems. Such disturbances are harmful to system performance, so rejection is one of the main objectives in the controller design. In industrial processes - like oil and metal industries - the production systems are usually influenced by external disturbances, such as variations in primal matter quality, production load fluctuations, and variations of complicated production environments. In the biomedical system, for exam-

ple, regulating blood glucose in diabetic patients, external disturbances are related to food intake, physical activity, and stress, among others.

Traditional feedback control schemes-such as PID controllers-attenuate disturbances relatively slowly. Although Feed-forward control provides an effective method for disturbances rejection, its implementation ideally requires that disturbances are measured by sensors. Unfortunately, in many cases, the disturbances are difficult to measure by sensors physically. For this purpose, disturbance observers provide a practical estimation of the perturbations for a wide range of dynamic systems.

This dissertation presents a new control scheme for dynamic systems with delay and parameter uncertainty. The approach uses the feedback controller design for uncertain systems and the active disturbance rejection control approach.

1.2. Objectives and scope of the research

1.2.1. General objective

To improve the dynamic performance of multivariable systems in presence of time delays, external disturbances and parametric uncertainty, through a robust feedforward-feedback control approach.

1.2.2. Specific objectives

In order to accomplish the general objective, the next specific ones were proposed:

1. To integrate the characteristics of feedback and feedforward controllers based on state observers for active disturbance rejection to obtain a robust scheme for system with parametric uncertainty and external disturbances.
2. To propose a predictive feedback-feedforward control for active disturbance rejection in time-delays systems with parametric uncertainty.
3. To validate the proposed control strategy for multivariable systems addressing problems of time delay, external disturbances and parametric uncertainty.

1.3. Organization of the dissertation

This dissertation is formulated into six chapters. The present chapter contains the introduction, motivation, and the key objective of the thesis. *Chapter 2* presents a brief literature review on some open problems in automatic control. The control problems studied are uncertain parameters, external disturbances, and time-delay. *Chapter 3* presents the theoretical framework, which covers topics such as fundamentals of active disturbances rejection control, differential flatness, limitations of classical controllers, and robust controller design based on quantitative control theory. The robust control proposal is presented in *Chapter 4*. This chapter presents the control scheme proposed in this thesis for uncertain systems with and without time delay.

Chapter 5 is assigned to the numerical and experimental validation of the robust control approach on kind of systems cases. Finally, *Chapter 6* presents some conclusions derived from this thesis and future work.

1.4. Academic Production

Published articles

1. Carreño-Zagarra, J. J., Guzmán, J. L., Moreno, J. C., Villamizar, R. (2019). Linear active disturbance rejection control for a raceway photobioreactor. Control Engineering Practice, 85, 271-279.
2. Carreño-Zagarra, J.J., Villamizar, R., Moreno, J.C., Guzmán, J.L. Active Disturbance Rejection and PID Control of a One-stage Refrigeration Cycle, IFAC-PapersOnLine, Volume 51, Issue 4, 2018, Pages 444-449, ISSN 2405-8963.
3. Carreño-Zagarra, J.J., Villamizar, R., Guzmán, J.L., Moreno, J.C. Predictive active disturbance rejection control for insulin in patients with T1DM, IFAC-PapersOnLine. (Accepted).

International conferences

1. 7th Symposium on System Structure and Control, Sept. 9-11, 2019, Sinaia, Rumania. Research presented: Predictive active disturbance rejection control for insulin in patients with T1DM. Authors: Jose Jorge Carreño Zagarra, Rodolfo Villamizar Mejía, Jose Carlos Moreno, Jose Luis Guzmán.

2. 3rd IFAC Conference on Advances in Proportional-Integral-Derivative Control, May 9-11, 2018, Gante, Bélgica. Research presented: Active Disturbance Rejection and PID Control of a One-Stage Refrigeration Cycle. Authors: J.J. Carreño-Zagarra, R. Villamizar, J.C. Moreno, J.L. Guzmán.

3. 14th IEEE International Conference on Control and Automation (ICCA), June 12-15, 2018, Anchorage, USA. Nonlinear robust control of offshore wind turbines based on flat filtering and reset compensation. Authors: J.J. Carreño-Zagarra; R. Villamizar.

4. XXXVIII Jornadas de Automática, sept. 6-8, 2017, Gijón, Spain. Research presented: Control Robusto del pH en Fotobiorreactores Mediante Rechazo Activo de Perturbaciones. Authors: J.J. Carreño- Zagarra, R. Villamizar, J.C. Moreno, J.L. Guzmán.

5. 12th International Conference on Informatics in Control, Automation and Robotics (ICINCO), July 21-23, 2015. Research presented: Design of Robust Control Strategy for Non-Linear Multivariable Systems with Delay, Parametric Uncertainty and External Disturbances. Authors: J.J. Carreño-Zagarra; R. Villamizar.

The information corresponding to the contribution made by each one of the authors in the written articles can be consulted in Table 1.

Table 1. Individual's contribution

PAPER INFORMATION	**CONTRIBUTION**
Carreño-Zagarra, J. J., Guzmán, J. L., Moreno, J. C., and Villamizar, R. (2019). Linear active disturbance rejection control for a raceway photobioreactor. *Control Engineering Practice*, 85, 271-279. https://doi.org/10.1016/j.conengprac.2019.02.007 Copyright: https://www.elsevier.com/about/policies/copyright	Carreño made substantial contributions to conception and design of project. He participed in the design of the control proposal; carried out the simulations, made the analysis of them; and wrote the manuscript. Guzmán participated in the implementation of the controllers in the experimental plant. Guzmán, Moreno and Villamizar served as advisers to the investigation. All authors read and approved the final manuscript. Level of contribution: Carreño (80 %), Guzmán (5 %), Moreno (5 %), Villamizar (5 %).

Carreno-Zagarra, J. J., Villamizar, R., Moreno, J. C., and Guzmán, J. L. (2018). Active disturbance rejection and pid control of a one-stage refrigeration cycle. *IFAC-PapersOnLine*, 51(4), 444-449. https://doi.org/10.1016/j.ifacol.2018.06.135 Copyright: https://www.ifac-control.org/publications/copyright-conditions	Carreño made substantial contributions to conception and design of project. He participed in the design of the control proposal; carried out the simulations, made the analysis of them; and wrote the manuscript. Villamizar, Moreno and Guzmán served as advisers to the investigation. All authors read and approved the final manuscript. Level of contribution: Carreño (85 %), Villamizar (5 %), Moreno (5 %), Guzmán (5 %).
Carreño-Zagarra, J. J., Villamizar, R., Moreno, J. C., and Guzmán, J. L. (2019). Predictive Active Disturbance Rejection Control for Insulin Infusion in Patients with T1DM. *IFAC-PapersOnLine*, 52(17), 105-110. https://doi.org/10.1016/j.ifacol.2019.11.035 Copyright: https://www.ifac-control.org/publications/copyright-conditions	Carreño made substantial contributions to conception and design of project. He participed in the design of the control proposal; carried out the simulations, made the analysis of them; and wrote the manuscript. Villamizar participated in the writing of the document and in the review of the simulations. Guzmán, Moreno and Villamizar served as advisers to the investigation. All authors read and approved the final manuscript. Level of contribution: Carreño (85 %), Villamizar (5 %), Moreno (5 %), Guzmán (5 %).
Carreño-Zagarra, J. J., and Vilamizar, R. (2018, June). Nonlinear robust control of offshore wind turbines based on flat filtering and reset compensation. In 2018 *IEEE 14th International Conference on Control and Automation (ICCA)*, 1186-1191. https://doi.org/10.1109/ICCA.2018.8444350 Copyright: https://www.ieee.org/publications/rights/index.html	Carreño made substantial contributions to conception and design of project. He participed in the design of the control proposal; carried out the simulations, made the analysis of them; and wrote the manuscript. Villamizar participated in the writing of the document and in the review of the simulations. All authors read and approved the final manuscript. Level of contribution: Carreño (90 %), Villamizar (10 %).

Carreño-Zagarra,J.J., Guzmán, J.L., Moreno, J.C., and Villamizar, R. (2017). Control robusto del pH en fotobiorreactores mediante rechazo activo de perturbaciones. In *Actas de las XXXVIII Jornadas de Automática*. Servicio de Publicaciones, 16-22. http://hdl.handle.net/10651/46411 Copyright: https://publicaciones.uniovi.es/reglamento	Carreño made substantial contributions to conception and design of project. He participed in the design of the control proposal; carried out the simulations, made the analysis of them; and wrote the manuscript. Guzmán participated in the review of mathematical model of the bioprocess. Guzmán, Moreno and Villamizar served as advisers to the investigation. All authors read and approved the final manuscript. Level of contribution: Carreño (85 %), Guzmán (5 %), Moreno (5 %), Villamizar (5 %).
Carreño-Zagarra, J.J., and Villamizar, R. V. (2016). Active Disturbance Rejection Robust Control for Uncertain Systems. Case: Floating Offshore Wind Turbine. *Science and Technology Publications*, 34-44.https:http://www.icinco.org/Abstracts/2016/DCINCO_2016_Abstracts.htm Copyright: https://www.scitepress.org/EthicsOfPublication.aspx	Carreño made substantial contributions to conception and design of project. He participed in the design of the control proposal; carried out the simulations, made the analysis of them; and wrote the manuscript. Villamizar participated in the writing of the document and in the review of the simulations. All authors read and approved the final manuscript. Level of contribution: Carreño (90 %), Villamizar (10 %).
Carreño-Zagarra, J.J., and Villamizar, R. V. (2015). Design of Robust Control Strategy for Non-linear Multivariable Systems with Delay, Parametric Uncertainty and External Disturbances. *Science and Technology Publications*, 34-44.https://www.scitepress.org/Papers/2015/55808/55808.pdf Copyright: https://www.scitepress.org/EthicsOfPublication.aspx	Carreño made substantial contributions to conception and design of project. He participed in the design of the control proposal; carried out the simulations, made the analysis of them; and wrote the manuscript. Villamizar participated in the writing of the document and in the review of the simulations. All authors read and approved the final manuscript. Level of contribution: Carreño (90 %), Villamizar (10 %).

Undergraduate project (Finished)

1. Diseño y Simulación de un Sistema de Control Predictivo para Administrar la Inyección de Insulina en Pacientes con Diabetes Mellitus Tipo 1. Ingeniería Electrónica, UIS. 2016. Personas orientadas: Yasser David Greyeb Ortiz y David Alberto Padilla Toloza.Trabajo dirijido como tutor principal.

2. Diseño de un Controlador Robusto QFT para el Control de Potencia Activa Generada y Velocidad de Rotación en una Turbina Eólica. Ingeniería Electrónica, UIS. 2016. Personas orientadas: Laura Mércedes Tulcan y Leonel Calderon Supelano. Trabajo dirijido como tutor principal.

3. Control Robusto QFT de un Campo de Colectores Solares Cilindro-Parabólicos basado en un Observador de Perturbaciones. Ingeniería Electrónica, UIS. 2016. Personas orientadas: Miguel Ángel Ardila Larrahondo y Alberto José Bermúdez Áreas. Trabajo dirijido como tutor principal.

4. Herramienta de Diseño Automático de Controladores Robustos LQG para la Regulación de los Niveles de Glucosa en Pacientes con Diabetes Mellitus tipo 1, Sintonizados Mediante Algoritmos Genéticos. Electronic Engineering. Universidad Industrial de Santander. 2015. Personas orientadas: Gabriel Herrera Zárate y Esteban López Herazo. Trabajo dirijido como cotutor.

Master's degree project (Ongoing)

1. Control predictivo robusto para la regulación automática de glucosa en pacientes con diabetes mellitus tipo 1. Tesis de Maestría en Ingeniería Electrónica. Universidad Industrial de Santander. Persona Orientada: David Padilla Toloza. Trabajo dirijido como cotutor.

2. LITERATURE REVIEW

2.1. Open problems in control systems

Today the PID controller is the most common solution to practical automatic control problems. Although proportional and integral action controllers have been in use for a long time, the PID controller's current form emerged with pneumatic controllers in the 1930s [6]. However, there are several characteristics not considered explicitly in the design of these PID controllers, such as delays, unmeasurable variables, parameter uncertainty, time-variant systems, nonlinearities, constraints, and multivariable interactions.

In this chapter a review of the results in the control of systems with delays, parameter uncertainty and external disturbances is carried out in order to explore possibilities that address control problems.

2.1.1. Dead time

Deadtime is the property of a physical system by which the response to an applied input is delayed. When material, information, or energy is physically transmitted from one location to another, a delay associated with the transmission is considered [118]. The control of these delays has been of great interest since they are the leading cause of instability and poor performance in control systems, such as thermal processes, long transmission lines in pneumatic systems, distillation processes, among others.

Figure 1. Delay in a feedback system

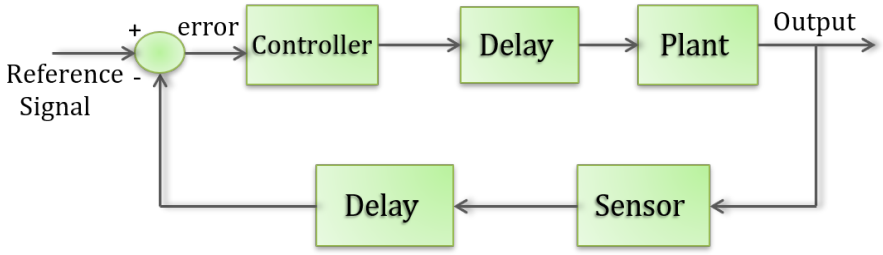

There are various sources of delay. One of these sources is the nature of the system, that is, the way the system works. For example, in chemical reactors, there

is a finite time reaction, and in an internal combustion engine, time is required to mix air and fuel. Another source of dead-time is the transport delay, which occurs when materials go through heat or mass transfer systems, as in a heating system where the transport delay occurs because of hot air. A delay could also be present in the communication between the parts of the system. For example, it takes time for signals to travel between controllers, sensors, and actuators in any typical closed-loop system, particularly in network control systems and high availability systems (see Fig. 1).

Figure 2. Step response of a time delayed system

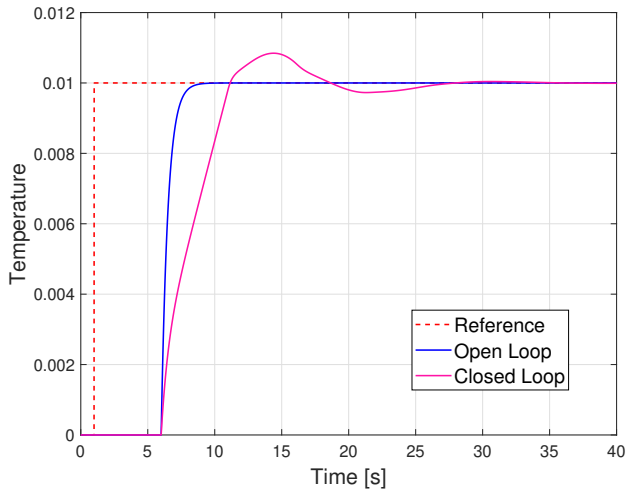

(a)

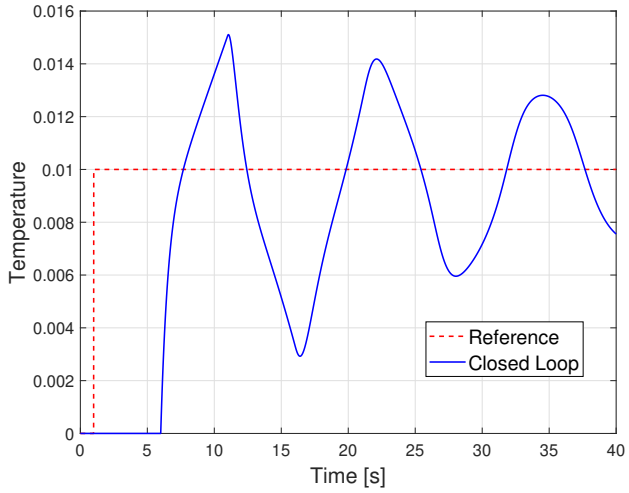

(b)

Figure 2 shows the typical operation of a central heating system, where T is the

temperature measured by a sensor placed in the room [78]. When a change of 1 % is introduced at the set-point, the settling time of the closed-loop control system with the PI controller is much longer than in the open-loop system (Fig. 2). The introduction of this PI element is a necessary modification to guarantee zero error in a stable state. If a faster response is attempted by modifying the proportional gain, oscillations could occur (as shown in Figure 2b) or even make the control system unstable.

A system with multiple delays in the state vector can be represented as:

$$\frac{\mathrm{d}x(t)}{\mathrm{d}t} = A_0 x(t) + \sum_{i=1}^{N} A_i x(t - \tau_i) \tag{2.1}$$

where $x(t)$ is the *n*-dimensional state variable, A_i, with $i = 0, 1, ..., N$, is an $n \times n$ matrix, N is a positive integer and τ_i is the time delay.

Moreover, the characteristic equation of eq. (2.1) is given by:

$$f\left(s; \tau_1, \tau_2, ...\tau_N\right) = \left| sI - A_0 - \sum_{i=1}^{N} A_i e^{-s\tau_i} \right| = 0 \tag{2.2}$$

Due to the presence of exponential terms, equation (2.2) is a quasi-polynomial and a transcendental equation, which has an infinite number of roots in the complex plane $\mathbb{C}$. Therefore, equation (2.1) is asymptotically stable only if all the roots of the above equation are on the left half-plane of the $j\omega$ axis. Verifying the asymptotic stability of equation (2.2) can be tricky since it has an infinite number of characteristic equations [106].

It is evident that delays are a crucial cause of instability and poor performance of dynamic systems, added to the fact that they are frequently found in various engineering and physical systems. The design of stability analysis and control of systems with time delay has attracted the attention of many researchers [66, 104]. The difficulty in controlling these processes is that downtime causes a phase delay that decreases the phase margin, deteriorating both the performance and the system's stability.

PID controllers

Due to the low cost and easy implementation, most of the controllers used in the industry are based on classic control schemes [7, 119]. In this approach, the idea is to tune the drivers, considering the inherent delay of the process. The design problem is to reduce highly conservative design conditions [18, 52, 83, 104]. The design and implementation of PID controllers in systems with variable time delays

are studied in [122], and in [98] an application of PID controllers with the dynamic adaptation of their parameters based on the measured delay is presented.

Although PID controllers can control many processes, they have many limitations. Consider, for example, the unity feedback system of Figure 3, with the transfer function of the plant as:

Figure 3. Feedback control scheme

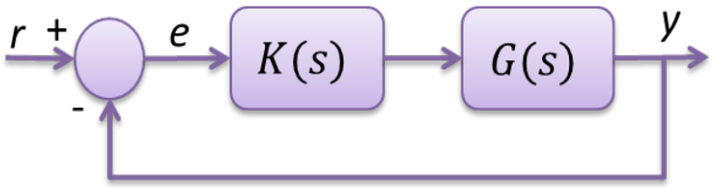

$$G(s) = \frac{K}{1+Ts}e^{-\tau s} \tag{2.3}$$

and PID control as:

$$K(s) = K_p\left(1 + T_d s + \frac{1}{T_i s}\right) \tag{2.4}$$

The transfer function in closed loop would be given by:

$$\begin{aligned} T(s) &= \frac{K(s)G(s)}{1+K(s)G(s)} \\ &= \frac{KK_p\left(T_dT_is^2+T_is+1\right)e^{-\tau s}}{\left(Ts+1\right)T_is+KK_p\left(T_dT_is^2+T_is+1\right)e^{-\tau s}} \end{aligned} \tag{2.5}$$

and the characteristic equation of the closed loop system is:

$$\left(Ts+1\right)T_is+KK_p\left(T_dT_is^2+T_is+1\right)e^{-\tau s}=0 \tag{2.6}$$

Since equation (2.6) is a transcendental equation stability analysis or designing a controller to ensure stability. In order to simplify the analysis, it is assumed that $T_i = T$. Then, the closed-loop transfer function becomes:

$$T(s) = \frac{KK_pe^{-\tau s}}{Ts+KK_pe^{-\tau s}} \tag{2.7}$$

This system is stable only when:

$$0 < K_p < \frac{\pi T}{2\tau K} \tag{2.8}$$

Therefore, the controller's gain is limited by the duration of the delay: the higher the delay, the lower the maximum gain allowed. Thus, a slower response is obtained.

Dead Time Compensation (DTC)

Control schemes for dead time compensation can be classified into two types: the Smith Predictor and Finite Spectrum Assignment (FSA). In 1957, the Smith Predictor is proposed in order to design controllers that isolate the feedback loop delay, obtaining significant simplifications in the system analysis and design of the controller [115].

Figure 4 shows the block diagram of a control system based on the Smith Predictor. $C(s)$ represents the controller, $G(s) = P(s)e^{-\tau s}$ is the controlled process and $Z(s) = P(s)(1 - e^{-\tau s})$ the Smith Predictor.

Figure 4. Control system based on the Smith predictor

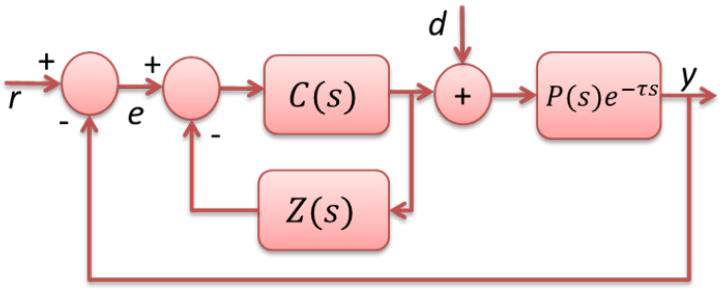

Assuming there are no disturbances in the system, the closed-loop transfer function is given by:

$$T(s) = \frac{C(s)P(s)}{1 + C(s)P(s)} e^{-\tau s} \tag{2.9}$$

Although this configuration allows the controller's design regardless of the magnitude of the delay, it has some limitations, such as not being able to apply to unstable processes, significant sensitivity to modeling errors, and external disturbances. It only applies to systems with constant delay and input (i.e., not applicable to systems with the delayed state) [130].

To overcome some limitations of Smith Predictor, in 1974, the technique of finite spectrum allocation was developed. This new approach is useful not only for the design of controllers for unstable systems with delay in the input but also in the states [73]. The technique is based on the transformation of the state vector of the process to eliminate delays of the characteristic equation of the system so that the closed-loop poles can be allocated from the required specifications of design [38]. This method does not require prior knowledge of the spectrum of the plant, only then spectral points, while the others left are automatically deleted [5].

Consider a system described in state space as:

$$\begin{aligned} \dot{x}(t) &= Ax(t) + Bu(t-\tau) \\ y(t) &= Cx(t) \end{aligned} \tag{2.10}$$

From this expression, the transfer function of the plant is:

$$G(s) = P(s)e^{-\tau s} = \begin{bmatrix} A & B \\ C & 0 \end{bmatrix} e^{-\tau s} \tag{2.11}$$

Finite Spectrum Assignment (FSA) takes on the following feedback control law [130]:

$$u(t) = Fx_p(t) \tag{2.12}$$

The state predicted $x_p(t)$ is given by:

$$x_p(t) = e^{A\tau}x(t) + \int_0^{\tau} e^{A\tau}Bu(t-\lambda)d\lambda \tag{2.13}$$

Similar to the control scheme based on the predictor, the delay term is removed from the design process. The resulting closed-loop system is stable if $A + BF$ is stable.

Although DTC structures are more complex and require more excellent knowledge for tuning than traditional PIDs, these have better compensation for delays, especially when process downtime is dominant [16]. However, because the state prediction is made from the model, these techniques have a high sensitivity to modeling errors, especially when the delay is considerable. If a high order model with delay to describe the dynamics of a process is needed, both a primary controller of higher-order in the DTC as a traditional (different to PID) controller is needed. In these cases, it is clear that the limitations on the performance of PID are due to model order and not to delay [16].

Sliding mode control

Sliding mode control is a robust control technique that uses non-linear switching elements to bring the system's states to the desired point of operation through a path defined in advance by the designer. This trajectory is called the surface or sliding line due through the commutation control law guarantees that from any point in the state space, the paths go towards it and slide until reaching the desired operating point.

Sliding mode control (SMC) supplies a powerful way to deal with a robust stabilization problem for dynamic systems of finite dimension (i.e., systems without delay). The presence of delay in a sliding mode control approach can produce oscillations in the design surface neighborhood. Some studies reveal possible behavioral changes (bifurcations) that arise in these types of systems [90]. This fact led to the research of SMC controller design for systems with input or state delays [93]. In [126], a control structure is proposed in sliding modes for the convergence in a finite time of systems with input delay.

The uncertainty of the plant model in systems with delay makes the control problem more complicated even for linear systems invariant over time. A possible way to handle this problem is to employ high gain or sliding mode control techniques, which are useful tools to reject the system uncertainty. However, the straight implementation of these robust control techniques without considering time delays can produce oscillations or instability of the closed-loop system [37]. To overcome these limitations, a predictor-based approach can be applied that compensates the time delay in the control input resulting in a delay-free closed-loop system. In [95] a sliding surface based on a predictor is exposed, which minimizes the effects of system entry delays, and derives a robust control law that guarantees the existence of a sliding mode and overcomes the delay and uncertainty of the system.

As is the case with other conventional control laws, if the delay is not taken into account when making the design, the system may become unstable or aggravate the effect of chattering [117]. In [45] a methodology to design controllers in sliding mode based on LMI (Linear Matrix Inequalities) for systems containing either one delay, multiple delays, constant delays, or variable delays is proposed. The conditions for the presence of the sliding status are studied by using the Lyapunov-Krasovskii and Lyapunov-Razumikhin functions, and an LMI scheme is used in the optimization procedure.

Delay scheduling

Delay Scheduling is a recent technique that improves the stability of multivariable systems by introducing hold buffers in the feedback loop. This idea of selectively increasing delays can add desired dynamic performance characteristics, such as

fast disturbance rejection. Since delayed data can make it difficult the tracking, the design goal is to reschedule them to improve the performance [81].

Let take the MIMO dynamics system as:

$$\dot{x}(t) = Ax(t) + Bu(t) \tag{2.14}$$

Suppose that (A, B) is a controllable pair, and the requested state trajectory to be trailed is given by $x^*(t)$. Using the conventional computerized torque method, the control law applies the delayed state information for its corrective actions in which multiplicative delays appear. Defining the state error vector as $e_x(t) = x^*(t) - x(t)$, Eq. (2.14) can be rewritten as follows:

$$\dot{e}_x(t) = Ae_x(t) + B\bar{u}(t) \tag{2.15}$$

where $\bar{u}(t)$ is the full-state feedback of the form $\bar{u}(t) = Ke_x(t)$, with the appropriate eigenvalue distribution of $A + BK$ for disturbance rejection. In the delay scheduling approach, the signal $\bar{u}(t)$ uses retarded data on $e_x(t)$. One way is to use *m* delayed parts of the vector e_x, that is, $e_1\,(t - \tau_1)$, $e_2\,(t - \tau_2)$,..., $e_m\,(t - \tau_m)$. In this way, the new error dynamics becomes:

$$\dot{e}_x(t) = Ae_x(t) + B\sum_{j=1}^{m} K_j e_x\,(t - \tau_j) \tag{2.16}$$

which is a popular class of LTI multiple time-delayed system (MTDS), whose stability property must be ensured. The error $e_x(t)$ must approximate zero and remain at that value for successful tracking. The following expression gives the characteristic equation of the system:

$$CE(s) = det\left[sI - A - B\sum_{j=1}^{m} K_j e^{-\tau_j s}\right] = 0 \tag{2.17}$$

These systems are recognized as LTI-MTDS of retarded type due to the existence of integer multiples of a delay, τ_j, such as $e^{-\tau_j s}$, $e^{-2\tau_j s}$, $e^{-3\tau_j s}$, etc.

Since time-delayed LTI systems could present multiple stable operating zones -known as pockets- in the delay space, the control problem is finding and experimentally testing such pockets [81]. For analytical pocket localization in [81], a novel technique known as Cluster Treatment of Characteristic Roots (CTCR) is used. Researches such as [80–82] have reported robust control performance for tracking and disturbance rejection in the face of long time delays.

Model predictive control (MPC)

MPC is a powerful control technique that has found great acceptance in industrial applications such as in academia. This success is possible due to the fact that systems are useful both in single variable and multivariable systems, considering the restrictions of the control system and inherently compensate for delays in the process [91].

Due to the MPC controllers' predictive environment, time delays are considered internally, which allows them to be compared with DTC algorithms [16, 78]. Each linear MPC can be stated as a DTC two degrees of freedom when the primary controller is calculated using an optimization process. The optimization structure of the internal DTC is defined as much by the process model as the model of disturbances, and is not dependent on the optimization procedure even when considering the restrictions. Figure 5 illustrates this idea.

Figure 5. Outline of model predictive control

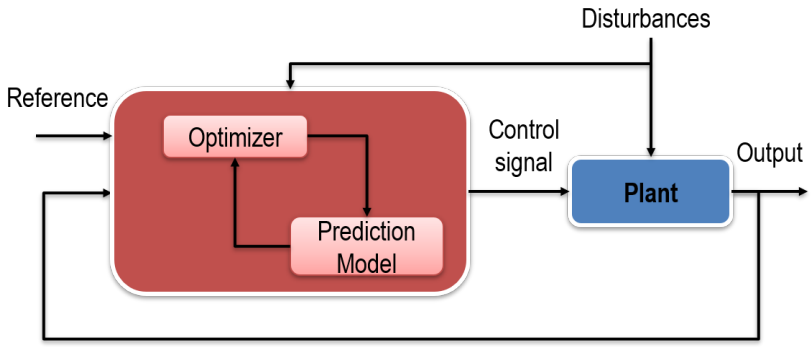

Figure 6 shows the general structure of an MPC controller predictor for a process with time delay. The prediction y_p consists of the addition of the output of the delay free ideal model $\hat{y}(t+d|t)$, and a correction based on the current plant output $y(t)$ and the predicted output $\hat{y}(t|t)$, passing through a filter [78].

Although the reference tracking is not dependent on the characteristics of the predictor, response to disturbance rejection, and robustness of the closed-loop system are associated with the predictor filter block MPC. Therefore, these two characteristics are affected by the dead time of the process, and in some applications, a greater scheme is required.

2.1.2. Uncertainty systems

Control system design depends significantly on the dynamic model of the plant or process. As a real process may be too complex to be described so absolutely precise

Figure 6. General structure of predictor MPC

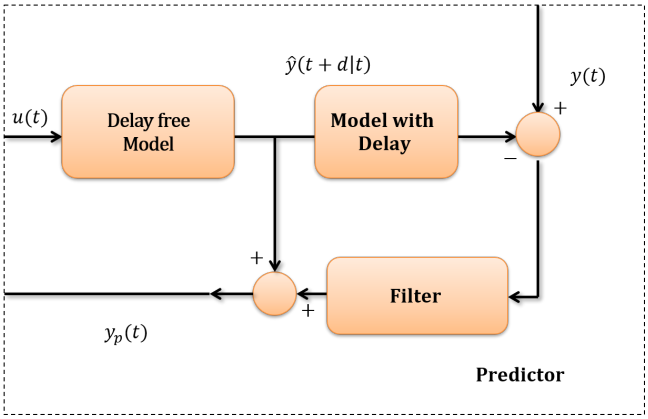

by a mathematical model, they always have modeling errors. The origins and causes of this discrepancy are many and control theory is referred collectively as uncertainty in the model: parametric uncertainty, little knowledge of the dynamics of the process, unknown entries and dynamic despised and simplifications in the model, among others [51, 97]. For example, if a model based on the linearized about a nominal operating point of a nonlinear system controller is designed, the nonlinearities are presented as modeling uncertainties (see Figura 7).

Figure 7. Control system with uncertainty in the plant model.

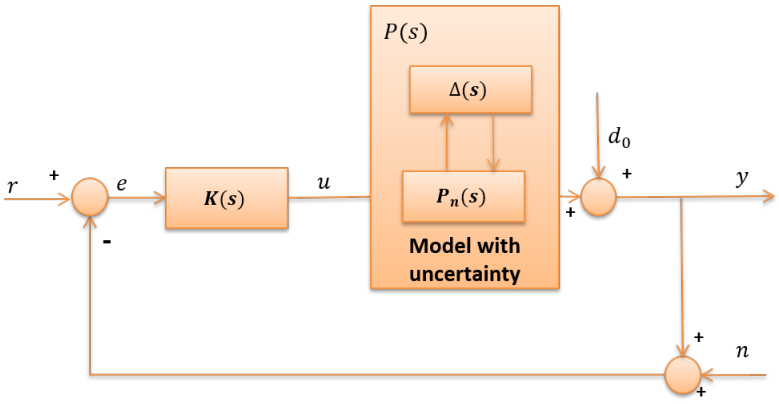

Items with uncertainty can be classified as structured and unstructured uncertainties. In the first class, sources of uncertainty of systems are localized, obtaining with this a tighter or structured modeling errors description. In the unstructured uncertainties, a magnitude dimension of the uncertainty is commonly known, usually depending on the frequency. These elaborate uncertainties generally are presented in the high-frequency range and could include uncertain time delays, parasitic coupling, hysteresis, and other non-linearities. An example of this type of uncertainty

occurs in the linearization of a non-linear system. If the real system is non-linear and the model used for its representation is linear, the difference operates as an unstructured uncertainty [74].

Unstructured uncertainties

Dynamic disturbances that take place in different regions of a system and can be grouped into an unique block of disturbance Δ, are known as unstructured uncertainty. This type of uncertainty can be described in different ways, and some of the most used models are: additive uncertainty, multiplicative uncertainty and feedback uncertainty. Some types of uncertainty are shown in Figure 8, where $P_n(s)$ is the nominal model of the system and $P(s)$ is the dynamics of the real disturbed system.

Table 2 shows the models of the different types of unstructured uncertainty. I is the identity matrix. The multiplicative uncertainty representations show relative errors, while additive descriptions provide an account of absolute error between the real behavior of the system and the nominal model used [47]. For this type of uncertainty a dimension of the magnitude of $\Delta(s)$ is known, generally dependent on the frequency:

Table 2. Modelling of unstructured uncertain systems

Model of uncertainty	Real plant
Additive uncertain	$P(s) = P_n(s) + \Delta(s)$
Input multiplicative uncertain	$P(s) = P_n(s)\,[I + \Delta(s)]$
Output multiplicative uncertain	$P(s) = [I + \Delta(s)]\,P_n(s)$
Input feedback uncertain	$P(s)^{-1} = [I + \Delta(s)]\,P_n(s)^{-1}$
Output feedback uncertain	$P(s)^{-1} = P_n(s)^{-1}\,[I + \Delta(s)]$
Plant feedback uncertain	$P(s)^{-1} = P_n(s)^{-1} + \Delta(s)$

$$\sigma\left[\bar{\Delta}(j\omega)\right] \leq \delta(\omega) \quad \forall\omega \tag{2.18}$$

Structured uncertainties

If the sources of the system's uncertainties are somehow located, a more adjusted or structured description of the modeling errors will be available. This can be constituted in turn by multiple localized and independent unstructured uncertainties $\Delta_i(s)$. These uncertainties may correspond to non-modeled dynamics of actuators, sensors and even the same plant. Therefore, the complete uncertainty of the system is of the form:

Figure 8. Modelling of uncertain systems

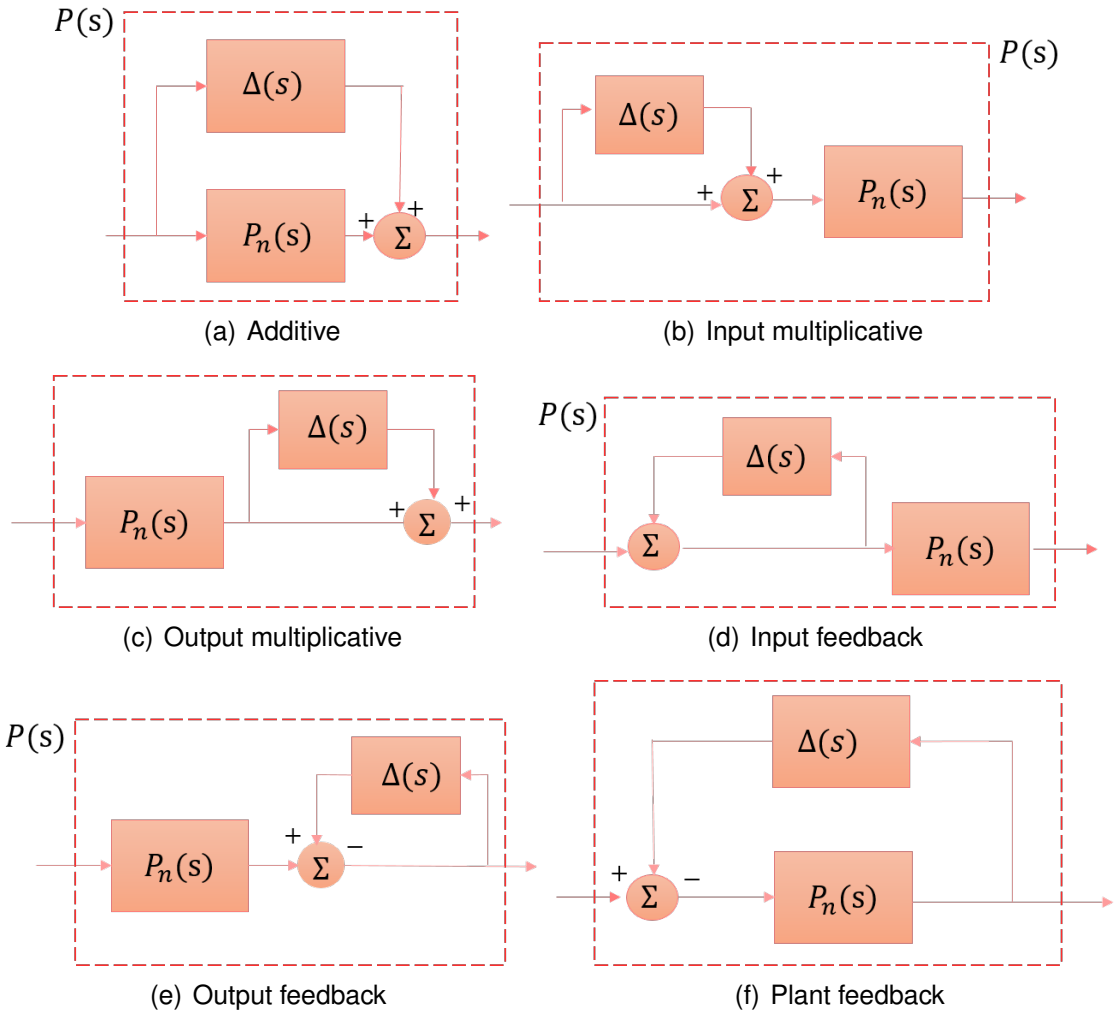

$$\Delta(s) = diag\{\Delta_i(s)\}; \quad i = 1, 2, ..., p \tag{2.19}$$

where p is the number of blocks.

In many industry control systems dynamic disturbances are produced by an inexact description of the characteristics of the components, the change of operating points, or the effects of wear on plant components, etc. Such disturbances can represent variations of determinate system parameters, around some feasible ranges of values. They affect the performance of the low frequency range and are called *parametric uncertainties* [47].

Consider for example a first order system whose transfer function is given by:

$$P(s) = \frac{K}{\tau s + 1} \tag{2.20}$$

Assume that in this process there is uncertainty around the pole, $\tau = \tau_0 + \delta\tau$, with τ_0 as the nominal value. The representation of this uncertainty can be done with a multiplicative model as follows:

$$\begin{aligned} P(s) &= \frac{K}{(\tau_0 + \delta\tau)\, s + 1} \\ &= \frac{K}{\tau_0 s + 1}\left[\frac{\tau_0 s + 1}{\tau_0 s + \delta\tau s + 1}\right] \\ &= \frac{K}{\tau_0 s + 1}\left(1 - \frac{\delta\tau s}{\tau_0 s + \delta\tau s + 1}\right) \\ &= P_n(s)(1 + \Delta(s)) \end{aligned} \tag{2.21}$$

where, in this case

$$\Delta(s) = \frac{-\delta\tau s}{\tau_0 s + \delta\tau s + 1} \tag{2.22}$$

When a dynamic system is depicted through the standard configuration in Fig. 9, and the uncertainty Δ has a particular structure (such as unmodelled dynamics and parameter variations), it is stated that it has a structured uncertainty. This block diagram is used to illustrate how the uncertainty influences the input/output relationship of the control system [47].

Control approaches of uncertain systems

Currently, two main approaches try to overcome the uncertainty in the model: adaptive control [100, 114] based on online identification process and adjustment of the slider to the desired conditions; and robust control [53, 84, 103], which guarantees the preservation of specific properties of the control loop for the whole family of controlled plants. Various strategies of adaptive control have been proposed considering uncertainty SISO and MIMO systems. Such controllers often involve some functions to approximate the unknown dynamics. However, the approximation error and disturbance - internal or external - can impair controller performance or even destabilize the closed-loop control system. Therefore, to ensure the controller's performance, the design of adaptive controllers incorporates various robust components, resulting in robust adaptive controllers [48, 58, 69, 124].

Figure 9. Standard $M - \Delta$ configuration

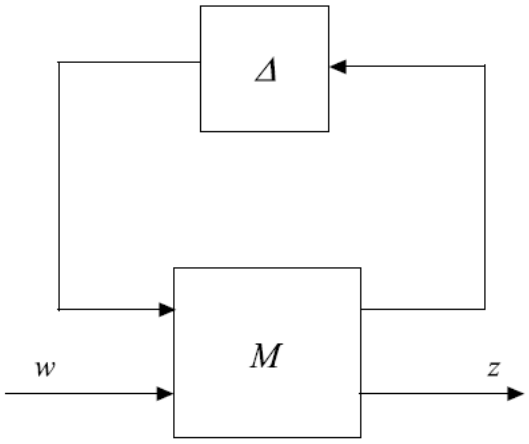

2.1.3. Disturbance rejection

The disturbance rejection dilemma is a perennial topic of research that encompasses the theory and control applications. Traditional control methods such as Proportional Integral Derivative (PID) and Linear Quadratic Regulatory (LQR) controllers are often unable to meet high precision control specifications in the presence of uncertainties and strong disturbances. The main reason is that these methods do not explicitly take into account the attenuation of the effect of such control problems [72]. Typical characteristics of the disturbance rejection methods are summarized below:

Adaptive Control: is a non-linear control technique that automatically modifies the controller parameters to guarantee that the closed-loop system's behavior maintains the essential design characteristics. Since this technique identifies the controlled model parameters online and then adjusts the controller parameters based on that estimate, it is generally very effective in dealing with model uncertainties. However, as successful adaptive control applications generally rely heavily on the laws of adaptation, when these critical parameters are difficult to identify or estimate online, these methods are not valid.

Robust Control: is an approach to controller design that explicitly deals with uncertainty. Robust control methods are designed to achieve robust performance and stability in the presence of parameters uncertain or disturbances defined within a set of values, which is generally compact. The robustness of this technique is usually obtained by sacrificing the transient performance of other highlights. Therefore, the robust control is often criticized for occasionally being conservative.

Sliding mode control: is a non-linear control technique that modifies the dynamics of a non-linear system by employing a discontinuous control signal that forces the system to "slip.[a]long a cross-section of normal system behavior. Although this techni-

que can suppress the effects of parameter variations and external disturbances, the discontinuous switching of the controller makes it prone to inducing high-frequency vibrations. Several modification methods can effectively reduce this problem; however, this leads to a deterioration of the performance to the rejection of disturbances [72].

Internal Model Control: is a linear control technique that makes use of a plant model to calculate the input movements to be made. Although due to its simple concept and intuitive design philosophy, this technique has received high acceptance in control theory, it is generally available for linear systems, and its application in high-dimensional systems usually presents a very high computational cost due to the need to calculate the inverse of a high-dimensional transfer matrix [72].

The objective of the cited control schemes is to reject disturbances through feedback, so this rejection is based on the tracking error between the measured outputs and the setpoints [52]. In the event of strong disturbances, such controllers cannot react fast enough, although ultimately they can suppress disturbances by regulating feedback relatively slowly. Due to this fact, these control approaches are commonly recognized as passive anti-disturbance control (PADC) methods [72].

To overcome the limitations of PADC methods in handling disturbances, the so-called active disturbance rejection control (ADRC) approach has recently been proposed. The idea of such a control approach is to directly counteract disturbances through an anticipated compensation control design based on disturbances' estimates through the use of observers. Usually, this control structure involves two parts: feedback control and feedforward control based on disturbance observer. Feedback control is generally employed to ensure monitoring and stabilizing the dynamics of the nominal controlled plant. At this stage, the disturbances and uncertainties do not necessarily need to be considered. A disturbance observer can estimate these characteristics in order to be compensated for by a progress controller [72].

3. THEORETICAL FRAMEWORK

3.1. Quantitative Feedback Theory

Control engineering occupies a monumental place in the design of technology. Control concepts are usually the key factor in achieving speed and precision in multidisciplinary systems, including aerospace missions, power plants, chemical processes, transportation, energy systems, robotics, and environmental projects [41].

The theory of automatic control began in the early thirties when feedback amplifiers for communication appeared in commercial use. At that time, the use of the feedback was initiated with the purpose to make the characteristics of the amplifier less sensitive to the uncertainties and physical anomalies of the electronic components. However, as is well known, the use of feedback creates serious stability problems.

In 1932 Nyquist presented his famous work entitled *Nyquist Stability Criterion*, which would be expanded by Back in 1934 to analyze the stability of feedback amplifiers. In 1945, after seven years of research in the *Bell Telephone* laboratories, Hendrick Bode published the most influential work in the automatic control of the twentieth century: his book *Network Analysis and Feedback Amplifier Design*. There, he presented the fundamentals of feedback, systems analysis and compensator design in the frequency domain.

In 1959, a scientist from the *Hughes Aircraft* company named Isacc Horowitz, would introduce a laborious formulation of the genuine frequency methodology founded by Bode with considerations of unawareness of the plant under quantitative analysis. In his book *Fundamental Theory of Automatic Linear Feedback Control Systems*, Horowitz presents the need to quantify the design of the controller according to the desired specifications and the uncertainty of the plant.

Four years later (1963), in his book *Synthesis of Feedback Systems*, Horowitz would formally broaden Bode's original concepts and provide novel proposals such as the control of two degrees of freedom. There, he handles a wide set of sensitivity problems in feedback control and exposes the first work in which a control problem was treated quantitatively in a systematic way [44]. However, until 1972, coinciding with the introduction of the Nichols diagram as a working tool, Horowitz and his doctoral student Marcel Sidi used the name of *Quantitative Feedback Theory* (QFT) for first time.

Since then, the QFT control theory has been widely used, with flying colors applied in monovariable and multivariable systems, linear and non-linear systems, delayed processes, minimum and non-minimum phase systems, discrete time systems, etc. Also it has been employed in multiple real-world applications, such as wind energy, light control, spacecraft, water treatment plants, mechanical and power systems, chemical reactors and motion control.

Figure 10 describes the big picture of QFT control system design, closing the gap between control theory and real-world applications. This figure shows the essential aspects of the design process of the control system, and provides an overview of what it means to achieve a practical and successful control system design, presenting the factors that aid to close the gap between the theory and the real world. When making a practical design of the control system, the engineer must consider that the objective of the design process is not only limited to a satisfactory robust design but also that the implementation must comply with the functional requirements [44]. In this process the model simulations are very useful in the early evaluation, but if the system works optimally, hardware tests must be carried out in the circuit and the system to verify the unmodified effects that have not been taken into account during the design and the phases implementation.

As shown in Figure 10, the key elements of QFT are the incorporation of performance specifications (at the beginning of the design process), the construction of templates to characterize the model of the plant at several frequencies, the capacity to inspect frequency responses of the linear time-invariant (LTI) plants that symbolize the nonlinear dynamical system at all its operating points, the design boundaries drawn on the Nichols chart and finally, the relationship of the closed-loop control system with the frequency domain design and the operating condition. To ensure a favorable control design, the control system must ensure that all requirements are met during the simulation and system test. If the control system failure in any of the simulation or system tests, then the designer can use the QFT components to mark that malfunction during the design process and provide any necessary adjustments [55].

3.1.1. Basic concepts of QFT

QFT is a control design methodology that reiterates the employment of feedback to mitigate the impact of plant uncertainty and fulfill functioning specifications. This methodology uses the classical frequency response examination that includes Bode diagrams, templates representations, and Nichols charts and hypothesizes that the feedback is needed primarily when the plant presents model uncertainty or when there are external disturbances operating on the plant [55].

The QFT design is based on the two-degree-of-freedom feedback scheme shown in Fig. 11, which structure incorporates many single-loop systems, cascaded-loop

Figure 10. QFT control system design: *closing the gap* [44].

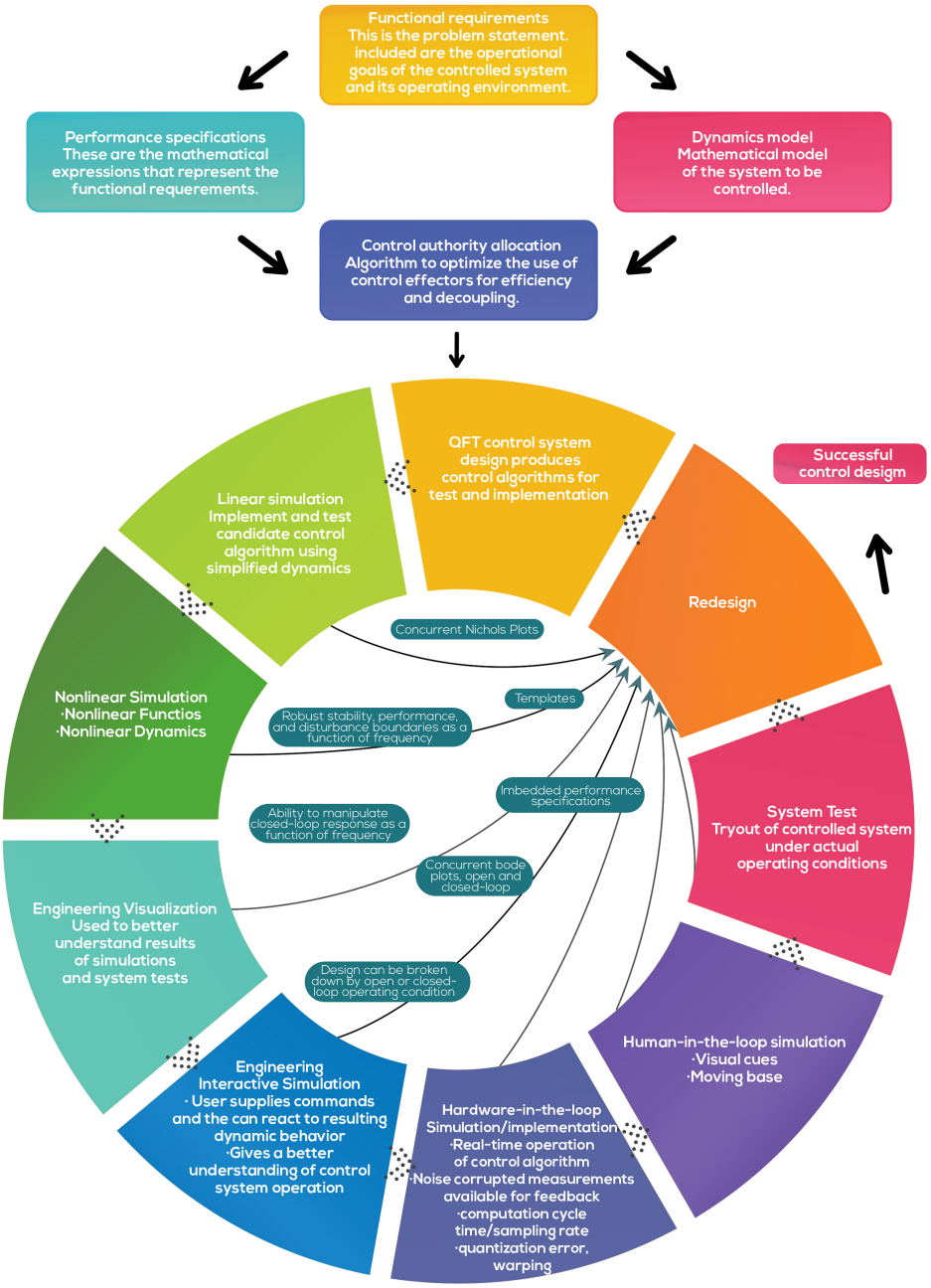

Figure 11. The single-loop feedback system

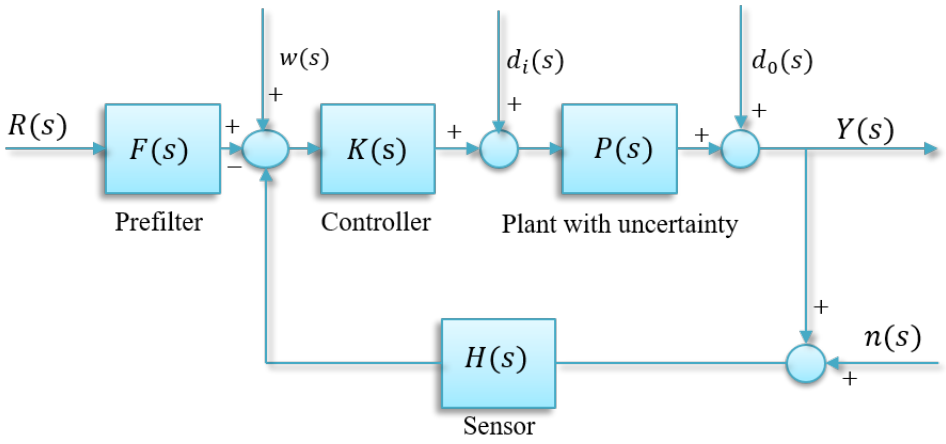

and multi-loop systems designed sequentially or decentralized. The feedback control system includes the set of plants with uncertainty $\Im P(j\omega)$, the controller $K(j\omega)$ and the prefilter $F(j\omega)$ to be designed, and the dynamics of the sensor $H(j\omega)$. The inputs of the system are: the reference $R(j\omega)$, the disturbances $W(j\omega)$, $D_1(j\omega)$ and $D_1(j\omega)$, and the noise $N(j\omega)$.

The methodology for designing QFT controllers consists of the following steps: (1) the model of the plant with uncertainty is defined; (2) the specifications in the frequency domain are defined; (3) based on the model with uncertainty and closed-loop specifications, the contours are calculated; (4) the controller is designed by adding poles and zeros to meet the specifications at each working frequency; (5) if the control system requires reference tracking specifications, a pre-filter is synthesized; (6) finally, after designing the controller $K(j\omega)$ and the filter $F(j\omega)$ its behavior is validated against the established specifications.

Define plant models and uncertainty

The description of the physics of the plant is fundamental to understand the possibilities and limitations of the control system, and to design an appropriate controller to meet the specifications. Consider an uncertain plant $\boldsymbol{P}$, where $\boldsymbol{P} \in \wp$, and $\wp$ is the set of possible plants due to uncertainty.

$\Im P(j\omega_i)$ is the template for the frequency ω_i, that is, the group of complex numbers that describe the frequency response of the uncertain plant at a fixed frequency. In other words, the templates are the representation of the *n*-dimensional parameter space in the Nichols diagram at each frequency of interest. This model uncertainty is a consequence of many factors, including inaccuracies measuring the parameters unknown dynamics, unknown high-frequency components, sensor and actuator errors, nonlinear dynamics, temperature changes, etc.

Figure 12. Templates for solar plant

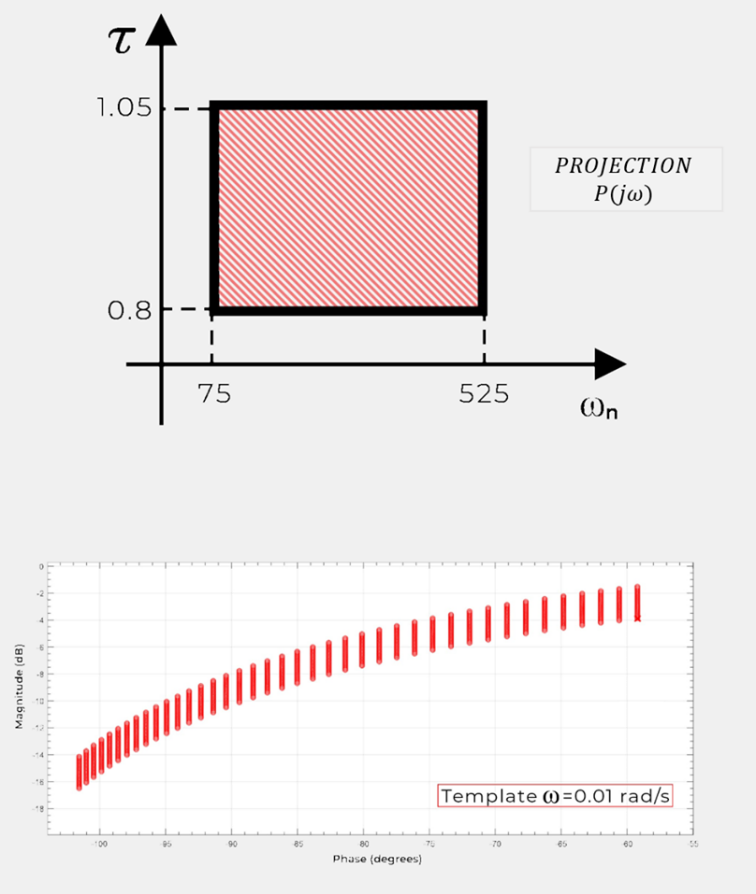

The template for the frequency $\omega = 0.001$ rad/s of a model of a solar plant is shown in Figure 12. The linear system, which includes the solar plant and a feedforward block, is represented by the following model with parametric uncertainty:

$$\wp(s) = \left\{ P(s) = \frac{K}{\tau s + 1} e^{-t_d s} : t_d = 39, \tau \in [75, 525], K \in [0.8, 1.05] \right\} \tag{3.1}$$

where K is the system gain in ^oC, t_d is the time delay (in seconds) and τ is the time constant (in seconds). A nominal plant is selected from the family of plants. The final controller designed by QFT will be the same, no matter what nominal plant is chosen.

Performance specifications

Robust stability and performance specifications (tracking, disturbance rejection, noise immunity, resonance frequency attenuation, etc.) can be done in terms of fre-

quency functions $\delta_k(\omega)$ that are allocated on the magnitude of the following system transfer functions:

$$y(s) = \frac{1}{1+KPH}\left[PD_1 + D_2 + PK(W+FR) - PKHN\right] \tag{3.2}$$

$$u(s) = \frac{1}{1+KPH}\left[K(W+FR) - KH(N+PD_1+D_2)\right] \tag{3.3}$$

$$e(s) = \frac{1}{1+KPH}\left[PHD_1 + HD_2 + PKHW + FR - HN\right] \tag{3.4}$$

Table 3 shows the stability and performance specifications in terms of transfer functions: $|T_k(j\omega)| = \delta_k(\omega)$, $k = 1, 2, ..., 5$. $\delta_1(\omega)$ restricts the transfer function $|L/(1+L)|$, $L = KP$, placing conditions on the robust stability, the control effort in the input disturbance rejection, and the sensor noise attenuation. $\delta_2(\omega)$ and $\delta_3(\omega)$ constrain the output and input disturbance rejection, respectively. $\delta_4(\omega)$ confines the control signal $|K/(1+L)|$ for the system output disturbance rejection, the noise attenuation, and the tracking of reference signals. The upper $\delta_{5b}(\omega)$ and lower $\delta_{5a}(\omega)$ models restrict the signal tracking [54].

Table 3. Single loop specifications (without loosing generality, $H(s) = 1$)

Specification	Application
$\lvert T_1(j\omega)\rvert = \left\lvert \frac{P(j\omega)K(j\omega)}{1+P(j\omega)K(j\omega)} \right\rvert \leq \delta_1(\omega)$	gain and phase margins; tracking bandwidth
$\lvert T_2(j\omega)\rvert = \left\lvert \frac{1}{1+P(j\omega)K(j\omega)} \right\rvert \leq \delta_2(\omega)$	Sensitivity reduction; rejection of disturbance at plant output
$\lvert T_3(j\omega)\rvert = \left\lvert \frac{P(j\omega)}{1+P(j\omega)K(j\omega)} \right\rvert \leq \delta_3(\omega)$	disturbance rejection at plant input
$\lvert T_4(j\omega)\rvert = \left\lvert \frac{K(j\omega)}{1+P(j\omega)K(j\omega)} \right\rvert \leq \delta_4(\omega)$	control effort minimization
$\delta_{5-lo}(\omega) \leq \left\lvert \frac{F(j\omega)P(j\omega)K(j\omega)}{1+P(j\omega)K(j\omega)} \right\rvert \leq \delta_{5-up}(\omega)$	Tracking problem

The specifications set is given by:

Stability specification The stability margins (gain margin and phase margin) are commonly used to calculate the degree of stability of a closed-loop system. A way to measure the stability is with M_c circles, which represent the locus of constant magnitude δ_1 of the closed-loop transfer function in the Nichols chart. As the M_c circles enclose $(0$ db,$-180)$ point, they are also related with the stability margins.

Equation (3.5) describes the M_c circle (δ_1) as a function of phase margin (PM), and equations (3.6) and (3.7) present PM and GM (gain margin) as a function of the M_c circles (δ_1), respectively.

$$\delta_1 = \frac{0.5}{\left[cos(\frac{\pi - PM}{2})\right]} \tag{3.5}$$

$$PM = \pi - 2cos^{-1}\left(\frac{0.5}{\delta_1}\right) \tag{3.6}$$

$$GM = 20\,log_{10}\left(1 + \frac{1}{\delta_1}\right) \tag{3.7}$$

In order to obtain a phase margin of 41.8 and a gain margin of 4.68dB for the solar plant model described in equation (3.1), $\delta_1 = 1.4$ is selected (see Figure 13).

Figure 13. Stability specification in the Nichols chart: $\delta_1 = 1.4$

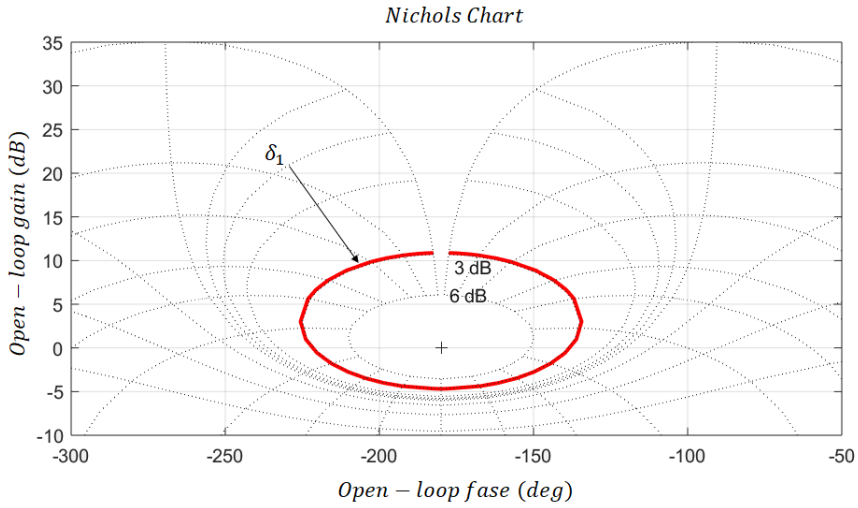

Disturbance rejection at plant output Unlike the stability, the sensitivity specification $\delta_2(\omega)$ is typically only define for selective low to middle frequencies. Due to this, the high frequency activity of the actuators is reduced and possible mechanical fatigue problems are avoided. A practical selection of $\delta_2(\omega)$ is shown in (3.8). The specification has also a slope of $-20dB/dec$ that reaches the $-3dB$ level at the frequency $\omega = a_d$, and has a 0 value for high frequency [41].

$$\delta_2(s) = \frac{s}{s + a_d} \tag{3.8}$$

Figure 14. Sensitivity or plant output disturbance rejection specification

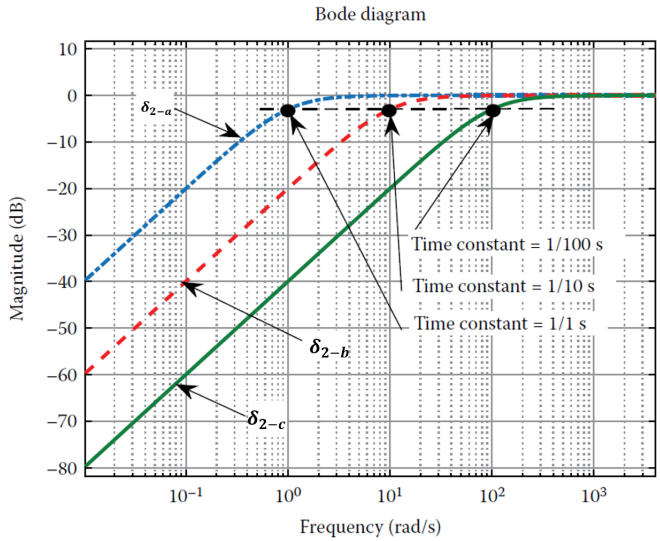

Sensitivity specification for different values of the parameter a_d -which is the inverse of the time constant- is presented in Figure 14. As can be seen, the expression gives a good disturbance rejection at low frequencies.

Figure 15 shows the time-domain response when a step disturbance is established in the plant for different levels of disturbance rejection. For large values of a_d, shorter rise times and settling times are obtained.

Figure 15. Step response for plant output disturbance

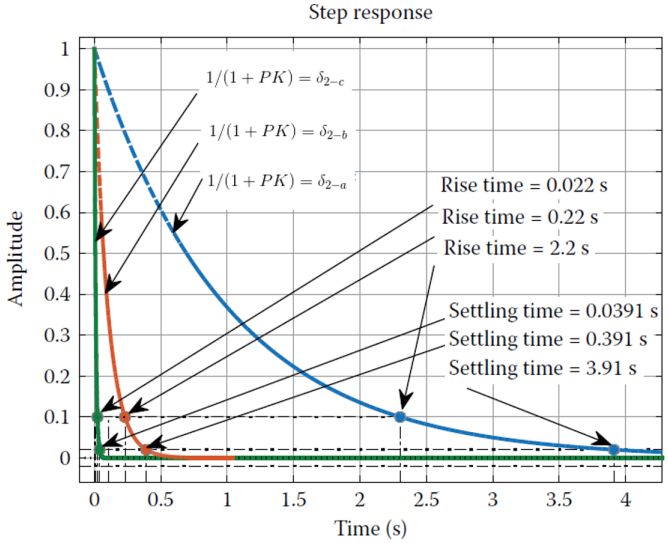

Reference tracking specification QFT methodology demands that the desired tracking control ratios be modeled in the frequency domain to accomplish the requi-

red gain and the desired time-domain performance specifications for a step input. Thus, the system's tracking performance specifications for a simple second-order system are based upon satisfying some or all of the step forcing function figures of merit for underdamped and overdamped responses [44].

In order to reduce the high frequency activity of the actuators and avoid possible mechanical fatigue problems, the reference tracking specifications are generally defined only for some low to mid frequencies. A practical choice is given by the following expressions:

$$\delta_{5-up}(s) = \frac{\omega_n^2/a(s+a)}{s^2 + 2\zeta\omega_n s + \omega_n^2} \tag{3.9}$$

$$\delta_{5-lo}(s) = \frac{1}{(\tau_1 s + 1)(\tau_2 s + 1)(\tau_3 s + 1)} \tag{3.10}$$

If, for example, a peak overshoot of 20 % and an establishment time close to 35min is desired for the solar collector system, the following transfer functions could be defined:

$$\delta_{5-up}(s) = \frac{0.002947s + 1.2 * 10^{-5}}{s^2 + 0.00381s + 1.2 * 10^{-5}} \tag{3.11a}$$

$$\delta_{5-lo}(s) = \frac{1}{1.8225 * 10^6 s^3 + 1.7212 * 10^5 s^2 + 740.11s + 1} \tag{3.11b}$$

Figure 16 shows the time response of $y(t)$ for both specifications. The variables $y(t)_U$ and $y(t)_L$ in the figure represent the upper and lower bounds, respectively, of the tracking performance specifications; that is, an admissible response $y(t)$ must lie between these bounds [54].

Figure 16. System time-domain tracking performance specifications.

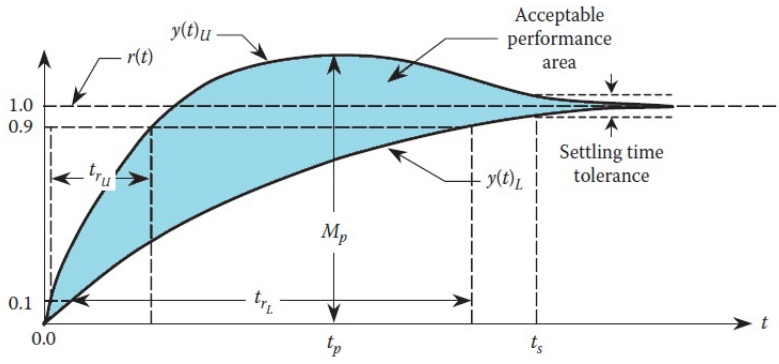

Computation of QFT bounds

Once the $P_0(j\omega)$ nominal plant has been selected, the QFT design methodology converts the closed-loop specifications - presented in Table 3 - and the uncertainty of the plant into a set of constraint curves or contours $B(j\omega)$ for each frequency of interest $j\omega_i \in \Omega$, drawn on the Nichols diagram.

Every plant in the ω_i-template can be expressed as $P(\omega_i) = pe^{j\theta} = p\angle\theta$. Similarly, the compensator polar form is $K(\omega_i) = ke^{j\phi} = k\angle\phi$, with $\phi \in [-2\pi, 0]$. By substituting the specifications in Table 3 the quadratic inequalities in Table 4 are obtained. The general form of these inequalities is given by the following expression:

$$I^m_{\omega_i} = (p, \theta, \delta_m, \phi) = ak^2 + bk + c \geq 0 \tag{3.12}$$

where p, θ y δ_m are known, ϕ varies between -2π and 0 rad, and k is unknown.

With an appropriate algorithm shown in [24], the quadratic inequalities in Table 4 are solved and translated into a set of curves on the Nichols chart for each frequency of interest and type of specification. These curves, known as bounds, can be solid or dashed lines. A solid line means that the area that satisfies the specification inequality is above the line, and a dashed line means that the area that satisfies the specification inequality is below the line [41].

After calculating and drawing the contours on the Nichols diagram, for each specification and at each frequency, these contours are intersected so that finally there is only one curve for each frequency: the most restrictive. Figure 17 shows both the union and the intersection of bounds computed for the tracking reference specifications described in (3.11a) and (3.11b), and stability specification fixed in δ_1 =1.4 for the solar plant model with uncertainty presented in (3.1).

Table 4. Quadratic inequalities

m	**Bound quadratic inequality**
1	$p^2\left[1-\frac{1}{\delta_1^2}\right]k^2 + 2p\,cos(\varphi+\theta)k + 1 \geq 0$
2	$p^2k^2 + 2p\,cos(\varphi+\theta)k + \left[1-\frac{1}{\delta_1^2}\right]$
3	$p^2k^2 + 2p\,cos(\varphi+\theta)k + \left[1-\frac{p^2}{\delta_3^2}\right]$
4	$\left[p^2-\frac{1}{\delta_4^2}\right]k^2 + 2p\,cos(\varphi+\theta)k + 1 \geq 0$
5	$p_e^2p_d^2\left[1-\frac{1}{\delta_5^2}\right]k^2 + 2p_ep_d\left[p_e\,cos(\varphi+\theta_d) - \frac{p_d}{\delta_5^2}cos(\varphi+\theta_e)\right]k + \left[p_e^2-\frac{p_d^2}{\delta_5^2}\right] \geq 0$

Figure 17. Bounds of two specifications: stability and tracking references

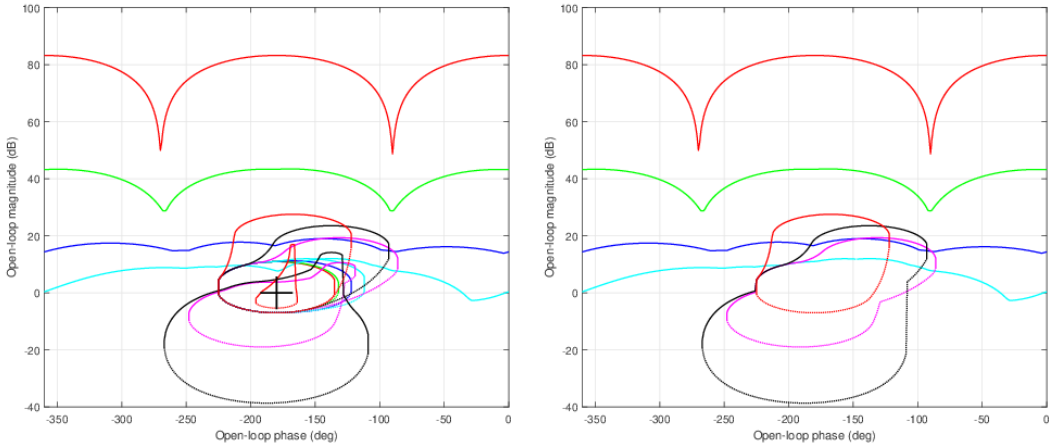

(a) Union of bounds (b) Intersection of bounds

Controller design

Once the contours are plotted in the Nichols diagram and the open loop function $L_0 = P_0 K$ is superimposed, the controller is designed including poles and zeros until all specifications in the frequency domain are met. This design process is known as *loop-shaping*.

As mentioned, the bounds define the uncertain plant model and the control specifications at each frequency. An robust controller is acquired if L_0 is exactly on top of the bounds at each frequency. In other words, a qualified controller design will place L_0 above the solid-line bounds and below the dashed-line bounds. This will provide the minimum possible controller magnitude at every frequency (minimum *cost of feedback*) to meet the required specifications with all the plants within the uncertainty [41].

A general expression for the controller structure $K(s)$ is the following transfer function:

$$K(s) = k_G \frac{\prod_{i=1}^{n_{rz}}(s/z_i + 1)\prod_{i=1}^{n_{cz}}(s^2/\omega_{ni}^2 + 2\zeta_i/\omega_{ni}s + 1)}{s^r \prod_{j=1}^{m_{rp}}(s/p_j + 1)\prod_{j=1}^{m_{cp}}(s^2/\omega_{nj}^2 + 2\zeta_j/\omega_{nj}s + 1)} \tag{3.13}$$

where k_G is the controller gain, p_j is a real pole, z_i is a real zero, ω_{ni} the natural frequency and ζ_i the damping of a complex zero, and ω_{nj} the natural frequency and ζ_j the damping of a complex pole. The controller may have also some integrators, with $r = 0, 1$ o 2, etc.

Looking at the intersection of bounds presented in Figure 17b a controller that meets these QFT bounds has been design, as shown in Figure 18. In this figure

Figure 18. Loop-shaping for solar plant

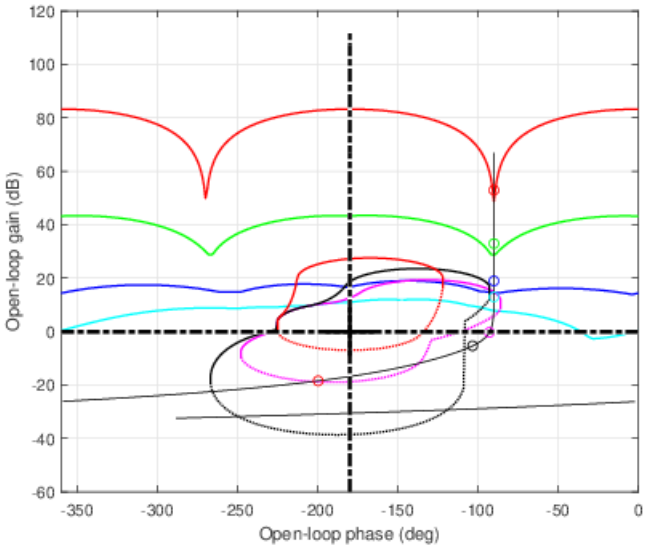

the small circles and numbers in the figure indicate the frequencies for the function $L_0(s) = P_0(s)K(s)$. The objective is to move each small circle above the solid-line bounds or below the dashed-line bounds. The proposed controller is given by the following expression:

$$K(s) = \frac{0.5555(s + 0.018)(s + 0.0077)}{s(s + 0.014)} \tag{3.14}$$

Synthetize Prefilter

Taking into account the controller $K(s)$ in eq. (3.14), and the reference tracking specifications given in equations (3.11a) and (3.11b), a prefilter $F(s)$ is designed to ensure that all the input/output functions $P(s)K(s)F(s)/[1 + P(s)K(s)]$ are inside the band defined by the limits $\delta_{5-up}(\omega)$ and $\delta_{5-lo}(\omega)$. Thus, while the basic objective of the $K(j\omega)$ controller is to reduce uncertainty and achieve stability and rejection of disturbance objectives, etc., the objective of the prefilter is to comply with the tracking specifications.

The prefilter for the solar plant described in eq. (3.1) is shown in the following expression and the input/output functions and limits in Figure 19:

$$F(s) = \frac{1}{150s + 1} \tag{3.15}$$

Figure 19. Prefilter $F(j\omega)$ for reference tracking specifications for solar plant

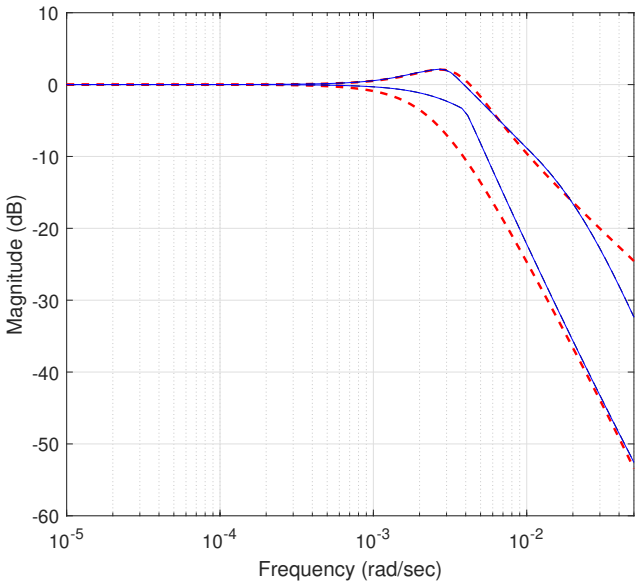

Analysis and Validation

Once the design of the controller and the filter is finished, its performance is analyzed against the given specifications, both in the time domain and in the frequency domain.

Figure 20 shows the analysis of the closed-loop stability in the frequency domain for the illustrative example of the solar plant. The red dashed line is the stability specification δ_1, defined in equation (4.30), and the solid line represents the worst case of the function $PK/(1+PK)$ at each frequency due to the model uncertainty.

3.2. Active Disturbance Rejection Control

The idea of feedback is deceptively simple and yet extremely powerful. Feedback can reduce the effects of disturbances, make the system robust to process variations, and ensure that it follows input signals appropriately. Feedback has also had a profound influence on technology. The feedback principle application has produced significant advances in the fields of control, communication, and instrumentation.

The PID controller is an easy realization of feedback. Such controllers are found in a large number of all industries and are presented in many different ways. They are a key element of motor control, very useful in distributed process control systems, and are also integrated into many special-purpose systems. It is estimated that in

Figure 20. Stability analysis for solar plant

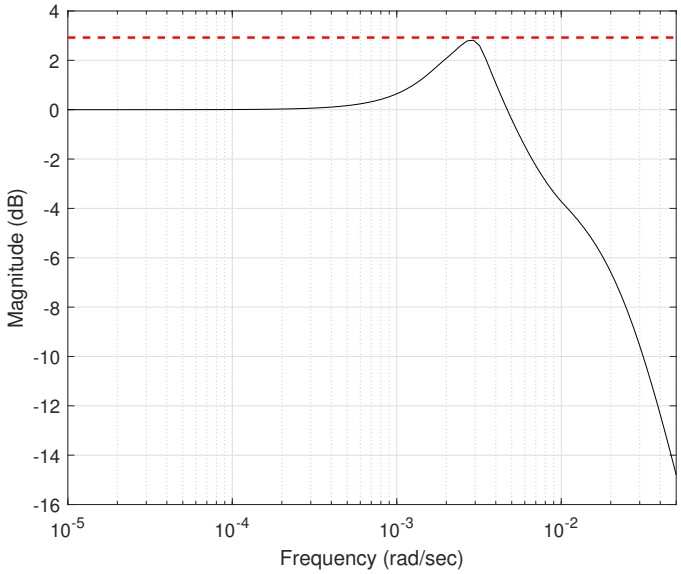

process control, more than 95 percent of control loops are of the PID type. Most ties are actually PI control [6].

However, it is well known that the PID is substantially burdened by the current demands of modern industry that, due to the search for efficiency and the cost of skilled labor, place much value on feedback control technologies. Despite the merit of its simplicity, some authors question whether PID control will temporarily outlive its usefulness and wonder what will replace this highly successful control mechanism while preserving its essential robustness and, at the same time, eliminating its restrictions [50].

Active Disturbance Rejection Control (ADRC) was one of the main research topics of the late Professor J. Han, which addressed the limitations of classical controllers. His vision of simplifying controller design via appropriate, simultaneous, state estimation and disturbance estimation, followed by disturbance cancellation and feedback, has proved to be a robust scheme embracing many fields of academic and industrial automatic control engineering. As a control design tool, it applies to linear and nonlinear, continuous and discrete, SISO and MIMO systems, Systems with delays at the inputs and systems described by fractional order time derivatives.

3.2.1. PID control limitations

Classical PID is a simultaneous feedback control mechanism widely used in industrial control systems, consisting of three different parameters: proportional, in-

Figure 21. PID control topology

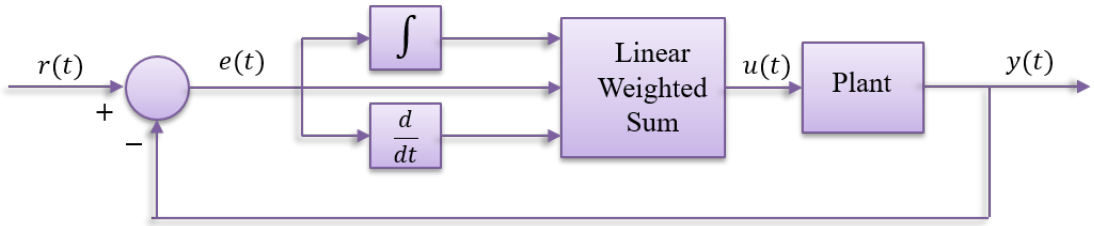

tegral, and derivative, as shown in Fig. 21, where the error between the setpoint y_{ref} =constant and plant $y(t)$, i.e., $e(t) = y_{ref} - y(t)$, as well as its integration $\int_0^t e(\tau)d\tau$ and differentiation $de(t)/dt$ are used in linear combination to provide the control law:

$$u(t) = k_p e(t) + k_i \int_0^t e(\tau)d\tau + k_d \frac{de(t)}{dt} \tag{3.16}$$

This PID controller has the capacity to remove errors in the steady state via integral action, and can predict the future with the derivative part. PI and PID controllers are necessary for many control problems, especially when the dynamics of the process are favorable and the behavioral requirements are not demanding [6].

Consider the second-order system whose transfer function is as follows:

$$\frac{y(s)}{u(s)} = \frac{k\omega_n^2}{s^2 + 2\zeta\omega_n s + \omega_n^2} \tag{3.17}$$

Let $e(t) = y_{ref} - y(t) = y_{ref} - x_1 = e_1$, $\dot{e}_1 = -\dot{x}_1 = e_2$, and $\ddot{e}(t) = -\ddot{x}_1$, and the error dynamics can be seen as

$$\begin{cases} \dot{e}_1(t) = e_2(t) \\ \dot{e}_2(t) = -\omega_n^2(e_1(t) - y_{ref}) - k\omega_n^2 u(t) - 2\zeta\omega_n e_2(t) \end{cases} \tag{3.18}$$

Denoting $e_0 = \int_0^t e(\tau)d\tau$, then $e = e_1 = \dot{e}_0$ and considering equation (3.16), the error equation can be written as:

$$\begin{aligned} \dot{e}_0 &= e_1 \\ \dot{e}_1 &= e_2 \\ \dot{e}_2 &= \omega_n^2 (y_{ref} - k_i k e_0) - \omega_n^2 (1 + k k_p) e_1 - \omega_n (k_d k \omega_n + 2\zeta) e_2 \end{aligned} \tag{3.19}$$

which is asymptotically stable if

$$\begin{cases} k_i k\omega_n^2 > 0, kk_p + 1 > 0, k_d k\omega_n^2 + 2\zeta\omega_n > 0 \\ \omega_n (kk_p + 1)(k_d k\omega_n + 2\zeta) > kk_i \end{cases} \tag{3.20}$$

The design goal $e_1 = e(t) = y_{ref} - y \to 0$, or $x_1 \to y_{ref}$, is achieved if the gains k_i,k_p and k_d are chosen to fulfill (3.20), for the values ζ, ω_n, $k \neq 0$ selected. Although for many plants of the form of (3.17), a collection of PID gains could be readily selected (either analytically or experimentally). Precisely said ease of adjustment and simplicity denote its fundamental restrictions, which are visible in the existence of progressively demanding control system performance [50].

In general, in the PID controller framework, four fundamental points must be handled. 1) PID is often implemented without part D due to noise sensitivity. 2) The integral expression, although to suppress the steady-state error, presents other problems such as saturation and reduced stability margin. 3) The reference signal is commonly a step function, which is not suitable for most dynamic systems as it is equivalent to requiring the control signal to perform a sudden jump.4) Although the weighted sum of the three terms in (3.16) is simple, it might not be the best control law based on the present and past of the error and its exchange rate [50].

3.2.2. Differential flatness

The differential flatness is derived from the algebraic differential approach as proposed by Fliess et al in 1995 [34]. This is a property of some controlled dynamic systems whose trajectories can be planned without solving differential equations and where the feedback controller design problem can be reduced to a set of decoupled LTI systems [108]. It can be found in continuous- and discrete-time systems, linear and nonlinear systems, finite-dimensional, single and multivariable systems, and even infinite-dimensional systems.

Consider the nonlinear system of the form:

$$\dot{x} = f(x,u), \quad y = h(x,u), \quad x \in \mathbb{R}^n, \quad u \in \mathbb{R}^m, \quad y \in \mathbb{R}^p \tag{3.21}$$

Let γ, α, β be finite multi-indices. System (3.21) is differentially flat if a vector known as the group of flat outputs exist, with dimension equal to the number of inputs:

$$z = \phi(x, \dot{x}, \cdots, x^{(\gamma)}) \epsilon\, \mathbb{R}^m \tag{3.22}$$

The components of these variables are differentially independent, so there are functions ψ and θ such that:

$$x = \psi(z, \dot{z}, \cdots, z^{(\alpha)}), \;\; u = \theta(z, \dot{z}, \cdots, z^{(\beta)}) \tag{3.23}$$

Flatness connotes that all variables in the system (inputs, outputs and states) can be differentially characterized according to the components of a vector z that is a combination of the state variables and a finite number of their time derivatives. Normally, the set of flat outputs is not unique [111].

On the other hand, to introduce the representation of flat systems in the multivariable linear case (MIMO), consider the linear time-invariant system:

$$\dot{x} = Ax + Bu, \quad x \in \mathbb{R}^n, \quad u \in \mathbb{R}^m \tag{3.24}$$

with $B = [b_1, b_2, ..., b_m] \ \in \mathbb{R}^{n \times m}$.

The Kalman controllability matrix is defined by the following non-square $n \times nm$ matrix:

$$\mathcal{K} = \left[B; AB; A^2B; \dots ; A^{n-1}B\right] \tag{3.25}$$

A system (A, B) is controllable whenever rank$(\mathcal{K}) = n$. If the system is controllable outside the matrix $\mathcal{K}$ a set of n linearly independent column vectors can always be extracted to form the controllability matrix $\mathcal{K}_c$. It can be assumed that the n-column full-rank controllability matrix $\mathcal{K}$ is of the form:

$$\mathcal{K}_c = \left[b_1; Ab_1; \cdots ; A^{\gamma_1 - 1}b_1; b_2; Ab_2; \cdots ; A^{\gamma_2 - 1}b_2; \cdots ; b_m; Ab_m; \cdots ; A^{\gamma_m - 1}b_m\right] \tag{3.26}$$

where the set of integers $\gamma_1, ..., \gamma_m$ are the *Kronecker controllability indices* of the inputs and they satisfy $\sum_{j=1}^{m} \gamma_j = m$.

The state coordinate transformation $z = \mathcal{K}_c^{-1}x$ leads to a system of the following form:

$$\dot{z} = Fz + Gu \tag{3.27}$$

where $F = \mathcal{K}_c^{-1}A\mathcal{K}_c$ and $G = \mathcal{K}_c^{-1}B$

The flat outputs are defined by the following expression:

$$Z = \left[\phi_1, \phi_2, \dots, \phi_m\right]^T z = \begin{bmatrix} \phi_1 \\ \phi_2 \\ \vdots \\ \phi_m \end{bmatrix} \kappa_c^{-1} x \tag{3.28}$$

with ϕ_j, $j = 1, 2, ..., m$, is of the form:

$$\phi_j = [\overbrace{0, \dots, 0}^{\gamma_1}, \underbrace{0, \dots, 0, 1}_{\gamma_j}, 0, \dots, 0] \tag{3.29}$$

where the 1 occupies the position $\sum_{i=1}^{j} \gamma_i$ in the n-dimensional row vector.

3.2.3. Extended state observers

ADRC based on observers is then introduced by examining, in an introductory manner, a small illustration that will also be useful for the desired generalization. Consider the following flat disturbed system:

$$\dot{y}(t) = u(t) + \xi(t) \tag{3.30}$$

where $\xi(t)$ is a uniformly completely bounded disturbance with, in addition, a uniformly completely limited first-order time derivative $\dot{\xi}(t)$ [111]. Consequently, let consider the presence of finite constants α_0 and α_1 such that:

$$\sup_t |\xi(t)| \leq \alpha_0, \quad \sup_t |\dot{\xi}(t)| \leq \alpha_1 \tag{3.31}$$

Regard, for $\lambda > 0$, the consequent disturbance observer for the first-order system:

$$\dot{\hat{y}} = u + z + \lambda (y - \hat{y}) \tag{3.32}$$

where z is an secondary variable to be defined based on the stability of the output estimation error and the perturbation prediction error, described by $\eta(t) = \xi(t) - z(t)$. The output prediction error $e_s(t) = y(t) - \hat{y}(t)$, then advance in accordance with:

$$\dot{e}_s = -\lambda e_s + \xi(t) - z = -\lambda e_s + \eta \tag{3.33}$$

Let ρ be a rigidly positive constant quantity. Regard the subsequent positive definite Lyapunov function candidate in the (e_s, η) space:

$$V(e_s, \eta) = \frac{1}{2} e_s^2(t) + \frac{1}{2\rho} \eta^2(t) \tag{3.34}$$

The time derivative of the function $V(e_s, \eta)$ associated with the estimation error dynamics has the following composition:

$$\begin{aligned} \dot{V}(t) &= e_s(t)\dot{e}_s(t) + \frac{1}{\rho}\eta(t)\dot{\eta}(t) \\ &= -\lambda e_s^2 + \eta e_s + \frac{1}{\rho}\eta(\dot{\xi} - \dot{z}) \\ &= -\lambda e_s^2 + \eta \left[e_s + \frac{1}{\rho}(\dot{\xi} - \dot{z}) \right] \end{aligned} \tag{3.35}$$

It can be noted that the alternative

$$\dot{z}(t) = \dot{\xi}(t) + \rho e_s(t) \tag{3.36}$$

guides to the negative semi-definite time derivative of function V, i.e., $\dot{V} = -\lambda e_s^2 \leq 0$. The observer paths asymptotically concur with $e_s(t) = 0$ and to $\eta(t) = z(t) - \xi(t) = 0$. Based on these conditions, the prediction error dynamics fulfills the asymptotically exponentially stable dynamics:

$$\ddot{e}_s = -\lambda \dot{e}_s - \rho e_s \tag{3.37}$$

However, since $\xi(t)$ is unknown, dynamics selected in advance for z, is unrealizable. For this reason, the following remodeled proposal for the dynamics of z is proposed:

$$\dot{z} = \rho e_s = \rho(y - \hat{y}) \tag{3.38}$$

In this case, the following observer is available for the perturbed system:

$$\begin{cases} \dot{\hat{y}}(t) = u(t) + z(t) + \lambda \left(y(t) - \hat{y}(t)\right) \\ \dot{z}(t) = \rho \left(y(t) - \hat{y}(t)\right) \end{cases} \tag{3.39}$$

This observer is commonly called the Extended State Observer (ESO) and the error estimate fulfills the following exogenous dynamics:

$$\begin{cases} \dot{e}_s(t) = \xi(t) + z(t) + \lambda e_s(t) \\ \dot{z}(t) = \rho e_s(t) \end{cases} \tag{3.40}$$

i.e.,

$$\ddot{e}_s + \lambda \dot{e}_s + \rho e_s = \dot{\xi}(t) \tag{3.41}$$

The prediction error dynamics is a disturbed linear system that will be globally asymptotically exponentially stable as long as the constants ρ and λ are selected to be rigidly positive. Suppose ϵ is a small and rigidly positive parameter employed in a singular disturbance approach to analyze the stability of the high-gain prediction error system. Let ρ and λ be as follows [111]:

$$\lambda = \frac{2\zeta\omega_n}{\epsilon}, \quad \rho = \frac{\omega_n^2}{\epsilon^2} \tag{3.42}$$

where are the natural frequency and the damping ratio desired in closed-loop. The choice of these parameters establishes that the injected dynamics to be:

$$\ddot{e} + \left(\frac{2\zeta\omega_n}{\epsilon}\right)\dot{e} + \left(\frac{\omega_n^2}{\epsilon^2}\right)e = \dot{\xi}(t) \tag{3.43}$$

In terms of a Lyapunov stability analysis, a Lyapunov function candidate $V(e_s, \eta)$ is prescribed as defined in (3.34). Considering the z dynamics in (3.40), the subsequent time derivative for V along the exogenous dynamics is obtained:

$$\begin{aligned} \dot{V} &= -\lambda e^2 + \frac{(\xi(t) - z)\dot{\xi}(t)}{\rho} \leq -\lambda e^2 + \frac{|(\xi - z)| \left|\dot{\xi}(t)\right|}{\rho} \\ &\leq -\lambda e^2 + \frac{|(\xi - z)| \alpha_1}{\rho} \end{aligned} \tag{3.44}$$

This expression guides the semi-definite time derivative of function V to be negative, therefore, the observer paths asymptotically converge to $e_s(t) = 0$ and to $\eta(t) = z(t) - \xi(t) = 0$ [111].

3.2.4. Generalities on GPI observers

GPI control, or control based on *integral reconstructors*, is a new advancement in the literature about automatic control. This method proposes the structural reconstruction of the state from inputs and outputs, modulates the effect of initial conditions and modulates the effect of classical disturbances: that is, constant, ramp, parabolic disturbances. As a result of these errors and due to the principle of superposition, the integral error compensation completes the stable feedback design [112].

Consider the perturbed system (3.30) next to the following uniform absolute boundedness supposition concerning to the second-order time derivative of the disturbance input:

$$\sup_t |\xi(t)| \leq \alpha_0, \quad \sup_t |\dot{\xi}(t)| \leq \alpha_1 \tag{3.45}$$

An extended observer for the disturbed first-order system may be the following:

$$\dot{y}_0 = y_1(t) \tag{3.46}$$

where $e_0 = y - y_0$ is the observation error of the output whose perturbed linear dynamics is given by:

$$\frac{d^3 e_0}{dt^3} + \lambda_2 \frac{d^2 e_0}{dt^2} + \lambda_1 \frac{de_0}{dt} + \lambda_0 e_0 = \frac{d^2 \xi(t)}{dt^2} \tag{3.47}$$

The selection of the observer design parameter set can be established according to the characteristic polynomial of a required asymptotically exponentially stable prediction error dynamics ([111]). For appropriate rigorously positive values p, ω_n and ζ, said polynomial can have the following form:

$$p_{cl}(s) = (\epsilon s + p)\left(\epsilon^2 s^2 + 2\zeta\omega_n \epsilon s + \omega_n^2\right) = 0 \tag{3.48}$$

Hence, the observer parameters can be selected as follows:

$$\lambda_2 = \frac{p + 2\xi\omega_n}{\epsilon},\ \ \lambda_1 = \frac{2\xi\omega_n p + \omega_n^2}{\epsilon^2},\ \ \lambda_0 = \frac{\omega_n^2 p}{\epsilon^3} \tag{3.49}$$

Using the expression (3.46) the corresponding estimation error dynamics for e_0 is given by:

$$\dot{e_0} = -\lambda_2 e_0 - \lambda_1 \int_0^t e_0(\sigma_1)d\sigma_1 - \lambda_0 \int_0^t \int_0^{\sigma_1} e_0(\sigma_2)d\sigma_2 d\sigma_1 + \xi(t) \tag{3.50}$$

Regardless of the system order, there is the option of expanding the typical observer using a suitable linear combination of estimation error integrators. This fact results in the probability of predicting some number of time derivatives of the perturbation signal [111].

Example Consider the following mathematical model of the two tank system in Fig. 22:

$$\begin{aligned} \dot{x}_1 &= -\tfrac{c}{A}\sqrt{x_1} + \tfrac{1}{A}u \\ \dot{x}_2 &= -\tfrac{c}{A}\sqrt{x_2} + \tfrac{c}{A}\sqrt{x_1} \\ y &= x_2 \end{aligned} \tag{3.51}$$

Regulating the output $y(t)$ of the system is desired, so that it tracks a given smooth trajectory $y_{ref}(t)$. System parameters A and c are assumed to be known.

The two tank system admits the following input-output model:

$$\ddot{y} = \frac{1}{2A}\left[\frac{c^2/A^2}{\dot{y} + \frac{c}{A}\sqrt{y}}\right]u - \frac{c}{2A}\frac{\dot{y}}{\sqrt{y}} - \frac{c^2}{2A^2} \tag{3.52}$$

Consider the following simplified system with a nonlinear input gain:

$$\ddot{y} = \frac{1}{2A}\left[\frac{c^2/A^2}{\dot{y} + \frac{c}{A}\sqrt{y}}\right]u + \xi(t) \tag{3.53}$$

where:

$$\xi(t) = -\frac{c}{2A}\frac{\dot{y}(t)}{\sqrt{y(t)}} - \frac{c^2}{2A^2} \tag{3.54}$$

Figure 22. A two tank system

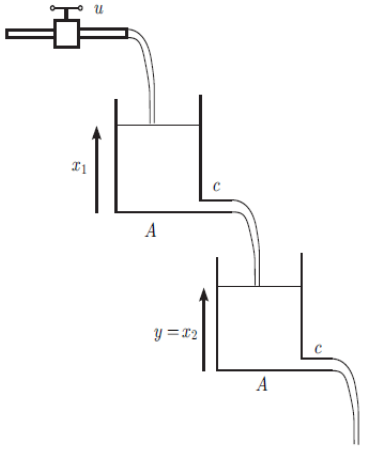

For the disturbed system defined in eq. (3.52) the following nonlinear control law is proposed:

$$u = 2A\frac{A^2}{c^2}\left(y_1 + \frac{c}{A}\sqrt{y}\right)v \tag{3.55}$$

$$v = -\hat{\xi}(t) + \ddot{y}_{ref}(t) - 2\zeta_c\omega_{nc}\left(y_1 - \dot{y}_{ref}(t)\right) - \omega_{nc}^2(y - y_{ref}(t)) \tag{3.56}$$

where y_1 is the estimated output velocity which is synthesized by the following GPI observer:

$$\begin{aligned}
\dot{y}_0 &= y_1 + \lambda_5(y - y_0)\\
\dot{y}_1 &= \tfrac{1}{2A}\left[\tfrac{c^2/A^2}{y_1 + \frac{c}{a}\sqrt{y}}\right]u + z_1 + \lambda_4(y - y_0)\\
\dot{z}_1 &= z_2 + \lambda_3(y - y_0)\\
\dot{z}_2 &= z_3 + \lambda_2(y - y_0)\\
\dot{z}_3 &= z_4 + \lambda_1(y - y_0)\\
\dot{z}_4 &= \lambda_0(y - y_0),\\
\hat{\xi}(t) &= z_1
\end{aligned} \tag{3.57}$$

The coefficients $\{\lambda_0, \lambda_1, \ldots, \lambda_5\}$ are chosen in accordance with the well known rule of equating the closed loop characteristic polynomial of the system to one with roots conveniently situated in the left half of the complex plane. One way to select these parameters is through the definition of the following characteristic equation for the estimation error:

$$p_{obs}(s) = \left(s^2 + 2\zeta_o\omega_{no}s + \omega_{no}^2\right)^3 = 0 \tag{3.58}$$

In other words:

$$\begin{cases} \lambda_0 = \omega_{no}^6, \quad \lambda_1 = 6\zeta_o\omega_{no}^5, \quad \lambda_2 = 3\omega_{no}^4\left(1+4\zeta_o^2\right) \\ \lambda_3 = 4\omega_{no}^3\zeta_o\left(3+2\zeta_o^2\right), \quad \lambda_4 = 3\omega_{no}^2\left(1+4\zeta_o^2\right), \quad \lambda_5 = 6\zeta_o\omega_{no} \end{cases} \tag{3.59}$$

In Fig. 23 the response of ADRC controlled two tank system is presented. As can be seen the controlled system quickly follows the set level reference. The parameters of the plant are given by $c = 1.2\ m^{2.5}/s$, $A = 4\ m^2$, the parameter of the controller are $\zeta = 1.5$ and $\omega_n = 5\ rad/s$, and the observer parameters are $\zeta_o = 2$ and $\omega_{no} = 40\ rad/s$. The block diagram in Simulink is presented in Figure 24.

Figure 23. Output trajectory tracking for ADRC controlled two tank system

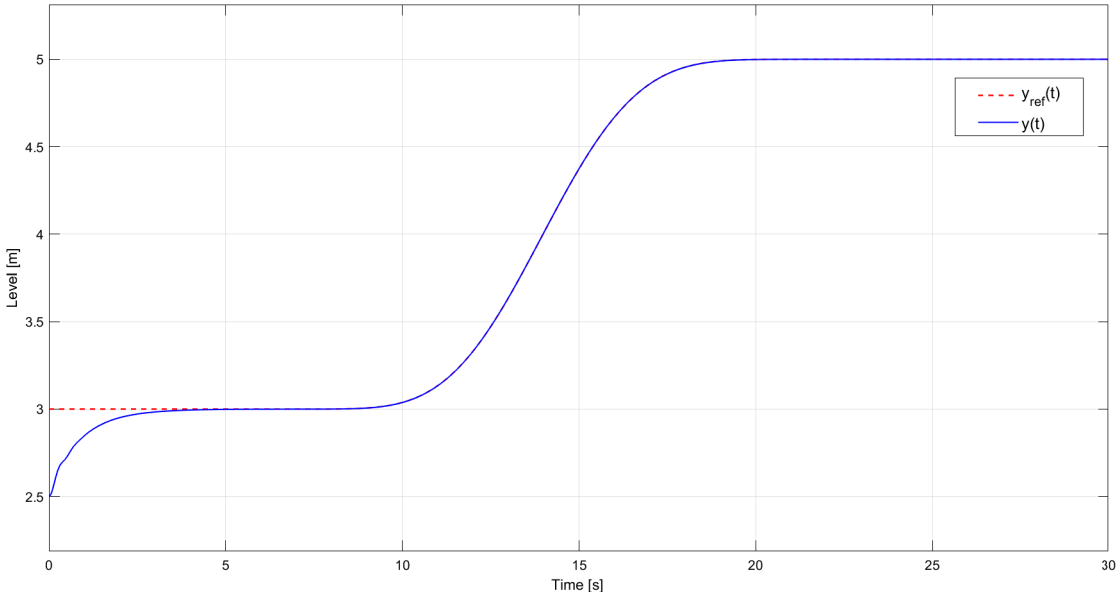

Figure 24. Block diagram in Simulink

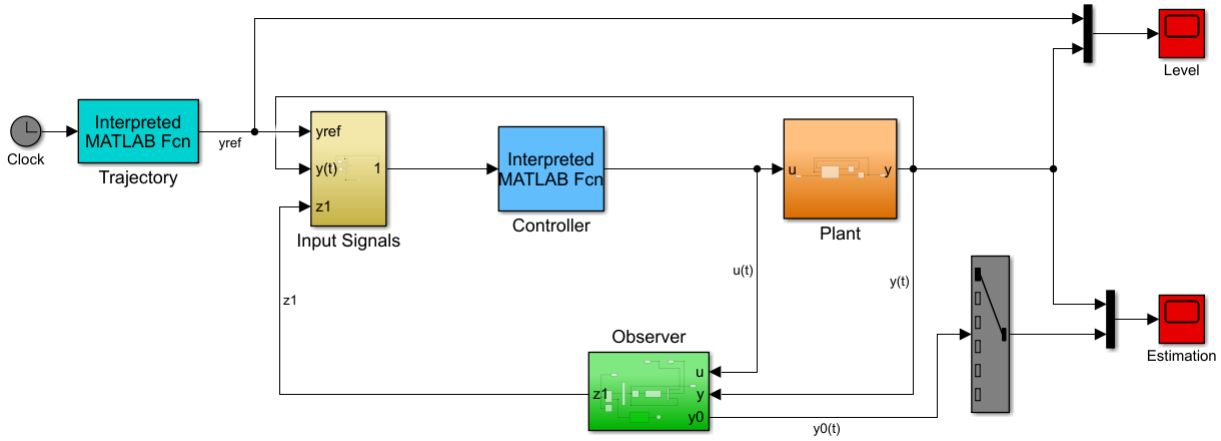

Program codes The code corresponding to the disturbance observer is presented below:

function Yh=Observador(u) ux=u(1); y0=u(2);
y0h=u(3); y1h=u(4);
z1=u(5); z2=u(6);
z3=u(7); z4=u(8);

%Parameters
c=1.2; A=4; zo=2; wno=40;
lam5=(6*zo*wno);
lam4=(12*wno$^2 * zo^2 + 3 * wno^2$);
$lam3 = (8 * wno^3 * zo^3 + 12 * wno^3 * zo)$;
$lam2 = (12 * wno^4 * zo^2 + 3 * wno^4)$;
$lam1 = 6 * wno^5 * zo$;
$lam0 = wno^6$;

%Observer
Yh(1,1)=y1h+lam5*(y0-y0h);
Yh(2,1)=c$^2/(2 * A^3) * ux/(y1h + c/A * sqrt(y0)) + z1 + lam4 * (y0 - y0h)$;
$Yh(3,1) = z2 + lam3 * (y0 - y0h)$;
$Yh(4,1) = z3 + lam2 * (y0 - y0h)$;
$Yh(5,1) = z4 + lam1 * (y0 - y0h)$;
$Yh(6,1) = lam0 * (y0 - y0h)$;

The program code of the control law is the following:

```
function uc=controlADRC(u)
c=1.2; A=4;wn=5; zi=1.5;

y0=u(1); yp=u(2); yr=u(3);
yrp=u(4); yrpp=u(5); z1=u(6);

%Control law
uc=2*A^3/c^2*(yp+c/A*sqrt(y0))*...
(-z1+yrpp+2*zi*wn*(yrp-yp)+wn^2*(yr-y0));
```

The program code for the trajectory path is the following:

```
function Fs=trayectoria(u)
t=u(1); a=0.275; b1=0.29;
b=0.33; eps=b/a;

t1=6; t2=23;
delt=t2-t1;
tdif = abs(t-t1);

z1in = 3;
z1f =5; z1dif = z1f-z1in;

tau=(tdif/delt);
tau2=tau*tau;
tau3=tau*tau2;
tau4=tau*tau3;
tau5=tau*tau4;
tau6=tau*tau5;
tau7=tau*tau6;
tau8=tau*tau7;
tau9=tau*tau8;

r1=12870;
r2=91520;
r3=288288;
r4=524160;
r5=600600;
r6=443520;
r7=205920;
r8=54912;
r9=6435;
```

```
z1st1 = z1in;
fr=r1-r2*tau+r3*tau2-r4*tau3+r5*tau4-r6*tau5+r7*tau6-r8*tau7+r9*tau8;
z1stt = z1in+z1dif*tau8*fr;
z1st2 = z1f;

if (t <= t1)
Fs=z1st1;
end

if (t > t1  t <= t2)
Fs=z1stt;
end

if (t > t2)

Fs=z1st2;
end
```

4. ROBUST CONTROL APPROACH

4.1. Introduction

Most of the controller design methodologies that exist are based on the mathematical description of the dynamics of the plant. Nevertheless, several physical systems in the real world are nonlinear, time-variant, and considerably uncertain, so precise numerical models of physical plants are generally unavailable in process control. A solution to this problem is the robust control, which allows to guarantee robust stability and robust behavior in the presence of bounded disturbances and uncertainties in the model.

Several approaches for robust stability and robust control design problems have been developed, however some of these methods are too conservative. Some works have solved H_∞ continuous and discrete time control problems through basic procedures in LMI. In [39], for example, a parameterization of two LMI-based all suboptimal H_∞ controllers was provided. Although this study was founded on Lyapunov's quadratic equations for stability and performance analysis, the controllers designed could be excessively conservative and difficult to implement in real plants [40].

Model uncertainty makes much more difficult the controller design, since specifications not only for a single plant with fixed parameters, but for each and every one of the plants within the uncertainty, must be accomplished. The independent study of a control solution for each plant within the uncertainty, that is the brute-force solution, is very time consuming or even impossible. To deal simultaneously with not just one, but many performance specifications at the same time, including stability, reference tracking, disturbance rejection, actuator limitations, reduction of vibrations, noise rejection, etc., for uncertain systems, Quantitative Feedback Theory (QFT) can be a powerful robust control design tool [41].

In situations where the disturbance can be measured, a feedforward block could add to mitigate or suppress the effect of the disturbance. Nevertheless, in processes where external disturbances cannot measure in a direct line, an active disturbance rejection control (ADRC) can be used. This method requires the least amount of information from the plant, tolerating the uncertainty in the model. The mixed effect of both external disturbances and unmodeled dynamics is dealt with as a secondary state, predicted by using an additional dimension represented for a Luenbergeer-type state observer [21, 23, 111]. Once the total perturbation is predicted, it can

Figure 25. Disturbance observer based control scheme

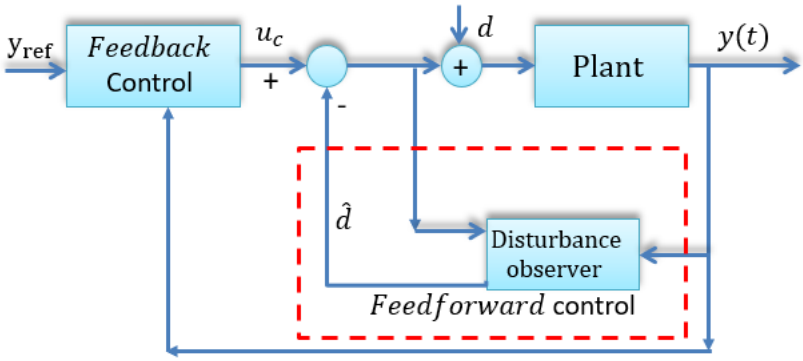

cancel out in the control law, reducing a complex non-linear control problem in a single linear invariant time.

One class of observers for active rejection of disturbances are the GPI observers, which naturally act as extended state observers and are an extension of these. These GPI observers are capable of on-line estimating a finite number of time derivatives of the disturbance input. The design consists of the incorporation of output error integral injections to cancel the effects of state-dependent and exogenous disturbance input signals, altering the plant's dynamics [111].

This chapter presents the control scheme proposed in this thesis for uncertain systems with and without time delay. As can be seen in Fig. 25, the design consists of combining feedforward and robust feedback controllers. The feedback control is employed for tracking and stabilizing the uncertain plant. The disturbances are compensated by a feedforward control where an extended observer estimates such disturbances.

First, the feedforward controller is designed, which consists of tuning parameters of the disturbance observer. Next, the robust feedback controller is designed for the equivalent plant (uncertain plant plus feedforward controller).

4.2. Feedforward Controller Design

A natural conception to deal with the problem of non-measurable disturbances is to estimate the perturbation from accessible variables, and then a suitable control signal is applied based on the estimation. This notion could be instinctively extended to deal the uncertainty as part of the disturbance [25].

In this dissertation, the use of GPI observers is proposed due to their robust phase variable regeneration feature and high-gain based perturbation estimation, in

addition to the prediction of a finite number of perturbation input time derivatives. This approach results in properties of mitigation or disturbance rejection and provides trajectory tracking, robust performance and output stabilization [107].

Consider a single-input single-output linear system, described by the subsequent frequency domain expression:

$$y(s) = P_r(s)\left[u(s) + d(s)\right] \tag{4.1}$$

where $u(s)$ is the input signal, $y(s)$ the controlled variable, $d(s)$ the external perturbation, and $P_r(s)$ the real plant.

Fig. 26 presents the blocks diagram for the disturbance observer, in the frequency domain, for system described by (4.1), where $Q(s)$ is the disturbance filter.

Figure 26. Blocks diagram of disturbance observer

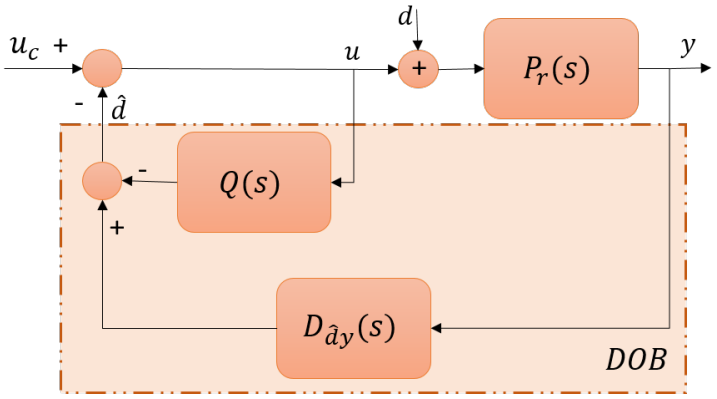

The transfer function of the equivalent plant with input $u_c(t)$ and output $y(t)$:

$$P_{eq}(s) = \frac{P_r(s)}{1 - Q(s) + D_{\hat{d}y}(s)P_r(s)} \tag{4.2}$$

In order to achieve that $P_{eq}(s) \approx P_r(s)$ it must be guaranteed that:

$$D_{\hat{d}y}(s) = Q(s)P_n^{-1}(s) \tag{4.3}$$

where, $P_n(s)$ is the nominal plant.

In this way, the transfer function is described as follows:

$$P_{eq}(s) = \frac{P_r(s)}{1 - Q(s)\left(1 - \frac{P_r(s)}{P_n(s)}\right)} \tag{4.4}$$

In order to show how the observer estimates the disturbances (external and internal), consider the estimated disturbance signal:

$$\hat{d}(s) = D_{\hat{dy}}(s)y(s) - Q(s)u(s) \tag{4.5}$$

By substituting (4.1) and (4.3) in (4.5), it is obtained that:

$$\hat{d}(s) = d(s)QP_rP_n^{-1} - Q\left[\left(1 - P_rP_n^{-1}\right)u(s)\right] \tag{4.6}$$

When $\lim_{s\to 0} Q(s)\left[\left(1 - P_rP_n^{-1}\right)u(s)\right] \approx 0$, the disturbance estimation error can be approximated as:

$$e_d(s) = \hat{d}(s) - d(s) \approx d(s)(Q(s) - 1) \tag{4.7}$$

The disturbance estimation error $e_d(s)$ will trend to zero as time goes to infinity, if the filter $Q(s)$ is selected as a low-pass form: that is, $\lim_{s\to 0} Q(s) = 1$.

The design of the $Q(s)$ filter has an important function in the observer design. To optimally predictive the effect of the disturbance, the filter $Q(s)$ should be unity gain over a frequency range. However, this fact could increase sensor noise and also make it impossible to implement the observer due to the inverse of the nominal plant $P_r(s)$ is required. Typically, the filter $Q(s)$ is designed in such a way that the degree of the denominator of the transfer function is greater than the degree of the nominal plant in order to ensure that the transfer function $D_{\hat{dy}}(s)$ is implementable. The selection of a pass filter is since the perturbation $\hat{d}(t)$ is usually low or medium, while the noise of the sensors is of medium or high frequency. Thus, the observer could predict the perturbation in a low and medium frequency range while also filtering out the high-frequency measurement noise.

4.2.1. Disturbance rejection of linear systems

As mentioned above, the Generalized Proportional Integral (GPI) observers were introduced by Sira-Ramirez and Feliu-Batlle in the framework of sliding-mode observers to be applied in the online detection of obstacles in the operation of flexible robots [110]. The great advantage of employing this type of observers is to use a design that inherently introduces iterated output error integral injections to attenuate the influence on the prediction error of external and state-dependent disturbance input signals actuating on the dynamics of the process [111].

Consider the n-dimensional flat system:

$$y^{(n)} = K(t,y)u + \psi(t) \tag{4.8}$$

where $K(t,y)$ is known, evenly bounded and far from zero, and the function $\psi(t)$ which is unknown and is uniformly absolutely bounded, as well as each of its temporal derivatives to a finite order m. Lets consider the following observer of grade $n+m$:

$$\begin{aligned}
\dot{y}_0 &= y_1 + \lambda_{m+n-1}(y - y_0) \\
\dot{y}_j &= y_{j+1} + \lambda_{m+n-j-1}(y - y_0), \\
&\quad j = 1, ..., n-2 \\
\dot{y}_{n-1} &= K_n u + z_1 + \lambda_m (y - y_0) \\
\dot{z}_l &= z_{l+1} + \lambda_{m-l}(y - y_0), \quad l = 1, 2, ..., m-1 \\
\dot{z}_m &= \lambda_0 (y - y_0)
\end{aligned} \tag{4.9}$$

where the transfer function of the disturbance filter is given by the following expression:

$$Q(s) = \frac{z_1(s)}{u(s)} = \frac{\lambda_{m-1}s^{m-1} + \lambda_{m-2}s^{m-2} + ... + \lambda_0}{s^{n+m} + \lambda_{n+m-1}s^{n+m-1} + ... + \lambda_0} \tag{4.10}$$

This observer is commonly called as Generalized Proportional Integral (GPI) and the disturbance estimation error can be reduced as small as desired if the observer gain parameters $\{\lambda_0, ..., \lambda_{m+n-1}\}$ are appropriately selected. This causes the estimation error of the time-varying disturbance to be confined to a sufficiently small neighborhood around the origin of the phase space of such estimation error.

The coefficients λ_j are selected such that the following polynomial in the complex variable *s*, is Hurwitz:

$$p_{obs}(s) = s^{m+n} + \lambda_{m+n-1}s^{m+n-1} + ... + \lambda_0 = 0 \tag{4.11}$$

The GPI observer is a generalized description of ESO since, by setting $m = 1$, the GPI is reduced by a linear ESO. For this reason, the GPI will provide greater accuracy of estimation in the presence of polynomial time series disturbances, that is, higher order time-varying disturbances. This type of observer achieves a more accurate disturbance estimate since, due to the integral chain, more information from the perturbation is used in the observer design. In other words, the internal model of

the perturbation is inherently incorporated into the observer for the prediction of the disturbance [25].

There are multiple ways to select the GPI observer parameters. By using the methodology proposed by [63], in order to mitigate typical peaking effects in high gain observers, the coefficient λ_0 can be chosen as:

$$\lambda_0 = \frac{T\alpha_0}{\lambda_{n+m}} \tag{4.12}$$

where α_0 is an arbitrary and strictly positive constant and the term $T > 0$ is known as the desired settling time or generalized time constant. The parameters $\lambda_0, \lambda_1 ... \lambda_{n+m}$ are determined by:

$$\lambda_i = \frac{T^i \alpha_0}{\alpha_{i-1}\alpha_{i-2}^2\alpha_{i-3}^3 ... \alpha_1^{i-1}\lambda_{n+m}}, i = 1, ..., n+m-1 \tag{4.13}$$

$$\lambda_{n+m} = \frac{T^{n+m}\alpha_0}{\alpha_{n+m-1}\alpha_{n+m-2}^2\alpha_{n+m-3}^3 ... \alpha_1^{n+m-1}} \tag{4.14}$$

From the above expressions, α_1 is the desired damping factor of the observer and it must be an adjustable constant parameter greater than 2. [63] proposes to calculate the remaining α_k coefficients by:

$$\alpha_k = \alpha_1 \frac{\sin\left(\frac{k\pi}{n+m}\right) + \sin\left(\frac{\pi}{n+m}\right)}{2\sin\left(\frac{k\pi}{n+m}\right)}, k = 2, ..., n+m-1 \tag{4.15}$$

4.2.2. Disturbance rejection of time-delay systems

One of the main problems of classic controllers is their behavior against plants with a considerable delay. Such delays may be due to the time spent in sensing, transmitting over large distances, calculating or sending the control law to the entrance of the plant or even because parts of the process require covering certain distances at finite speeds before having a measurement.

Despite being a new control design framework, ADRC applications continue to grow, but they are not without constraints. For example, most successful ADRC solutions have been achieved with systems with small time delays, and processes with large delays still represent a major challenge. This work proposes a new Smith predictor scheme with active disturbance rejection for systems with time delay and parametric uncertainty.

Consider the n-dimensional, time-delay smooth dynamic system:

$$\begin{aligned} f^{(n)}(t) &= K(t, f, \dot{f}, .., f^{(n-1)})u(t - t_d) + \xi(t) \\ y(t) &= c_o f + c_1 \dot{f} + ... + c_{n-1} f^{(n-1)} \end{aligned} \tag{4.16}$$

where t_d is the time-delay, $K(t, f, \dot{f}, .., f^{(n-1)})$ is the nonlinear input gain matrix, evenly bounded, known and far from zero; y is the output of the system and the function $\xi(t)$ can be unknown and uniformly absolutely bounded as well as each of its temporal derivatives to a finite order m. f is the flat output of the system described in (4.16), such that the input u and the output y can in turn be expressed as a linear combination of the flat output and a finite number of its derivatives, i.e., that y and u differential functions of the flat output f [109].

Lets consider the following extended state observer of grade $n + m$:

$$\begin{aligned} \dot{f}_0 &= f_1 + \lambda_{m+n-1}(f - f_0) \\ \dot{f}_j &= f_{j+1} + \lambda_{m+n-j-1}(f - f_0), \\ & \quad j = 1, ..., n - 2 \\ \dot{f}_{n-1} &= K_n u(t - t_d) + z_1 + \lambda_m(f - f_0) \\ \dot{z}_l &= z_{l+1} + \lambda_{m-l}(f - f_0), \quad l = 1, 2, ..., m - 1 \\ \dot{z}_m &= \lambda_0(f - f_0) \end{aligned} \tag{4.17}$$

where K_n is the nominal gain of the plant. This observer is commonly called as Generalized Proportional Integral (GPI) and the disturbance estimation error can be reduced as small as desired if the observer gain parameters $\{\lambda_0, ..., \lambda_{m+n-1}\}$ are appropriately selected. The coefficients λ_j are selected such that the following polynomial in the complex variable *s*, is Hurwitz:

$$p_{obs}(s) = s^{m+n} + \lambda_{m+n-1} s^{m+n-1} + ... + \lambda_0 = 0 \tag{4.18}$$

Let $d(t)$ be the disturbance at plant input, defined as $d(t) = \xi(t)/K(t, y)$ and z_1 the estimate of such disturbance, i.e. $z_1 = \hat{d}(t)$. The transfer function between the control signal and the input disturbance estimation is given by: $u(s)/z_1(s) = -Q(s)e^{-t_d s}$, where:

$$Q(s) = \frac{\lambda_{m-1} s^{m-1} + \lambda_{m-2} s^{m-2} + ... + \lambda_0}{s^{n+m} + \lambda_{n+m-1} s^{n+m-1} + ... + \lambda_0} \tag{4.19}$$

By using the methodology proposed by [65], in order to mitigate typical peaking effects in high gain observers, the coefficients λ_i can be chosen.

The fundamental objective of controlling delayed systems is to design a GPI observer that estimates, even if approximately, the state-dependent $\xi(t)$ disturbance of the original system. The GPI observer must also be able to predict the future values, $\xi(t + t_d)$, of the unknown disturbance $\xi(t)$, in order to compensate them from the controller designed for the advanced system and thus be able to follow the advanced output reference asymptotically while the generated control is shared with the plant.

Robust Smith Predictor Scheme

The Smith predictor (SP) is undoubtedly the most widely used downtime compensator in time delay plant control due to its high effectiveness and simple implementation. Its main advantage is to mitigate the effect of time delay in the characteristic equation of the closed loop control system in systems without uncertainty [79]. However, this control structure has several limitations, such as low performance in uncertain plants, it cannot be applied in the control of plants with integrators or unstable, it does not work well when there is a time delay variable in time, and it presents low robustness to external measurable or non-measurable disturbances.

This work proposes a methodology for the robust design of Smith predictors for disturbance rejection in systems with delay and parametric uncertainty. Consider the control scheme based on disturbance observer (DOB) in Fig. 27. The transfer function between the output and the input disturbance is given by:

$$P_{dy}(s) = \frac{[1 - Q(s)e^{-\hat{t}_d s}]P(s)e^{-t_d s}}{1 + \left[\frac{P(s)}{P_n(s)}e^{-t_d s} - e^{-\hat{t}_d s}\right]Q(s)} \tag{4.20}$$

where P_n is the average model used in the Smith Predictor and the disturbance observer.

Figure 27. Predictive Disturbance Observer for Time-Delay systems

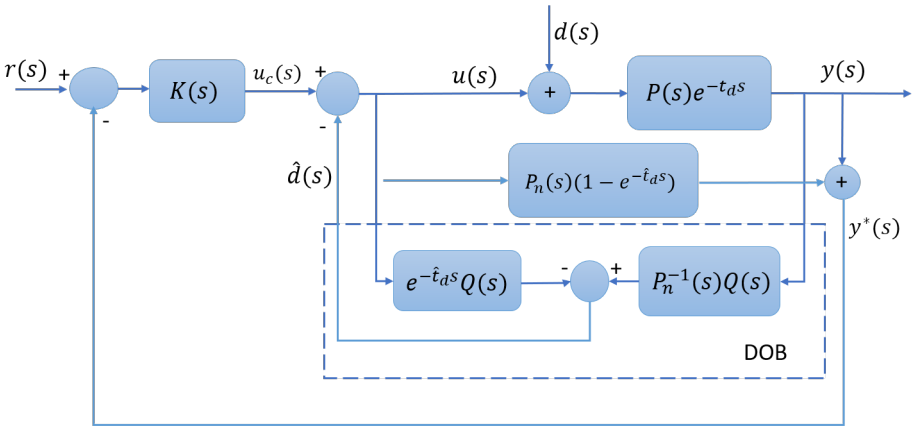

In the block diagram of the Fig. 27 the GPI observer is the basis of a estimation approach of the advanced disturbance $d(t + t_d)$, with the purpose of canceling said disturbance in the advance system called, $P_n(s)$. This makes it possible to reduce the problem of non-linear control with input delay, to a weakly disturbed linear system with input delay. The approximate cancellation of the disturbance input for the system in advance allows to utilize the classical Smith predictor in the consequence dominant linear problem. According to Smith's predictor methodology, a linear feedback controller $K(s)$ can be proposed, which takes into account the error between the output of the plant and the delayed exit of the system in advance.

The transfer function from controller signal to the output of the plant -which will be called equivalent plant of the system- is given by the following expression:

$$P_{eq}(s) = \frac{P(s)e^{-t_d s} + P_n(s)(1 - e^{-\hat{t}_d s})}{1 + \left[\frac{P(s)}{P_n(s)}e^{-t_d s} - e^{-\hat{t}_d s}\right] Q(s)} \tag{4.21}$$

$$\frac{y(s)}{y^*(s)} = \frac{e^{-t_d s}}{\left(1 - e^{-\hat{t}_d s}\right)\frac{P_n(s)}{P(s)} + e^{-t_d s}} \tag{4.22}$$

The diagram shown in Fig. 27 is rearranged to an equivalent structure, as shown in Fig. 28, where the expression $P_{eq}(s)$ is presented in eq. (4.21) and $H(s)$ is the denominator of eq. (4.22).

Figure 28. Equivalent Structure of the Smith Predictor

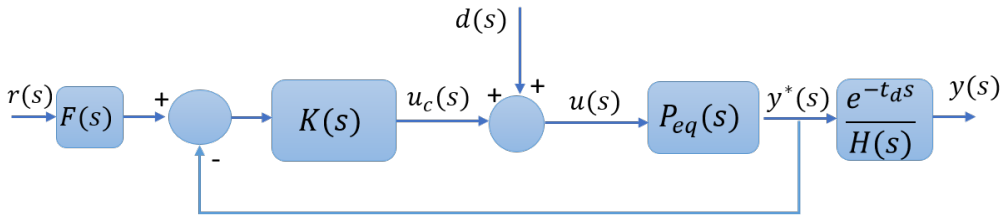

An inspection of the equivalent plant configuration shows that, if there is no uncertainty in the model, the design of the controller can be done without considering the effect of the disturbance observer. Nevertheless, if there is a model-plant mismatch the expression $P_{eq}(s)$ is different from $P(s)e^{-t_d s}$. As a result, the control system is influenced by the uncertainty and a robust control technique must be considered.

4.3. Robust feedback controller

As mentioned, in real systems there is always a certain degree of uncertainty. Such uncertainty implies that the output of a system cannot accurately predicted

even if the inputs and model are known. Therefore, it is preferable that the controller is robust, that is, the controller is insensitive to uncertainty, affirming that a robust control system retains its stability and performance properties against model uncertainties in the plant.

The robust control theory aims to ensure that the designed controller works well when implemented in the actual process. This objective can be considered to be composed of a series of sub-objectives, which are presented in Table 3. It is not always possible to achieve good rejection of disturbances together with robustness, so compromise solutions must be adopted in the design. To reach appropriate compromise solutions to the conditions of disturbances and uncertainty in the system considered, it is useful to have indices that ”measure”the sensitivity and robustness properties of a given controller. Two indexes traditionally used are the sensitivity functions of the loop.

Table 5. Description of control sub-objectives

Sub-objective	Description
Nominal stability	It is the main sub-objective. The system must be stable in closed loop for given or nominal working conditions.
Nominal performance	The controller must supply adequate suppression of disturbance signals (at the plant, sensors and actuators) and measurement noise, and must ensure tracking reference commands for the nominal plant.
Robust stability	The control system must be stable in closed loop for the set of possible plants that may occur as a result of the uncertainty in the model parameters.
Robust performance	The controller must supply adequate disturbance signals rejection and measurement noise attenuation, and must ensure adequate tracking and decoupling of reference commands, for all models of the plant in some set defined by a uncertainty model.

Reviewing the closed-loop response of the 2 degree of freedom control system in Fig. 11, it can be said that it is governed by four transfer functions, collectively called sensitivity functions:

$$T(s) = \frac{P(s)K(s)}{1 + P(s)K(s)}, \quad S(s) = \frac{1}{1 + P(s)K(s)} \tag{4.23}$$

$$S_i(s) = \frac{P(s)}{1 + P(s)K(s)}, \quad S_u(s) = \frac{K(s)}{1 + P(s)K(s)} \tag{4.24}$$

These transfer functions correspond to the sensitivity ($S(s)$), complementary sensitivity ($T(s)$), input sensitivity ($S_i(s)$) and control sensitivity ($S_u(s)$), and are algebraically related as follows:

$$\begin{aligned} S(s) + T(s) &= 1 \\ S_i(s) = S(s)P(s) &= \frac{T(s)}{K(s)} \\ S_u(s) = S(s)K(s) &= \frac{T(s)}{P(s)} \end{aligned} \tag{4.25}$$

In addition to specify the response of the system to signals, the $T(s)$ and $S(s)$ functions serve to specify the robustness properties of the system. As the reference signal normally has a low frequency spectrum, $T(s)$ is specified as a low-pass filter, and thus reject the measurement noise, usually high frequency.

The sensitivity function $S(s)$ is crucial in feedback system design because it takes care of several design performance requirements. The tracking error, relative stability and disturbance attenuation properties depends on $S(s)$. Generally, $|S(j\omega)|$ is constrained to be small at low frequencies, but gradually tends to increase to unity as $\omega \to \infty$ for system in which the open loop transfer function is strictly proper.

Assume that uncertainty is represented in model $\Delta(s)$ with multiplicative structure:

$$P(s) = P_n(s)\,(1 + \Delta(s)) \tag{4.26}$$

where $P_n(s)$ is the nominal plant, and the level of uncertainty is known:

$$|\Delta(j\omega)| \leq W_T(\omega) \tag{4.27}$$

Typically, $W_T(\omega)$ is an increasing function with the frequency ω (that is, the model is more uncertain at higher frequencies). Then, if the control system of Fig. 11 is stable with the $P_n(s)$ plant, it will be stable with the $P(s)$ plant if and only if:

$$|T_n(j\omega)| < \frac{1}{W_T(\omega)} \Longleftrightarrow |W_T(\omega)T(j\omega)| < 1, \quad \forall\, \omega \tag{4.28}$$

where $T_n(j\omega)$ is the nominal complementary sensitivity.

The nominal performance of the system can be specified by defining the form of $|S_n(j\omega)|$ with a given weight function $W_S(\omega)$ requiring that:

$$|S_n(j\omega)| < \frac{1}{W_S(\omega)} \Longleftrightarrow |W_S(\omega)S_n(j\omega)| < 1, \quad \forall\, \omega \tag{4.29}$$

If eq. (4.29) is preserved from the nominal plant to the real plant, and stability is also preserved, the system has robust performance. Robust performance, as intuitively can be expected, requires robust stability as a necessary condition.

This dissertation proposes the use of different feedback controllers to achieve robust performance and stability specifications in the presence of uncertainty in the parameters of the plant model. The use of quantitative control theory, the design of robust PI controllers of 2 degrees of freedom and the use of resets controllers is proposed.

4.3.1. Quantitative robust controller

QFT is a robust control engineering methodology that can simultaneously handle several performance specifications at the same time, such as stability, reference tracking, disturbance rejection, model uncertainty, actuator limitations, noise rejection, vibration reduction, etc. This versatility has allowed QFT to be successfully applied in different applications, including monovariable and multivariable, stable and unstable, and linear and nonlinear systems, among others.

The reliability of the final controller depends on the adequate description of the uncertainty. If the uncertainty covers the entire operating range of the plant, a controller that complies with all QFT bounds will guarantee good performance for each possible plant. However, a large uncertainty would make it more difficult to obtain a suitable controller for the problem, due to a trade-off between the size of the uncertainty and the achievable performance of the controller [41].

In order to take advantage of the potential of QFT in the control of uncertain systems, this dissertation proposes the use of this technique, both in systems with delay and in systems free of delay. Based on the scheme in Fig. 28, the use of the following design specifications is proposed:

Stability specification

$$\left|\frac{y^*(j\omega)}{F(j\omega)r(j\omega)}\right| = \left|\frac{K(j\omega)P_{eq}(j\omega)}{1+K(j\omega)P_{eq}(j\omega)}\right| \leq \delta_U(\omega) \tag{4.30}$$

where $K(j\omega)$ is the controller and $P_{eq}(j\omega)$ is the equivalent-plant.

The stability specification has to be achieved at every frequency of interest, where this inequality imposes a maximum over-impulse in closed-loop system response. It also guarantees minimum phase and gain margins, which reflects the degree of stability of the control system.

Disturbance rejection at plant output

$$\left|\frac{y^*(j\omega)}{d_o(j\omega)}\right| = \left|\frac{1}{1+K(j\omega)P_{eq}(j\omega)}\right| \leq \delta_s(j\omega) \tag{4.31}$$

Unlike the stability, the sensitivity specification $\delta_s(\omega)$ is usually only defined for some low to middle frequencies. In this way, the high frequency activity of the actuators is reduced and possible mechanical fatigue problems are avoided.

Reference tracking specification Two functions $T_U(\omega)$ and $T_L(\omega)$ are given that indicate the output specifications of the closed-loop transfer function magnitude:

$$T_L(j\omega) \leq \left|\frac{y^*(j\omega)}{r(j\omega)}\right| = \left|\frac{F(j\omega)K(j\omega)P_{eq}(j\omega)}{1+K(j\omega)P_{eq}(j\omega)}\right| \leq T_U(j\omega) \tag{4.32}$$

In order to reduce the high frequency activity of the actuators and avoid possible mechanical fatigue problems, the reference tracking specifications are generally only defined for some low to mid frequencies. A practical choice is given by the following expressions [41]:

$$\begin{aligned} T_U(s) &= \frac{\omega_n^2/a(s+a)}{s^2+2\zeta\omega_n s+\omega_n^2} \\ T_L(s) &= \frac{1}{(\tau_1 s+1)(\tau_2 s+1)(\tau_3 s+1)} \end{aligned} \tag{4.33}$$

As mentioned above, the scheme in Fig. 28 has been proposed for the design of controllers for systems with delay. However, the same scheme can be used for delay-free systems, only if the block which contains the delay is omitted.

Reset mechanism

In order to improve the performance of linear controllers designed in QFT, a reset mechanism of the state can be added. The reset state of the controller (or one of its coordinates) applies only when a certain condition is met. The condition that activates or triggers the reset is normally the zero crossing of the tracking error.

The first reset mechanism, called the Clegg integrator (reset control scheme in Fig. 29) was proposed in 1958. This component has the following dynamics:

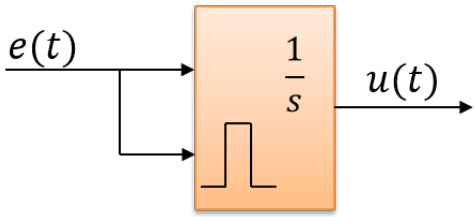

Figure 29. Clegg Integrator (CI)

$$\begin{cases} \dot{u}(t) = e(t) & \text{if} \quad e(t) \neq 0 \\ u(t^+) = 0 & \text{if} \quad e(t) = 0 \end{cases} \tag{4.34}$$

The first expression of the above equation represents the continuous mode (the integral action) and the second the discrete mode or reset, which is triggered at the zero crossing of the input, causing a zero restart of the control action [9].

To understand the advantages of using resets control schemes consider the transfer function of a plant $P(s) = 1/s(s + 0.5)$. Figure 30 shows the step response of this system for a classic controller and the same controller but with reset mechanism. The figure shows the improvement achieved with reset control: a noticeable reduction in overshoot and faster response than the linear system. In this way, reset control emerges as a good option to overcome the typical linear design trade-offs between robustness and bandwidth, or other competing objectives [9].

It can be verified that like a normal integrator, the CI provides -20dB/dec, but with a phase of only about -38° (instead of -90°). This property is very appropriate to achieve bandwidth and phase margin without the trade-off of fundamental linear limitations [10].

In order to obtain better performance, the following P + CI present in [9] can be used:

$$\begin{cases} u(t) = k_p \left(e(t) + \frac{1}{\tau_i} \int_0^t e(\sigma) d\sigma \right) & \text{if} \quad e(t) \neq 0 \\ u(t^+) = k_p e(t) & \text{if} \quad e(t) = 0 \end{cases} \tag{4.35}$$

The previous expression indicates that when $e(t) \neq 0$ a proportional-integral control scheme is presented, but when there is a zero crossing of the error the control action is proportional.

The frequency response of this control scheme is given by the following expression:

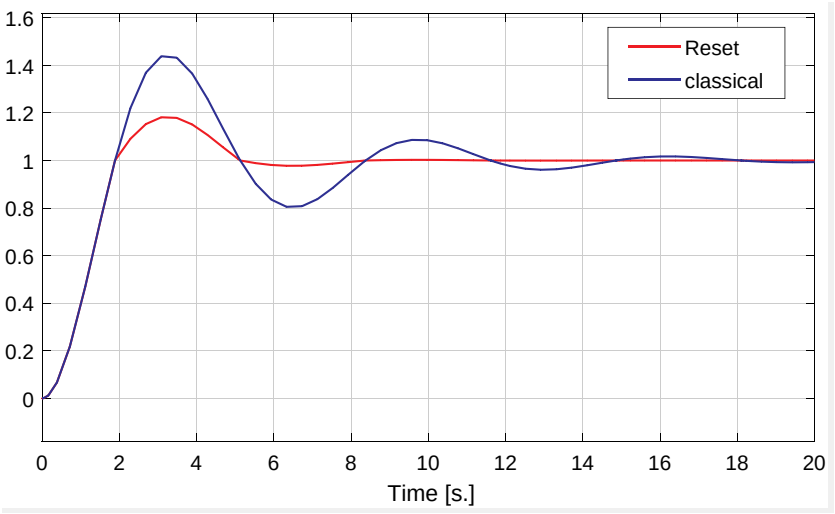

(a) Step response of linear and reset system.

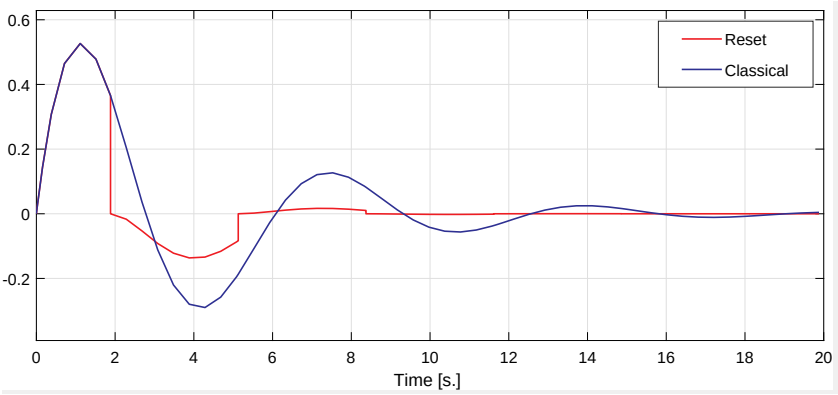

(b) Manipulated variable classic controller and reset controller.

Figure 30. Comparison of linear controller and reset system.

$$(P+CI)(j\omega) = k_p\left[\frac{j\left(\omega\tau_i + 4/\pi\right)+1}{j\omega\tau_i}\right] \tag{4.36}$$

With this structure a phase lead up to 52° is achieved with respect to its base linear PI control. Then the P+CI structure allows better performance in terms of bandwidth and robustness.

For systems with uncertainty, the design of the reset controller can be done by using the QFT technique. In this case, the open-loop transfer function is described by $L(s) = G(s)P(s)$, where the frequency response of the feedback compensator is given by the PI + CI compensator (4.36), that is, $G(j\omega) = (PI + CI)(j\omega)$. This open-loop transfer function can be used to design the compensator, guaranteeing that the

response has the desired oscillatory characteristic for the reset to be effective and in the presence of large plant uncertainty [9].

4.3.2. Robust 2-DoF PI controller

Although in most industrial process control applications the requested set-point of the output variable typically is kept constant, in some cases, in order to alternatively guarantee the operation of disturbance rejection and set point monitoring, it is necessary to change the implementation of a one degree of freedom controller to a two degree of freedom (2-DoF) implementation. The additional parameter provided by the 2-DoF control algorithm improves its servo control operation while considering the performance of regulatory control and the robustness of the closed-loop control system [3].

This subsection presents the design of 2-DoF (two degree of freedom) PI robust control scheme that includes the GPI observer presented in the previous section.

Consider the following 2-DoF PI control algorithm:

$$u_c(s) = K_p \left[\beta r(s) - y(s) + \frac{r(s) - y(s)}{T_i s} \right] \tag{4.37}$$

where the controller parameters to be tuned are $\theta = \{K_p, T_i, \beta\}$. Then, the controller output (4.37) is rearranged as follows (See Fig. 31):

$$u_c(s) = C_r(s) r(s) - C_y(s) y(s) \tag{4.38}$$

where $C_r(s)$ and $C_y(s)$ are given by:

$$C_r(s) = K_p \left(\beta + \frac{1}{T_i s} \right) \tag{4.39}$$

$$C_y(s) = K_p \left(1 + \frac{1}{T_i s} \right) \tag{4.40}$$

Optimization of Cost Functionals

From Figure 31 and equation (4.38), considering measurement noise, the reference, and disturbance, the controlled variable can be obtained by the following relation:

$$y(s) = M_{yr}(s) r(s) + M_{yd}(s) d(s) + M_{yn}(s) n(s) \tag{4.41}$$

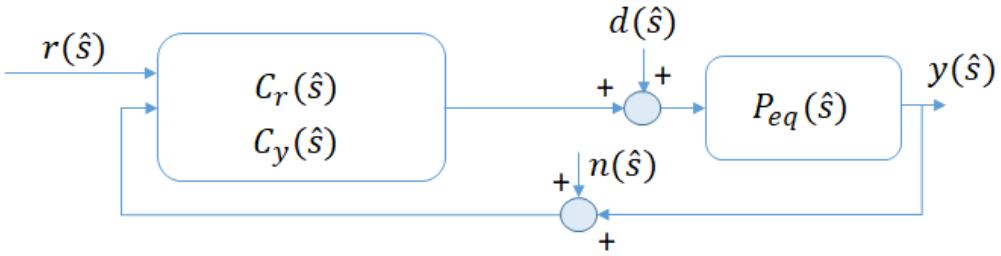

Figure 31. Two-degrees-of-freedom closed-loop control system

where

$$M_{yr}(s) = \frac{C_r(s)P(s)}{1 + C_y(s)P(s)} \tag{4.42}$$

$$M_{yd}(s) = \frac{P(s)}{1 + C_y(s)P(s)} \tag{4.43}$$

$$M_{yn}(s) = \frac{-C_y(s)P(s)}{1 + C_y(s)P(s)} \tag{4.44}$$

M_{yr} is the transfer function from the setpoint to the controlled variable (or servo-control closed loop transfer function), M_{yd} is that from the load-disturbance to the output variable (regulatory control closed-loop transfer function) and M_{yn} is the transfer function from the noise signal to the output variable [2].

Therefore, the target global control system noise free output is computed as follows:

$$y^{tg}(s) = M_{yr}^{tg}(s)r(s) + M_{yd}^{tg}(s)d(s) \tag{4.45}$$

and in the time domain as follows:

$$y^{tg}(t) = y_r^{tg}(t) + y_d^{tg}(t) \tag{4.46}$$

For the model-reference regulatory control and the servo-control response optimization, the cost functionals to be optimized are respectively defined as follows [2]:

$$J_d(\theta_p, \theta_{cy}, \theta_d) = \int_0^\infty \left[y_d^{tg}(\theta_p, \theta_{cy}, \theta_d, t) - y_d(\theta_p, \theta_{cy}, t)\right]^2 dt \tag{4.47}$$

$$J_r(\theta_p, \theta_c, \theta_d) = \int_0^\infty \left[y_r^{tg}(\theta_p, \theta_c, \theta_d, t) - y_r(\theta_p, \theta_c, t)\right]^2 dt \tag{4.48}$$

where θ_d are the design parameters selected so that the control system robustness matches a target value measured using the maximum sensitivity, θ_p the equivalent plant parameters, θ_{cy} are the parameters of the expression (4.40), θ_{cr} are the

parameters of the expression (4.39) and $\theta_c = \theta_{cr} \cup \theta_{cy}$ the controller parameters. $y_d^{tg}(\theta_p, \theta_{cy}, \theta_d, t)$ and $y_r^{tg}(\theta_p, \theta_c, \theta_d, t)$ are the target regulatory control closed-loop step response and the target step response of the servo-control closed-loop transfer function. Both step signals are of unit magnitude.

For the 2-DoF controller design, the following overall cost functional is optimized:

$$J_T(\theta_p, \theta_c, \theta_d) = J_r(\theta_p, \theta_c, \theta_d) + J_d(\theta_p, \theta_{cy}, \theta_d) \tag{4.49}$$

With this cost functional, the same importance is assigned to the disturbance rejection and the references tracking. The controller parameters θ_c^* are obtained by solving the optimization problem defined by the following equation:

$$J_T^* = J_T\left(\theta_p, \theta_c^*, \theta_d\right) = \min_{\theta_c} J_T\left(\theta_p, \theta_c, \theta_d\right) \tag{4.50}$$

The controlled process model can be expressed as a quotient of polynomials in s:

$$P(s) = \frac{N_p^-(s) N_p^+(s)}{D_p(s)} \tag{4.51}$$

where $N_p^+(s)$ is the controlled process model non-invertible part (right-half plane zeros and/or dead-time).

Substituting (4.40) and (4.51) in (4.43), the target regulatory control-loop transfer function is given by:

$$M_{yd}^{tg}(s) = \frac{\left(T_i/K_p\right) s N_p^+(s)}{D_M\left(\theta_p, \theta_{cy}, \theta_d, s\right)} \tag{4.52}$$

where $D_M\left(\theta_p, \theta_{cy}, \theta_d, s\right)$ is the denominator of all the control system closed-loop transfer functions with $D_M(s=0) = 1$. Substituting (4.39), (4.40) and (4.51) in (4.42), the target servo-control transfer function is:

$$M_{yr}^{tg}(s) = \frac{\left(\beta T_i s + 1\right) N_p^+(s)}{D_M\left(\theta_p, \theta_{cy}, \theta_d, s\right)} \tag{4.53}$$

According to [2], to achieve a non-oscillatory output signal and, as a secondary consequence a smooth control signal, the target closed-loop transfer functions (4.52) and (4.53) are fixed such that the target global control system output $y^{tg}(s)$ (4.45) for a first-order plus dead-time system is as follows:

$$y^{tg}(s) = \frac{e^{-\lambda s}}{\tau_c \tau s + 1} r(s) + \frac{\left(T_i/K_p\right) s e^{-\lambda s}}{\left(\tau_c \tau s + 1\right)^2} d(s) \tag{4.54}$$

The variable τ_c is a dimensionless design parameter, indicating the closed-loop system response speed in relation to the open-loop process speed [2], and is selected in order to achieve a non-oscillatory and smooth response with no steady-state error.

Robustness

A way of expressing system robustness is to use the stability margin M_s, which is the smallest length from the Nyquist curve to the critical point (-1,0). This measure is the complementary value of the maximum peak of the sensitivity function, or Maximum sensitivity, defined as follows:

$$M_s = \max_{\omega} \left| \frac{1}{1 + K(j\omega)P(j\omega)} \right| \tag{4.55}$$

where $K(j\omega)$ is the frequency response of the controller.

It is feasible to acquire the normalized controller parameters and the consequence control system robustness as functions of the performance specification, τ_c, and the model parameters, θ_p. Nevertheless, to reduce the design method, the controller parameters are expressed as functions of the closed-loop control system robustness parameter, M_s. In this way, the control system robustness M_s uses the relative speed τ_c as the design parameter.

Parameters design θ_d from (4.49) are chosen just like that the control system robustness with is adjusted to a objective value (robust design) measured by the maximum sensitivity [2]. Low values of M_s imply Nyquist curve distant from the critical point, and consequently greater robustness [19].

By using (4.45) with (4.47) and (4.48) in order to optimize (4.49), the closed-loop response relative speed τ_c is tuned to acquire a objective robustness level M_s^t.

4.4. Feedforward and feedback controllers integrated design

An alternative form of robust design is to tune simultaneously the feedforward and feedback controller using the QFT methodology, and in this way the uncertain system parameters are considered in the tuning stage.

For example, consider the linear perturbed SISO observable system in Fig. 32, where $y(t)$ is the output signal, $\xi(t)$ is the external perturbation input and the group of

parameters $\{a_0, a_1, \ldots, a_{n-1}, b\}$ are uncertain but limited by a set of closed intervals in the real axis, $a_i \in [a_{i,min}, a_{i,max}]$, and $b \in [b_{min}, b_{max}]$ [57].

The idea is to develop an ADRC scheme that is robust with respect to the polynomial disturbance inputs of the form

$$\xi(t) = \sum_{i=0}^{r-1} p_i t^i \tag{4.56}$$

where all parameters p_i are fully uncertain.

The linear system has the subsequent state representation in observable canonical manner:

$$\dot{\hat{x}} = A\hat{x} + \lambda_x(y - \hat{y}) + B\,(u + \omega) \tag{4.57a}$$

$$\dot{z} = Fz + \lambda_z(y - \hat{y}) \tag{4.57b}$$

where $C_z = [1, 0, 0, \ldots, 0]$, $\omega = C_z z$ and $\hat{y} = C\hat{x}$. The state transition matrices for the linear SISO system in the figure are as follows:

$$A = \begin{bmatrix} -a_{n-1} & 1 & 0 & \cdots & 0 & 0 \\ -a_{n-2} & 0 & 1 & \cdots & 0 & 0 \\ \vdots & \vdots & \ddots & \ddots & \vdots & \\ -a_1 & 0 & 0 & \cdots & 0 & 1 \\ -a_0 & 0 & 0 & \cdots & 0 & 0 \end{bmatrix}, \quad B = \begin{bmatrix} 0 \\ 0 \\ \vdots \\ 0 \\ b \end{bmatrix}_{(n\times 1)} \tag{4.58}$$

$$\lambda_x = \begin{bmatrix} \lambda_{n+r-1} \\ \lambda_{n+r-2} \\ \vdots \\ \lambda_{r+1} \\ \lambda_r \end{bmatrix}, \quad F = \begin{bmatrix} 0 & 1 & 0 & \cdots & 0 \\ 0 & 0 & 1 & \cdots & 0 \\ \vdots & \vdots & \vdots & \ddots & \vdots \\ 0 & 0 & 0 & \cdots & 1 \\ 0 & 0 & 0 & \cdots & 0 \end{bmatrix}_{(r\times r)} \tag{4.59}$$
$$\lambda_z = \begin{bmatrix} \lambda_{r-1} & \lambda_{r-2} & \cdots & \lambda_1 & \lambda_0 \end{bmatrix}^T$$

By taking the Laplace transform for the eq. (4.57b), the following expression is obtained:

$$\begin{aligned} sz(s) &= Fz(s) + \lambda_z(Y(s) - C\hat{x}(s)) \\ (sI - F)z(s) &= \lambda_z(Y(s) - C\hat{x}(s)) \\ z(s) &= (sI - F)^{-1}\lambda_z\,(Y(s) - C\hat{x}(s)) \end{aligned} \tag{4.60}$$

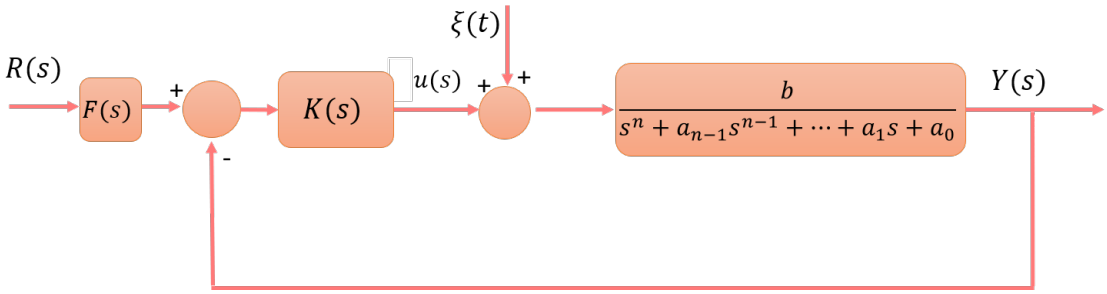

Figure 32. Control of linear perturbed SISO system combining LADRC and QFT

where,

$$\Lambda = (sI - F)^{-1}\lambda_z \;\; \Rightarrow z(s) = \Lambda(Y(s) - C\hat{x}) \tag{4.61}$$

Now, by applying Laplace transformation in eq. (4.57a) and replacing the expression in eq. (4.61), the transfer function of $Y(s)$ with respect to $\hat{x}(s)$ is obtained:

$$\begin{aligned} s\hat{x}(s) &= A\hat{x}(s) + \lambda_x(Y(s) - C\hat{x}(s)) + Bu + BC_z z(s) \\ (sI - A + \lambda_x C)\hat{x}(s) &= \lambda_x Y(s) + Bu + BC_z\Lambda(Y(s) - C\hat{x}(s)) \\ (sI - A + \lambda_x C + BC_z\Lambda C)\hat{x}(s) &= Bu + (\lambda_x + BC_z\Lambda)Y(s) \\ \hat{x}(s) &= \Gamma\left[Bu + (\lambda_x + BC_z\Lambda)Y(s)\right] \end{aligned} \tag{4.62}$$

where,

$$\Gamma = (sI - A + \lambda_x C + BC_z\Lambda C)^{-1} \tag{4.63}$$

With the suggested GPI observer, the subsequent ADRC approach for the trajectory tracking of the specified plant with uncertainty is presented:

$$u = -\hat{\xi}(t) + \frac{[y^*(t)]^{(n)} - \sum_{j=0}^{n-1}\kappa_j(y_j - [y^*(t)]^{(j)})}{b} \tag{4.64}$$

where $y^*(t)$ is the requested output reference trajectory, and the collection of constant coefficients $\{\kappa_0, \kappa_1, \ldots, \kappa_{n-1}\}$ are the controller design parameters.

The control law described in eq. (4.64) can be rewritten as follows:

$$u = \bar{K}_f(R - \hat{x}) - C_z z \tag{4.65}$$

where R is the reference input and $\bar{K}_f \in \mathbb{R}^n$ is a constant vector given by:

$$\bar{K}_f = \frac{[\kappa_0, \kappa_1, \ldots, \kappa_{n-1}]}{b} \tag{4.66}$$

By combining the equations (4.65), (4.61) and (4.62) an expression for $u(s)$ in terms of $Y(s)$ and $R(s)$ is obtained

$$\begin{aligned} u(s) &= \bar{K}_f(R-\hat{x}(s)) - C_z\Lambda(Y(s)-C\hat{x}(s)) \\ u(s) &= \bar{K}_f R - (\bar{K}_f - C_z\Lambda C)\hat{x}(s) - C_z\Lambda Y(s) \\ u(s) &= \bar{K}_f R - (\bar{K}_f - C_z\Lambda C)\Gamma\left[Bu + (\lambda_x + BC_z\Lambda)Y(s)\right] - C_z\Lambda Y(s) \\ \left[1 + (\bar{K}_f - C_z\Lambda C)\Gamma B\right] u(s) &= \bar{K}_f R - \left[(\bar{K}_f - C_z\Lambda C)\Gamma(\lambda_x + BC_z\Lambda) + C_z\Lambda\right] Y(s) \end{aligned} \tag{4.67}$$

The previous equation can be written as

$$\begin{aligned} u(s) &= \frac{D_2(s)}{D_1(s)}\left[\frac{D_3(s)}{D_2(s)}R(s) - Y(s)\right] \\ &= K(s)\left[F(s)R(s) - Y(s)\right] \end{aligned} \tag{4.68}$$

where $K(s)$ and $F(s)$ are the feedback controller and prefilter of the block diagram in Fig. 32. Such transfer functions can be calculated as:

$$K(s) = \frac{D_2(s)}{D_1(s)} \tag{4.69}$$

$$F(s) = \frac{D_3(s)}{D_2(s)} \tag{4.70}$$

with:

$$\begin{aligned} D_1(s) &= \left[1 + (\bar{K}_f - C_z\Lambda C)\Gamma B\right] \\ D_2(s) &= (\bar{K}_f - C_z\Lambda C)\Gamma(\lambda_x + BC_z\Lambda) + C_z\Lambda \\ D_3(s) &= \bar{K}_f\left[1, \quad 0, \quad \cdots, \quad 0\right] \end{aligned} \tag{4.71}$$

In order to show the advantages of a combination between the linear active disturbance rejection control and the quantitative feedback theory, an illustrative example is presented below.

Example Consider the inverted pendulum shown in Fig. 33. The equation that describe is given by the following expression:

$$\begin{aligned} (M+m)\ddot{x} &= u(t) - mL\ddot{\theta}\cos\theta + mL\dot{\theta}^2\sin\theta - k\dot{x} \\ \left(I + mL^2\right)\ddot{\theta} &= mgl\sin\theta - mL\ddot{x}\cos\theta \end{aligned} \tag{4.72}$$

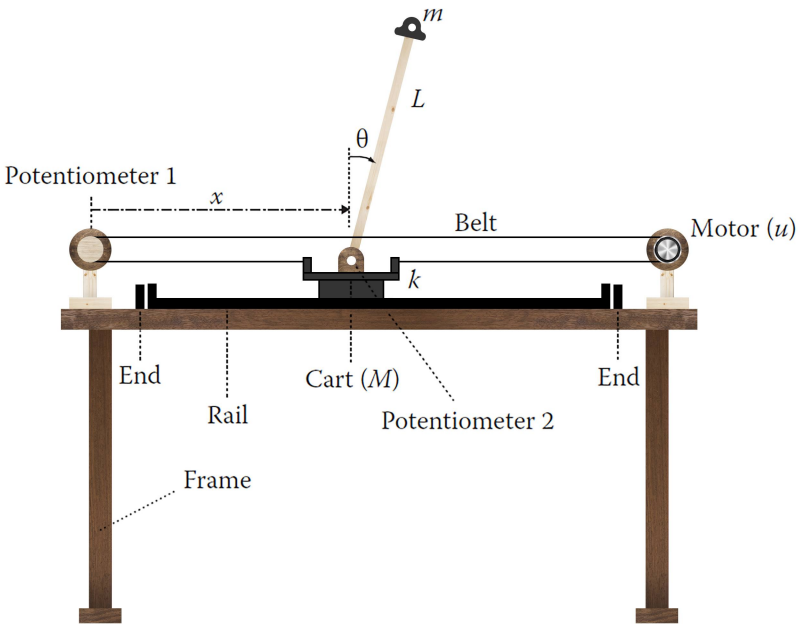

Figure 33. Inverted pendulum on a cart

where,

$u(t)$ is the force applied to the cart

$\theta(t)$ is the pendulum angle to be controlled

$x(t)$ is the position of the cart

m is the end mass

M is the cart mass

$L = 0.5m$ is the stick length

k is the friction coefficient between the rail and the cart

I is the stick inertia

$g = 9.8m/s^2$ is the gravity

The uncertain parameters are

$$M \in [0.9, 1.1]kg, \quad m \in [0.1, 0.2]kg$$
$$k \in [0.1, 0.2]Ns/m, \quad I \in [5, 10]10^{-3}kgm^2$$

By linearizing the non-linear multivariable model close to the operation point, the state space description is given by:

$$\dot{\mathbf{x}} = \begin{bmatrix} 0 & 1 & 0 & 0 \\ 0 & \frac{-k(I+mL^2)}{(M+m)I+mL^2M} & \frac{m^2L^2g}{(M+m)I+mL^2M} & 0 \\ 0 & 0 & 0 & 1 \\ 0 & \frac{mLk}{(M+m)I+mL^2M} & \frac{mLg(M+m)}{(M+m)I+mL^2M} & 0 \end{bmatrix} \mathbf{x} + \begin{bmatrix} 0 \\ \frac{I+mL^2}{(M+m)I+mL^2M} \\ 0 \\ -\frac{mL}{(M+m)I+mL^2M} \end{bmatrix} u \tag{4.73}$$

$$y = \begin{bmatrix} 0 & 0 & 1 & 0 \end{bmatrix} \mathbf{x}$$

Given the state variables:

$$\mathbf{x} = [x_1, x_2, x_3, x_4]^T = \left[\Delta x, \Delta \dot{x}, \Delta \theta, \Delta \dot{\theta}\right]^T$$

The goal is to design a robust controller $K(s)$ to keep the pendulum in the vertical position for the following stability and performance specifications [44]:

-A minimum phase margin of 45°

-Disturbance rejection plant output:

$$\left| \frac{1}{1 + P(j\omega)K(j\omega)} \right| < \left| \frac{0.05\left((j\omega/0.05) + 1\right)}{(j\omega + 1)} \right| \tag{4.74}$$

The system in Eq. (4.73) is flat. By combining the equations (3.25), (3.27) and (3.28), the flat output is given by the following expression:

$$F = -\frac{mML^2 + IM + Im}{m^2L^2g} \left[mL\Delta x + (I + mL^2)\Delta\theta\right] \tag{4.75}$$

For an ADRC treatment of the control problem one would take:

$$F^{(4)} = u(t) + \xi(t) \tag{4.76}$$

For the previous disturbed system the following GPI observer is proposed:

$$\begin{aligned} \dot{F}_0 &= F_1 + \lambda_4 (F - F_0) \\ \dot{F}_1 &= F_2 + \lambda_3 (F - F_0) \\ \dot{F}_2 &= F_3 + \lambda_2 (F - F_0) \\ \dot{F}_3 &= z_1 + u + \lambda_1 (F - F_0) \\ \dot{z}_1 &= \lambda_0 (F - F_0) \end{aligned} \tag{4.77}$$

Assume that the state feedback control law in Eq. (4.66) is replaced by a PI controller, such that:

$$\bar{K}_f = \frac{k_p s + k_i}{s} \tag{4.78}$$

By combining the equations (4.78), (4.76) and (4.69), the following feedback controller is obtained:

$$K(s) = \frac{k_p s^6 + \alpha_5 s^5 + \alpha_4 s^4 + \alpha_3 s^3 + \alpha_2 s^2 + \alpha_1 s + \lambda_0 k_i}{s^2 \left(s^4 + \lambda_4 s^3 + \lambda_3 s^2 + \lambda_2 s + \lambda_1\right)} \tag{4.79}$$

where,

$$\alpha_5 = (\lambda_4 k_p + \lambda_0 + k_i)\,; \quad \alpha_4 = (\lambda_3 k_p + \lambda_4 k_i)$$

$$\alpha_3 = (\lambda_2 k_p + \lambda_3 k_i)\,; \quad \alpha_2 = (\lambda_1 k_p + \lambda_2 k_i)\,; \quad \alpha_1 = (\lambda_0 k_p + \lambda_1 k_i)$$

Because it may be difficult to tune a sixth-grade controller (as it appears in eq. (4.79)), the method described in equations (4.12) - (4.15) is used to avoid the peak effect in the estimation of the disturbance.

Selecting the parameters for the observer $\alpha_0 = 1$, $\alpha_1 = 3$ and $T = 0.35$ [s], and $k_p = 80$, $k_i = 100$ for the controller, the results in Fig. 34 are obtained.

Simulation results indicate that the combination of QFT and ADRC more quickly rejects external disturbances. Another notable advantage in the proposed control scheme is its low energy consumption compared to the results obtained with the QFT controller without observer.

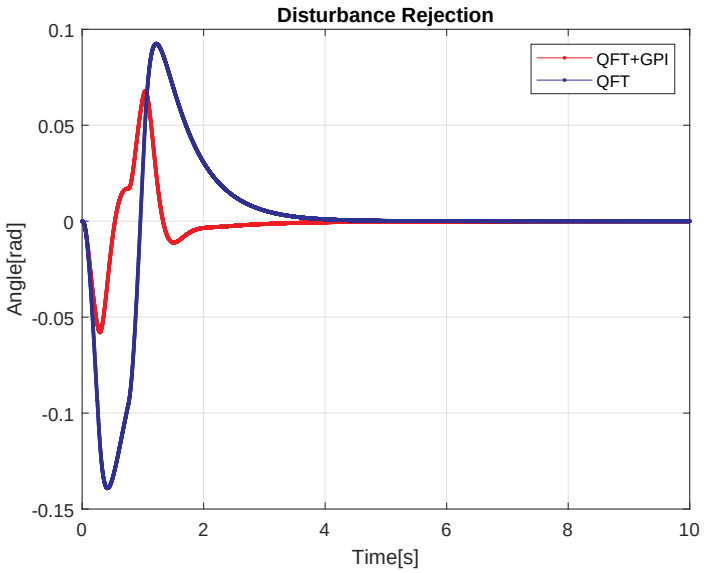

(a)

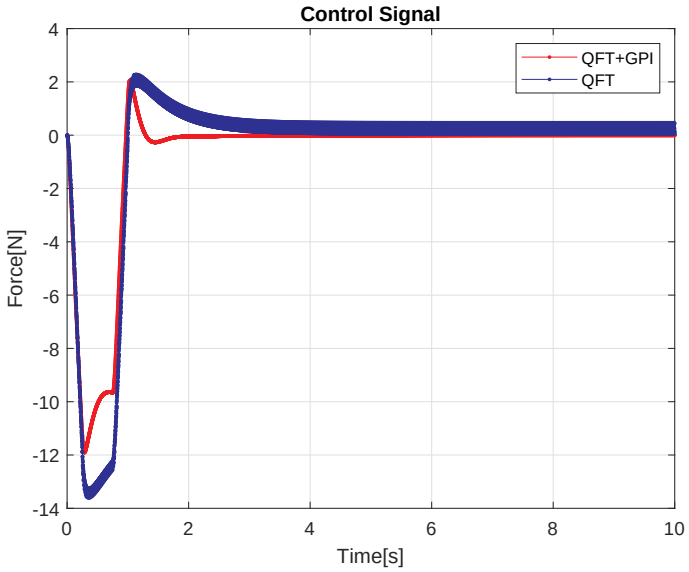

(b)

Figure 34. Control of inverted pendulum

5. NUMERICAL VALIDATION

This chapter validates the performance of the control scheme proposed in this doctoral thesis in three cases of simulation of non-linear multivariable systems: a one-state refrigeration cycle, an offshore wind turbine model and a glucose regulation system in patients with diabetes type 1 mellitus. The discussions presented in this chapter have been taken from [20, 22, 23], which are research published by the author during the execution of this doctoral thesis. In all cases, numerical validation required the use of MATLAB version 9.6 and the robust control toolbox presented in [41].

5.1. Numerical Case 1: One-Stage Refrigeration Cycle

Refrigeration by steam compression is one of the most widely used technologies for generating cold, more in industrial than domestic refrigeration [92]. The power demand range varies from 1 kW to 1 MW, which implies a high energy consumption and consequently, a substantial impact on economic and environmental balances. For example, supermarkets -which are high energy consumers- consume between 2 and 3 MW per year, and approximately $50\,\%$ of this energy is consumed in the cooling processes. Besides, around $30\,\%$ of the energy in the world is employed for ventilating, heating, and air conditioning (HVAC systems), in conjunction with refrigerators and water heaters [59]. Accurately, several researchers reflect that air conditioners and refrigerators demand $28\,\%$ of energy expenditure at home in the USA [12]. Thus, improving energy efficiency in the refrigeration cycle could lead to a significant reduction in energy consumption.

Steam compression refrigeration systems are highly non-linear multivariable systems, with cross-coupling variables, thus their dynamic modeling is not trivial. Due to advances in the technology industry, variable speed compressors and electronic expansion valves have progressively displaced current single-speed compressors and thermostatic expansion valves, respectively. This fact must lead to advanced control schemes, which save energy and mitigate fluctuations in the output variables, thus obtaining more precise control and better system performance.

In this section the stated robust control problem is solved for a one-stage refrigeration cycle using the active disturbance rejection approach through the design of

GPI observers in the internal control loops and PID controllers in the external loops by means of QFT methodology [53].

5.1.1. Process model

According to Fig. 35, a refrigeration cycle consists of: i) variable-speed compressor, ii) electronic expansion valve, iii) evaporator and iv) condenser, where the goal of each period is to suppress heat from the secondary flux at the evaporator and turn off the heat at the condenser by transporting it to the secondary flux. The inverse Rankine cycle is implemented. The refrigerant passes into the evaporator at a low temperature and pressure and evaporates at the same time that suppressing heat from the secondary evaporator flux [13]. Then, the compressor raises the refrigerant pressure and temperature, and it passes into the condenser, where its temperature declines, condenses, and turns into subcooled liquid in the time that transporting heat to the secondary condenser flux. The expansion valve ends the cycle by keeping the pressure difference between the condenser and the evaporator [13].

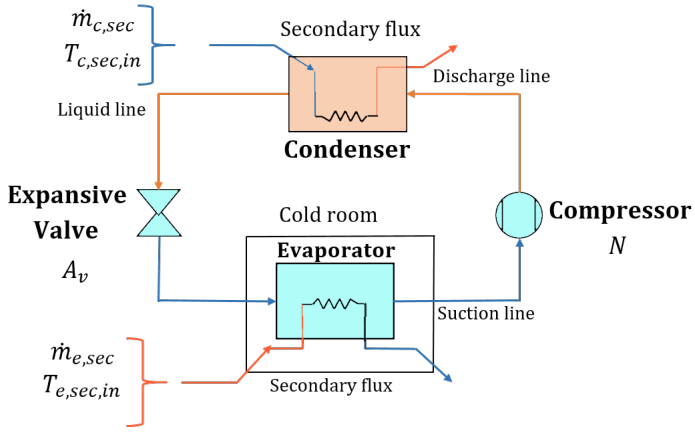

Figure 35. Vapour compression system [11]

A large variety of refrigeration cycle system models can be found: from very complex to simple models. The latter is oriented to multivariable control strategies. The dynamical model used in this work is inspired by [70]. The heat exchangers are modeled using the switched moving boundary method [92], where the heat exchanging zone is divided into variable-length subzones of superheated, two-phase or/and subcooled refrigerant. Depending on the quantity and classification of existing subzones, up to five model characterizations or methods for the condenser and two modes for the evaporator are defined [4].

For every mode, the state vectors $\mathbf{x}_c$ and $\mathbf{x}_e$ in (5.1) gather the most relevant information at each instant of condenser and evaporator, respectively.

$$
\begin{aligned}
\mathbf{x}_c &= [h_{c,sh}\ P_c\ h_{c,sc}\ \zeta_{c,sh}\ \zeta_{c,tp}\ \gamma_c]^T \\
\mathbf{x}_e &= [\zeta_{e,tp}\ P_e\ h_{e,sh}\ \gamma_e]^T \\
\mathbf{x}_{cycle} &= [\mathbf{x}_c\ \mathbf{x}_e]^T
\end{aligned} \tag{5.1}
$$

The state vectors $\mathbf{x}_e$ and $\mathbf{x}_c$ contain mixed elements such as the evaporation and condensation pressures, P_e and P_c, specific enthalpies relating the single-phase zones such as $h_{c,sh}$, $h_{c,sc}$ and $h_{e,sh}$, the zone lengths $\zeta_{c,sh}$, $\zeta_{c,tp}$ and $\zeta_{e,tp}$, and the mean void fractions at both heat exchangers γ_c and γ_e [12].

The uniform state vectors facilitate, through the heat exchanger modes, the establishment of a permanent dynamic system structure formulated in the form of a non-linear descriptor that is presented subsequently [4]:

$$
\begin{aligned}
\mathbf{Z}_c\left(\mathbf{x}_c, \mathbf{u}_c\right)\dot{\mathbf{x}}_c &= \mathbf{f}_c\left(\mathbf{x}_c, \mathbf{u}_c\right) \\
\mathbf{Z}_e\left(\mathbf{x}_e, \mathbf{u}_e\right)\dot{\mathbf{x}}_e &= \mathbf{f}_e\left(\mathbf{x}_e, \mathbf{u}_e\right)
\end{aligned} \tag{5.2}
$$

Each mode in both heat exchangers has its own coefficient matrix **Z(x,u)**, forcing function **f(x,u)** to store thermodynamic variables, and mass and energy balance terms [4]. The choice of model outputs will depend on the interfaces of other system components models:

$$
\begin{aligned}
\mathbf{u}_c &= [\dot{m}_{c,sec}\ T_{c,sec,in}\ \dot{m}_{c,in}\ \dot{m}_{c,out}\ h_{c,in}]^T \\
\mathbf{u}_e &= [\dot{m}_{e,sec}\ T_{e,sec,in}\ \dot{m}_{e,in}\ \dot{m}_{e,out}\ h_{e,in}]^T
\end{aligned} \tag{5.3}
$$

where $\dot{m}$ is he mass flow and T is the temperature. The subscripts are defined as: c: condenser, e: evaporator, sec: secondary flux, in: inlet and out: outlet.

In this work neither the mass flow $\dot{m}_{e,sec}$ nor the inlet temperature $T_{e,sec,in}$ are intended to be regulated. Consequently, the cooling requirement could be presented as a target on the outlet temperature of the secondary evaporator flux $T_{e,sec,out}$, where the mass flow and inlet temperature operate as measurable perturbations. Concerning the condenser, the inlet temperature $T_{e,sec,in}$ and mass flow $\dot{m}_{c,sec}$ of the secondary flux are also treated as perturbations. The manipulated variables are the compressor speed N and the expansion valve opening A_v [13].

Uncertain linear model

In order to describe the fundamental dynamic behaviour of the refrigerator system and to design the robust controller, linear models were identified at different operating points by means of a step response. Each model is expressed in the continuous transfer matrix form:

$$\begin{bmatrix} \Delta T_{e,sec,out}(s) \\ \Delta T_{SH}(s) \end{bmatrix} = G(s) \begin{bmatrix} \Delta A_v(s) \\ \Delta N(s) \end{bmatrix} \tag{5.4}$$

where,

$$G(s) = \begin{bmatrix} G_{11}(s) & G_{12}(s) \\ G_{21}(s) & G_{22}(s) \end{bmatrix} \tag{5.5}$$

and

$$G_{ij} = \frac{k_{ij}\left(T_{z_{ij}}s+1\right)}{\left(\tau_{p_{ij}}s+1\right)\left(T_{f_{ij}}s+1\right)}; \quad i,j=1,2. \tag{5.6}$$

The fixed parameters of the obtained model are the following:

$\tau_{p_{11}} = 26.133\ [s]$, $\tau_{p_{12}} = 30.494\ [s]$, $\tau_{p_{21}} = 27.5\ [s]$, $\tau_{p_{22}} = 39.927\ [s]$,

$T_{z_{11}} = 42.6\ [s]$, $T_{z_{12}} = 9.1954\ [s]$, $T_{z_{21}} = 38.6\ [s]$, $T_{z_{22}} = 52.675\ [s]$.

And the uncertain parameters of the dynamic model are the following:

$k_{11} = [-0.02532, -0.015204]$ °C, $k_{12} = [-1.96, -1.49]\,10^{-3}$ °C

$k_{21} = [-0.407, -0.229]$ °C, $k_{22} = [0.137, 0.172]$ °C

$T_{f_{11}} = [0.1, 0.27]\ [s]$, $T_{f_{12}} = [0.25, 0.57]\ [s]$,

$T_{f_{21}} = [0.0146, 0.247]\ [s]$, $T_{f_{22}} = [5.76, 7.68]\,10^{-2}\ [s]$.

The so-called fixed parameters were kept constant at the different points of operation of the identification process while the so-called uncertain parameters changed in value in each test. Table 6 includes the accepted range of the input variables, used in the identification of the uncertain parameters model.

5.1.2. Feedforward control design

By considering that the linear system the Eq. (5.6) is controllable, its flat outputs, f_i, are given by:

$$f_i = \frac{k_{ii}u_i(s)}{\left(\tau_{p_{ii}}s+1\right)\left(T_{f_{ii}}s+1\right)}; \quad i=1,2. \tag{5.7}$$

Table 6. Input variable ranges

Variable	Range	Units
A_v	$[10, 100]$	$\%$
N	$[30, 50]$	Hz
$T_{c,sec,in}$	$[27, 33]$	^oC
$T_{e,sec,in}$	$[-22, -18]$	^oC
T_{surr}	$[20, 30]$	^oC
$\dot{m}_{c,sec}$	$[125, 175]$	gs^{-1}
$\dot{m}_{e,sec}$	$[0.0075, 0.055]$	gs^{-1}
$P_{c,sec,in}$	–	bar
$P_{e,sec,in}$	–	bar

Therefore, controlled temperatures are determined by the following differential equation:

$$T_i = T_{z_{ii}} \frac{df_i}{dt} + f_i; \quad i = 1, 2. \tag{5.8}$$

Now, from Eq. (5.7) the following simpler perturbed system can be obtained:

$$f^{(2)} = k_{ii} u_i + \xi(t) \tag{5.9}$$

where $\xi(t)$ is the disturbed signal that included depreciated dynamics.

An GPI observer (5.10) is designed for the system (5.9), which provides simultaneous estimations of the phase variables associated with the flat output f and the disturbance $\xi(t)$

$$\begin{aligned} \dot{f}_0 &= f_1 + \lambda_3 (f - f_0) \\ \dot{f}_1 &= k_{ii} u_i + z_1 + \lambda_2 (f - f_0) \\ \dot{z}_1 &= z_1 + \lambda_1 (f - f_0) \\ \dot{z}_2 &= \lambda_0 (f - f_0) \end{aligned} \tag{5.10}$$

where f_0 is the estimation of the flat output f, f_1 is the first derivative of f_0 and $z_1 = \hat{\xi}(t)$ is the disturbance estimation. To guarantee an establishment time at around 20 seconds of the estimation error, the observer gain parameters in equations (4.12) - (4.15) were set as: $T = 6\ [s]$, $\alpha_0 = 4$ and $\alpha_1 = 4$. In this way the estimation error characteristic polynomial is defined by $p_{obs}(s) = s^4 + 21.85s^3 + 59.68s^2 + 23.87s + 1.194 = 0$.

5.1.3. Feedback control design

For the design and validation of the controller, an operation point is selected within the uncertainty of the plant model. Let $P_r(s, \theta)$ be the transfer function of the plant with uncertainty θ, the nominal plant is given by:

$$P_n(s) = P_r(s, \theta_n) \tag{5.11}$$

where θ_n is the parameters vector of the operation point, which was selected as:

$$\theta_n = \frac{\theta_{max} + \theta_{min}}{2} \tag{5.12}$$

where θ_{min} and θ_{max} are the lower and the upper parameters vector, respectively, of the uncertainty set.

In order to analyse the interaction of the inputs and outputs of the system, the Bristol relative gain matrix is used, which is defined by:

$$R = P_n(0). * P_n^{-T}(0) \tag{5.13}$$

In the case of the selected nominal plant, the obtained result is:

$$R = \begin{bmatrix} 0.85 & 0.15 \\ 0.15 & 0.85 \end{bmatrix} \tag{5.14}$$

This indicates that the pairs input-output $u_1 - y_1$ and $u_2 - y_2$ should be taken to utilize the design of two single-input $\&$ single-output (SISO) controllers.

Table 7 shows the stability, sensitivity and reference tracking specifications given by (4.30), (3.8), (3.9) and (3.10) for the equivalent plants $P(s)$ of $G_{11}(s)$ and $G_{22}(s)$.

By using loop shaping on the Nichols chart with bounds computed from the template of the equivalent plant, the 2DOF controller is obtained as follows:

$$K(s) = K_p + \frac{K_i}{s} + \frac{K_d s}{(s/\beta + 1)} \tag{5.15}$$

$$F(s) = \frac{1}{\lambda s + 1} \tag{5.16}$$

Table 8 shows the controller and filter parameters for each SISO system.

Figure 36 shows the block diagram of the *feedback-feedforward* control for the one-cycle refrigeration system.

Table 7. Performance specifications

Parameter	Units	For $G_{11}(s)$	For $G_{22}(s)$
δ_U	–	1.66	1.45
a_d	–	0.01	0.0001
ω_n	rad/s	0.6	0.2
ζ	–	0.5	0.5
a	–	1	1
τ_1	s	2	6
τ_2	s	3	7
τ_3	s	4	8

Table 8. Parameters of filters and controller

Parameter	For $G_{11}(s)$	For $G_{22}(s)$
K_p	-2.2	1.44
K_i	-5	1
K_i	-0.228	0.41
β	100	16
λ	2	5

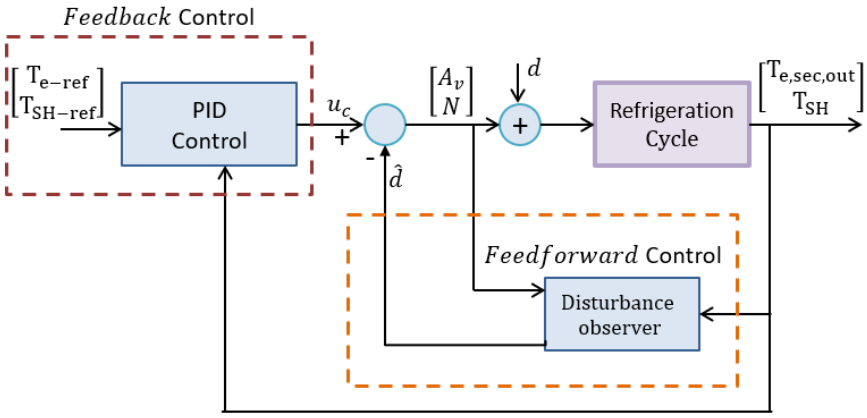

Figure 36. Block diagram of one-cycle refrigeration control system

5.1.4. Numerical validation and analysis

Fig. 37 shows the stability, sensibility and tracking reference analysis in the frequency domain, where the dashed line is the specification in the frequency domain and the solid line in each plot represents the worst case. Fig. 37(a) presents the analysis of the closed-loop stability specification, defined in (4.30), for $G_{11}(s)$ and Fig. 37(d) for $G_{22}(s)$. The control system meets the stability specification since the solid line is below the dashed line δ_U in all the analysed cases.

Fig. 37(b) shows the frequency-domain analysis of the sensitivity specification for $G_{11}(s)$ and Fig. 37(e) for $G_{22}(s)$. The control system meets the sensitivity specification in all the studied cases, since the solid line is below the dashed line δ_s. Fig. 37(c) and Fig. 37(f) present the limits $T_L(j\omega)$ and $T_U(j\omega)$ in (4.32) in order to analyse the reference tracking specification in the time-domain. The control system meets the specification (is between the upper and lower limits) in all the studied cases.

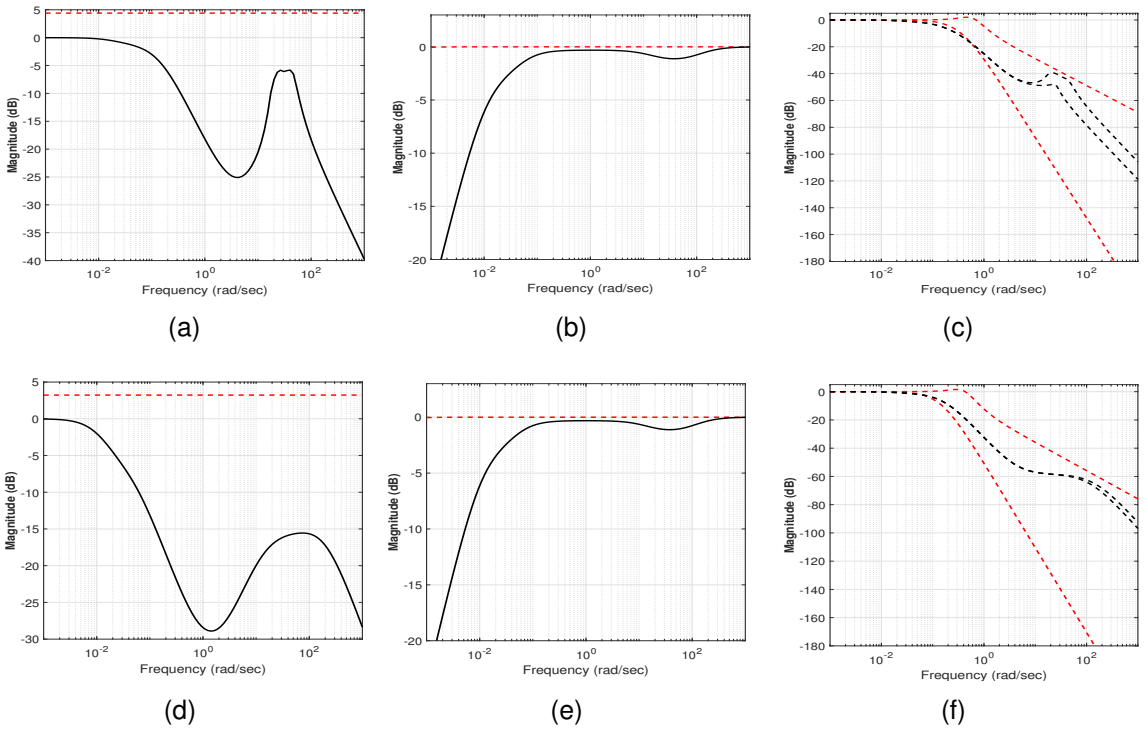

Figure 37. Robustness Specifications Analysis. Stability: (a) $G_{11}(s)$, (d) $G_{22}(s)$; Disturbance rejection: (b) $G_{11}(s)$, (e) $G_{22}(s)$; Reference tracking: (c) $G_{11}(s)$, (f) $G_{22}(s)$. Specification (dashed line) and worst case within the uncertain plants at each frequency (solid line).

On other hand, Fig. 38 shows the reference tracking of the controlled variables T_{SH} and $T_{sec,evap,out}$ within the considered range. Fig. 38(a) plots the manipulated variables, corresponding to A_v and N. The PID controller with disturbance observer reacts quickly to the reference changes, despite the non-measurement of the perturbation variables and the existing dynamic coupling of the multivariable system (Fig. 38(b)).

In order to carry out a quantitative comparison between the two controllers, the average of eight performance indices is evaluated. The first two indicators are the Ratios of Integrated Absolute Error (RIAE), considering that both the outlet temperature of evaporator secondary flux $T_{sec_evap_out}$ and the amplitude of superheating (T_{SH}) must follow the trajectories set for each one. The third indicator is the Ratio of Inte-

grated Time multiplied Absolute Error (RITAE) for the output signal $T_{sec_evap_out}$, considering that numerical validation usually includes a step change in its set-point. The fourth, fifth, and sixth indicators are the Ratios of Integrated Time multiplied Absolute Error (RITAE) for the second output signal (T_{SH}), considering that that numerical validation includes three sudden changes in its set-point. The seventh and eighth indicators are the Ratios of Integrated Absolute Variation of Control signal (RIAVU) for the two control signals, the valve opening A_v, and the compressor speed N. The mixed index is presented as the average value of the eight individual indices [13]. Therefore, the combined performance index is described by:

$$J\left(C_1, C_2\right) = \frac{1}{8}\sum_{i=1}^{8} R_i\left(C_1, C_2\right) \tag{5.17}$$

where each $R_i\left(C_1, C_2\right)$ is the ratio between the i-th performance index of C_2 (PID controller with observer) and the i-th performance index C_1 (PID controller without observer). These indices are presented in the following expressions:

$$\begin{aligned} IAE_i &= \int_0^{time} \left|e_i(t)\right| dt \\ ITAE_i &= \int_{t_c}^{t_c+t_s} \left(t - t_c\right)\left|e_i(t)\right| dt \\ IAVU_i &= \int_0^{time} \left|\frac{du_i(t)}{dt}\right| dt \end{aligned} \tag{5.18}$$

Since the index $J\left(C_1, C_2\right)$ in (5.17) is equal to 0.4, the PID controller with GPI observer has a better performance than the reference controller.

5.1.5. Conclusions

In this section, the problem of robust control of a one-stage refrigeration cycle is solved by using GPI observers designed and robust PID controllers designed by QFT methodology. The observer's efficiency is since the unknown parameters, and external perturbations of the flat input-output dynamics are considered an added additive perturbation, which is a function of time with the assumption of being uniformly bounded. This non-linear perturbation and the phase variables associated with the flat output are sufficiently accurately estimated in line through linear high-gain Luenberger observers, called GPI observers.

The proposed method is easy to implement, making it an appealing solution for refrigeration systems. Reference tracking analysis and a combined performance index show that the robust controller reacts quickly to the reference changes, despite

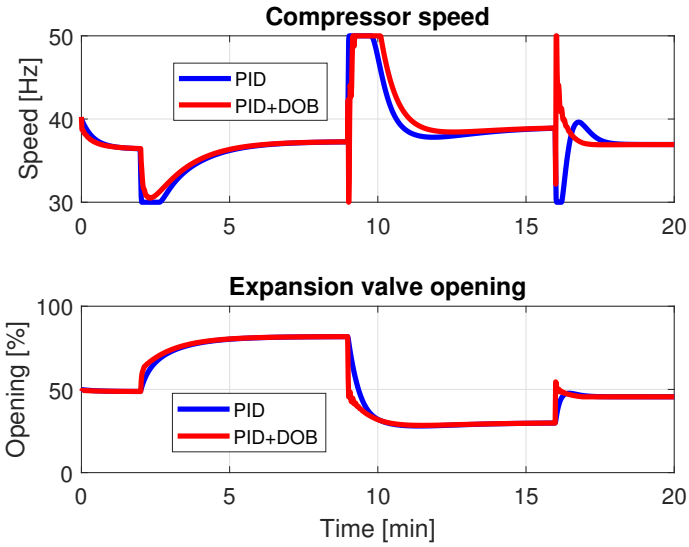

(a)

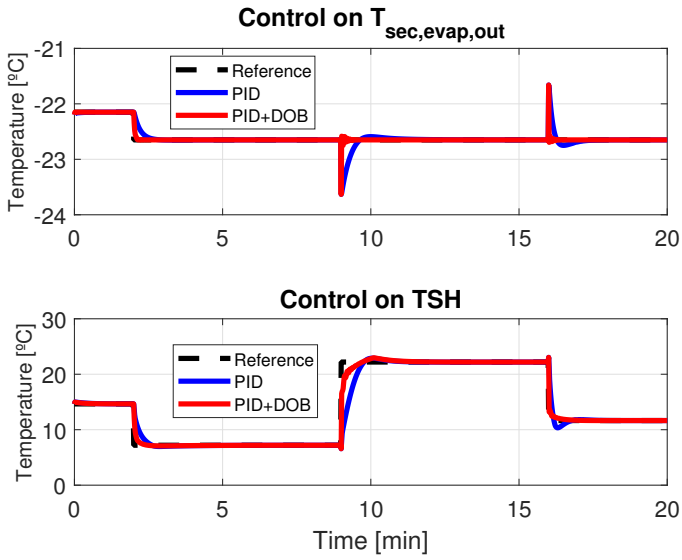

(b)

Figure 38. Comparison of the descentralized PID controller with the ADCR-PID controller: (a) Input variables; (b) Output variables.

the non-measurement of the disturbance variables and the dynamic coupling of the multi-variable system, compared to decentralized PIDs proposed with the benchmark. Besides, stability and sensitivity specifications are reached throughout the range of uncertainty of the identified model.

5.2. Numerical Case 2: Offshore Wind Turbine

Wind turbines are complex systems, with large flexible structures working under unpredictable and turbulent environmental conditions. High uncertainty and nonlinear models, substantial variations of wind speed, mechanical fatigue, and stability problems are the main challenges for designing advanced control systems [44], [121]. Thus, in this control approach, manipulated variables such as torque and pitch, controlled variables such as rotor speed and tower displacement, and actuator constraints were also taken into account.

Most of the control techniques applied to these systems are: decentralized PID [125], optimal LQG [8], [102], predictive [60], [128], H_∞ [76], [94], based on fuzzy logic [105], based on neural networks [17], [71], based on the estimated wind speed [61] and adaptive control [116], [36], [85].

On the other hand, floating wind turbines offer the opportunity of being used with offshore wind energy. However, movements of their platform make these systems much more dynamic compared with the ground-landed ones. This fact demands high requirements on the control system, especially on the blades angle control pitch. Thus, novel controllers should be designed to regulate the rotor speed and reduce structural loads during the floating platform's low-frequency motion.

This section compares the dynamic performance of a nonlinear control approach based on flat filtering concerning a baseline controller on an offshore wind turbine. Feedback linearization and Generalized Proportional Integral (GPI) compensator are used to reduce load and mechanical fatigue in the collective pitch blade, at the same time, a PI reset controller is designed to regulate the rotor speed for an uncertain parameter model of the generator torque. To validate the control approach, a baseline controller is used, which combines an Indirect Speed Controller (ISC) and a collective blade pitch controller (CPC). Simulation results show that the controller based on flatness and reset mechanism significantly reduces rotor speed and power variations in full load conditions and perfect wind preview.

5.2.1. Wind turbine modeling

A typical system wind energy conversion can be represented as in Fig. 39, where wind energy captured by the turbine is converted into mechanical torque through the drive train and then transformed into electrical energy by a doubly-fed induction generator connected, for example, to the grid. The aerodynamic torque can be expressed as Eq. (5.19).

$$M_a = 0.5\rho\pi C_P(\lambda,\beta)R^3v^2/\lambda \tag{5.19}$$

where R [m] is the length of the blades, $\lambda = \omega_t R/v$ is the speed ratio, ω_t [rad/s] is the turbine speed and $C_P(\lambda, \beta)$ is the non-linear power coefficient.

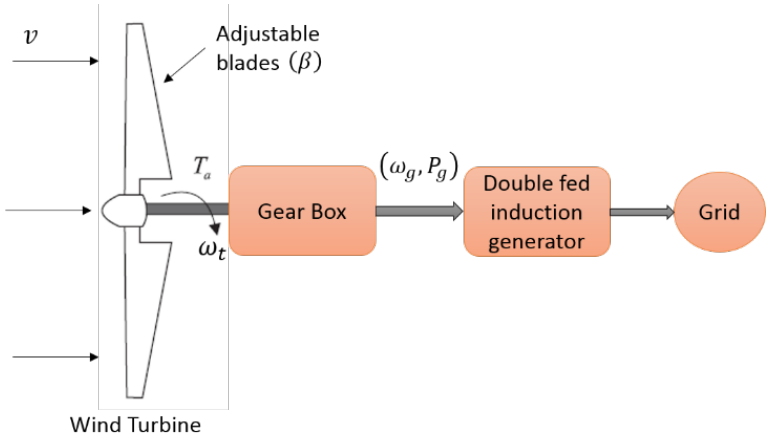

Figure 39. A typical conversion system for wind energy

On the other hand, a two-mass drive train model with flexible shaft can be expressed by the equations (5.20) and (5.21).

$$J_t \dot{\omega}_t = M_a - N M_g \tag{5.20}$$

$$m_{eT}\ddot{x}_T + c_{eT}\dot{x}_T + k_{eT}(x_T - x_{0T}) = F_a \tag{5.21}$$

where J_t [kg/s^2] is the inertia of turbine, M_g [Nm] is the electrical generator torque, x_T [m] is the tower top force-aft displacement, N is the gear box ratio m_{eT} [kg], c_{eT} [N-s/m] y k_{eT} [N/m] are the tower equivalent modal mass, structural damping, and bending stiffness, respectively.

The aerodynamic thrust is given by Eq. (5.22).

$$F_a = 0.5\rho\pi C_T(\lambda, \beta) R^2 v^2 \tag{5.22}$$

where C_T is the effective thrust coefficient.

5.2.2. Feedforward-feedback control design

As turbines increase in size, alleviating structural loads plays an important role in the design of controllers. Therefore, one of the main purposes of the control system is to maintain both the maximum mechanical loads in the turbine structure and the mechanical fatigue within the design limits [44]. The block diagram of the robust control approach for the wind generation system proposed in this dissertation is presented in Fig. 40.

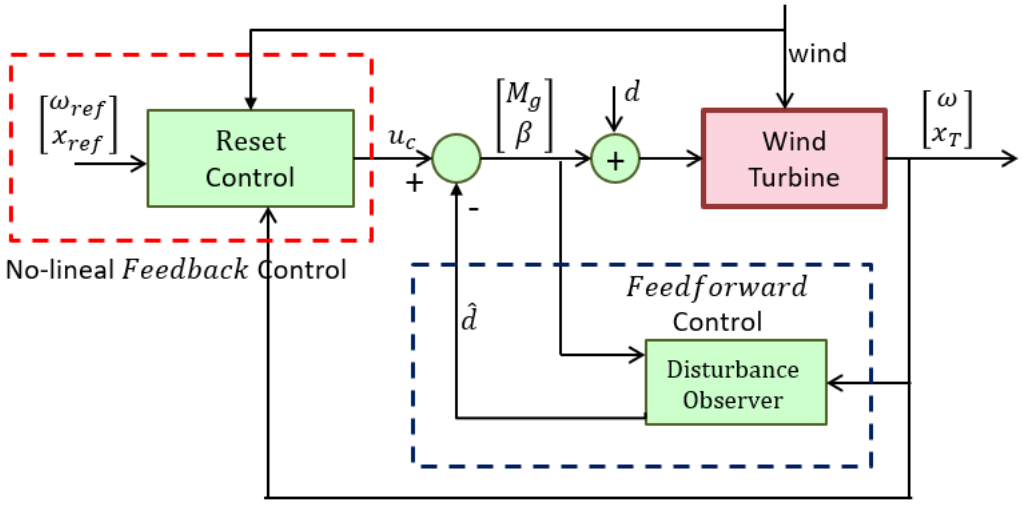

Figure 40. *Feedback-Feedforward* control approach for offshore wind turbine

Pitch control

For pitch control a feedback linearization based on differential flatness is proposed. Let a class of non-linear systems representable in the form of Eq. (5.23):

$$\begin{aligned}\dot{x}_1 &= x_2\\ \dot{x}_2 &= x_3\\ &\vdots\\ \dot{x}_n &= f_n(x_1, x_2, ..., x_n) + u g_n(x_1, x_2, ..., x_n)\end{aligned} \tag{5.23}$$

These kinds of systems represented by Eq. (5.23) are exactly linearizable by redefining the control variable in terms of the state and an external auxiliary input. This redefinition can be interpreted as a non-linear feedback process by transforming the coordinate of the control variable.

Multivariable systems, which are exactly linearizable by means of state coordinate transformation, and static state feedback, constitute the simplest class of flat systems [108].

By defining the auxiliary input as Eq. (5.24), a linear system that exhibits a pure integration chain structure occurs.

$$w = f_n(x_1, x_2, ..., x_n) + u g_n(x_1, x_2, ..., x_n) \tag{5.24}$$

For Eq. (5.22) the auxiliary variable can be defined by the following expression:

$$w = \ddot{x}_T = \frac{F_a - c_{eT}\dot{x}_T - k_{eT}(x_T - x_{0T})}{m_{eT}} \tag{5.25}$$

Then, the output tracking error is governed by:

$$\ddot{e}_{x_T} = e_w \tag{5.26}$$

where $e_{x_T} = x_T - x_{ref}$, $e_w = w - \ddot{x}_{ref}$ and x_{ref} is the desired steady state value for x_T

A stabilizing state feedback control law is given by:

$$e_w = -k_2\dot{e}_{x_T} - k_1 e_{x_T} \tag{5.27}$$

In order to consider the integral reconstruction of $\dot{e}_{x_T}$ the control law and the above equation can be modified by the following expression [35], [112], [110]:

$$e_w = -k_2\hat{\dot{e}}_{x_T} - k_1 e_{x_T} - k_0 \int_0^t e_{x_T}(\sigma)d\sigma \tag{5.28}$$

where the estimated $\hat{\dot{e}}_{x_T}$ is computed by integrating the next equation :

$$\hat{\dot{e}}_{x_T} = \int_0^t e_w(\sigma)d\sigma \tag{5.29}$$

In Laplace transform terms the subsequent expression for the suggested output error feedback controller is obtained:

$$\left(1 + \frac{k_2}{s}\right) e_w(s) = -\left(k_1 + \frac{k_0}{s}\right) e_{x_T} \tag{5.30}$$

The robust controller presents the subsequent combined time and frequency domain notation:

$$w(s) = -\left[\frac{k_1 s + k_0}{s + k_2}\right](x_T - x_{ref}) \tag{5.31}$$

The characteristic polynomial of the closed loop system is then given by the following fourth order polynomial:

$$p_k(s) = s^3 + k_2 s^2 + k_1 s + k_0 = 0 \tag{5.32}$$

whose roots are defined and achieved by appropriately selecting the coefficients $\{k_0, k_1, k_2\}$. By choosing the coefficients k_0, k_1, k_2 such that $p_k(s) = (s+\alpha)(s^2 + 2\zeta\omega_n s + w_n^2)$ is possible to maintain the tracking error vector in a small area around the origin. The design parameters of the characteristic polynomial of the observer were set to be:

$$\omega_n = 2 \ [rad/s], \quad \zeta = 0.5, \quad \alpha = 10$$

By combining equations (5.22) and (5.25), the following control law is obtained:

$$C_T(\lambda, \beta) = \frac{m_{eT} w + c_{eT} \dot{x}_T + k_{eT}(x_T - x_{0T})}{k_v} \tag{5.33}$$

where $k_v = 0.5\rho\pi R^2 v^2$.

By using a inverse function of the look-up table $C_T(\lambda, \beta)$, the desired pitch angle is obtained:

$$\beta_d = \beta(\lambda, C_T) \tag{5.34}$$

Torque Control

By linearising equation 2 around the point of operation $P_0 = (w_{t0}, v_0, \beta_0)$ the following linear equation is obtained:

$$J_t \Delta\dot{\omega}_t = \alpha_\omega \Delta\omega_t + \alpha_v \Delta v + \alpha_\beta \Delta\beta - N\Delta M_g \tag{5.35}$$

with

$$\alpha_\omega = \left.\frac{\partial M_a}{\partial \omega_t}\right|_{P_0}, \quad \alpha_v = \left.\frac{\partial M_a}{\partial v}\right|_{P_0}, \quad \alpha_\beta = \left.\frac{\partial M_a}{\partial \beta}\right|_{P_0}$$

Then, the uncertain linear model with lumped disturbance is the following:

$$\frac{\Delta\omega_t(s)}{\Delta M_g(s)} = \frac{K_a}{s+a} + d(s) \tag{5.36}$$

where $K_a = -N/J_t$ and $a = \alpha_\omega / J_t = [0.0774, 0.444]$, for wind speed between 13 and 25 m/s.

By using a PI controller, the characteristic equation of the system is as follows:

$$s^2 + (a + K_a k_p)s + K_a k_i = 0 \tag{5.37}$$

The parameters k_i (integral gain) and k_p (proportional gain) of the controller can be selected based on the desired sensitivity function, defined as:

$$S(s) = \frac{s(s+a)}{s^2 + (a + K_a k_p)s + K_a k_i} \tag{5.38}$$

The parameters k_p and k_i can be selected in such a way that the following sensitivity specification is obtained:

$$|S(s)| \leq \frac{s}{s+10} \tag{5.39}$$

Reset Control

In order to improve the robustness and speed of the torque controller the following P + CI control based in [9] is proposed:

$$\begin{cases} u(t) = k_p \left(e(t) + \frac{1}{\tau_i} \int_0^t e(\sigma) d\sigma \right) & \text{if} \quad e(t) \neq 0 \\ u(t^+) = k_p e(t) & \text{if} \quad e(t) = 0 \end{cases} \tag{5.40}$$

The previous expression indicates that when $e(t) \neq 0$ a proportional-integral control scheme is presented, but when there is a zero crossing of the error the control action is proportional.

The frequency response of this control scheme is given by the following expression:

$$(P + CI)(j\omega) = k_p \left[\frac{j\left(\omega\tau_i + 4/\pi\right) + 1}{j\omega\tau_i} \right] \tag{5.41}$$

With this structure a phase lead up to 52° is achieved with respect to its base linear PI control. Then the P+CI structure improves its performance in terms of bandwidth and robustness.

Baseline Controller

The baseline controller is described in [62] and combines an Indirect Speed Controller (ISC) and a collective blade pitch controller (CPC). Both controllers use the generator speed as the input and they are designed to work independently in the below-rated and above-rated wind speed range. *Baseline Collective Pitch Controller*

The collective blade pitch control signal is calculate using a gain-scheduled PI controller on the speed error between the filtered and the rated generator speed [62]:

$$\Delta\beta = GK(\beta)\left(K_P\Delta\omega_g + K_I\int_0^t \Delta\omega_g(\tau)d\tau\right) \tag{5.42}$$

where the dimensionless gain-correction factor $GK(\beta)$ is given by the following expression:

$$GK(\beta) = \left(1 + \frac{\beta}{\beta_k}\right)^{-1} \tag{5.43}$$

β_k is the blade-pitch angle at which the pitch sensibility is twice its value at the rated operating point. In other words,

$$\frac{\partial P_a}{\partial\beta}(\beta = \beta_k) = 2\frac{\partial P_a}{\partial\beta}(\beta = 0) \tag{5.44}$$

In order to ensure a second order characteristic response given by $\omega_{n\phi} = 0.6$ [rad/seg] and ζ_ϕ =0.6 to 0.7, [62] proposes the following Proportional-Integral constants:

$$K_P = \frac{2J_t\hat{\omega}_t\zeta_\phi\omega_{n\phi}}{-\frac{\partial P_a}{\partial\beta}(\beta = 0)}; \quad K_I = \frac{J_t\hat{\omega}_t\omega_{n\phi}^2}{-\frac{\partial P_a}{\partial\beta}(\beta = 0)} \tag{5.45}$$

Baseline Torque Controller

For the torque controller, the operation is divided into five control regions: $1, 1\frac{1}{2}, 2, 2\frac{1}{2}$ and 3. In region 1, the wind speed is too low for extracting power. Region 2 is a control region for optimizing power capture. The generator torque needed to maintain the maximum power coefficient $C_{P,max}$ in this region can be determined by the Indirect Speed Controller (ISC) [101]:

$$M_g = k_{isc}\omega_g^2 \tag{5.46}$$

where $k_{isc} = \frac{\rho\pi R^5 C_{P,max}}{(\lambda_{opt}N)^3}$

In region 3, the torque controller regulates wind power by inverting the equation of the electrical power:

$$M_g = \frac{P_{g,rated}}{\eta_g\omega_g} \tag{5.47}$$

The transition regions $1\frac{1}{2}$ and $2\frac{1}{2}$ use a linear function as state feedback and link the region 2 to region 1 and 3, respectively [101].

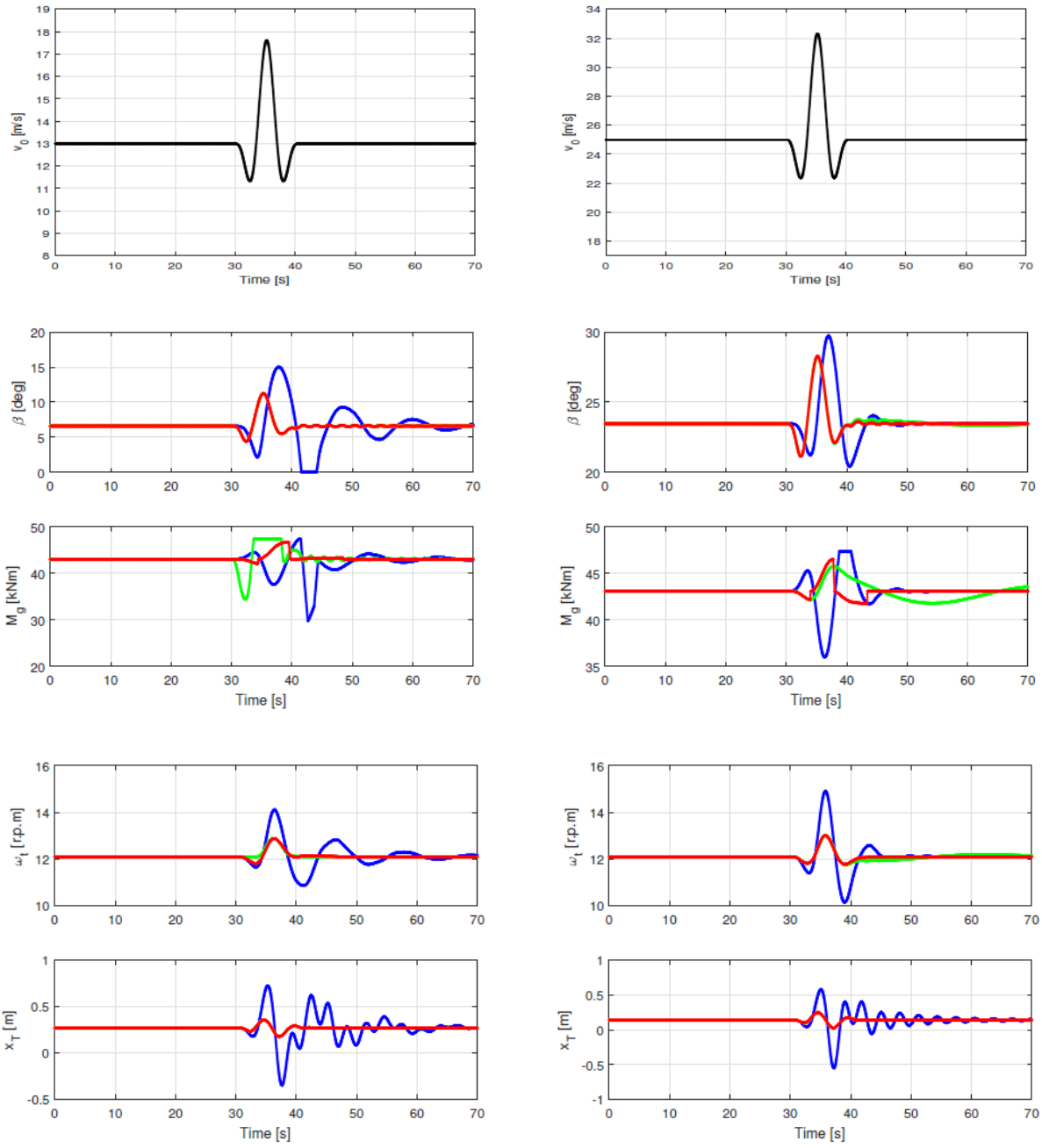

Figure 41. Reaction to an EOG at 13m/s (left) and 25m/s (right) in the case of perfect wind preview using the 5MW reference wind turbine. Simulated with reduced SLOW model: Baseline controller (blue), Non-linear GPI (green) and Non-linear GPI with reset (red).

5.2.3. Numerical results and discussions

In this section, the non-linear GPI pitch controller and the reset torque controller are compared with respect to a baseline controller. The control goal is to maintain

constant the rotor speed at 12 r.p.m, generator power at 5MW and to reduce structural loads.

In order to validate the performance of the proposed control methodology two Extremes Operating Gust signals (EOGs) -also known as ”The Mexican Hat”due to its shape- are applied according to Commission IE et al. [27] to the Simplified Low Order Wind Turbine SLOW model (SLOW) developed by Schlipf [101].

Figure 41 shows the reaction for EOG signals at 13 and 25 m/s, in the case of perfect wind preview using the 5MW reference wind turbine. Both the non-linear controller and the GPI non-linear controller with reset provide an active rejection of the perturbations, greater than the Baseline controller, ensuring that the rotor speed and the tower displacement recover their values quickly at a steady-state. However, the reset mechanism allows a rapid stabilization of rotor speed with considerable less control effort for both wind speed profiles. For the wind speed of 13 m/s the non-linear controller without reset reaches saturation and the generator torque M_g has sustained oscillations for the wind speed of 25 m/s. This situation does not occur if the reset mechanism is added since for both wind speed values the generator torque recovers rapidly after the rotor speed passes for through its nominal value.

5.2.4. Conclusions

In this section, a control scheme based on GPI and reset controllers for a nonlinear model of an offshore wind turbine is presented and numerically validated. The GPI controller's coefficients are calculated in a trivial form, with assumes global pole placement effort for the closed-loop dominant stability. The combination of the feedback controller and the observer works appropriately, and the extended observer design is not required. This approach could easily be amplified to simplify control of nonlinear, uncertain, and exogenously disturbed systems.

The proposed controller scheme for offshore wind turbines actively rejects disturbances, ensuring maximum efficiency in the wind energy system conversion. The 5MW reference wind turbine simulation results show that the nonlinear controller with reset mechanisms performs more efficiently than the baseline feedback controller for EOG at 13 and 25 m/s, in the perfect wind preview.

Finally, one of the main advantages of the GPI controller is that the tuning of the control parameters at different points of operation of the wind generation system is not required, however, the active disturbance rejection is guaranteed.

5.3. Numerical Case 3: Glucose Control in Type 1 Diabetes Mellitus Patients

Diabetes is a hard illness in which the body either cannot produce or appropriately use insulin. This disease causes high blood sugar levels, and thus could cause damage to the organs, blood vessels and nerves, and is considered the fifth cause of death worldwide after communicable diseases, cardiovascular diseases, cancer and injury [131].

Glucose regulation is a topic that has been studied for several decades, and different solutions have been proposed. With the appearance of new technologies in glucose sensing and insulin infusion, acting upon glucose levels using real-time measurements is now possible since the sampling period of most continuous glucose monitors (CGM) is 5 minutes or less [86]. Therefore, a technological effort focused on developing artificial pancreas systems to control insulin delivery has increased.

Due to the glucose-insulin system being a time-delayed process, the control design is more demanding since an additional phase lag is introduced, which limits the bandwidth and reduces the stability margin. In these cases, a greater effort of the compensator is needed to achieve the desired performance specifications, within the physical limits imposed by the time delay [42]. The well-known predictor of Smith has been the main method to treat such systems, since it can increase the closed-loop bandwidth by eliminating the effect of time delay in the closed-loop. The prerequisite is an accurate system model available; otherwise, the non-perfect time-delay cancellation in the loop can cause instability.

To deal simultaneously with not just one, but many performance specifications at the same time, including stability, reference tracking, disturbance rejection, actuator limitations, reduction of vibrations, noise rejection, etc. in the presence of uncertainty in the model, quantitative feedback theory (QFT) can be a powerful robust control design tool [41]. In [43] and [42] a Smith Predictor based on QFT is proposed to deal with processes with large delays and uncertainty. The method is applicable in the presence of uncertainty both in the model of the minimum phase part and in the time delay.

This section presents a methodology for the design of feedback controller and disturbances observer for a set of adult patients with type 1 diabetes by using the QFT technique.

5.3.1. Mathematical model of gluco-regulatory system

The well-known Bergman's model contains the minimal number of parameters and is widely used in physiological researches to estimate glucose effectiveness

and insulin sensitivity in the Intravenous Glucose Tolerance Test (IVGTT) [15]. This model represents the response of the blood glucose concentration to an intravenous glucose tolerance test and describes the behavior of glucose concentration in plasma, $G(t)$, and insulin concentration in plasma, $I(t)$, which are connected by an insulin-effect remote compartment denoted as $I_{is}(t)$:

$$\begin{aligned} \frac{dG(t)}{dt} &= -p_1\left(G(t)-G_b\right) - I_{is}(t)G(t) + d(t) \\ \frac{dI_{is}(t)}{dt} &= -p_2 I_{is}(t) + p_3\left(I(t)-I_b\right) \\ \frac{dI(t)}{dt} &= -nI(t) + u(t)/V_1 \end{aligned} \tag{5.48}$$

where G_b [mg/dL] and I_b [pmol/L] correspond to the glucose and insulin basal level, respectively. Intravenous glucose injection is defined as disturbance $d(t)$ and the actuating variable is the intravenous insulin infusion rate $u(t)$. Parameter p_1 represents the rate at which glucose is removed from the plasma. p_2 and p_3 are the fractional transfer coefficients of insulin in and out of the remote compartment where insulin action is expressed. n is the fractional disappearance rate of insulin and V_1 is an assumed intravenous insulin distribution volume. Fig. 42 illustrates a schema of mass transport according to Eq. (5.48). The continuous lines denote mass transports and the dashed line indicates the effect of one concentration on another.

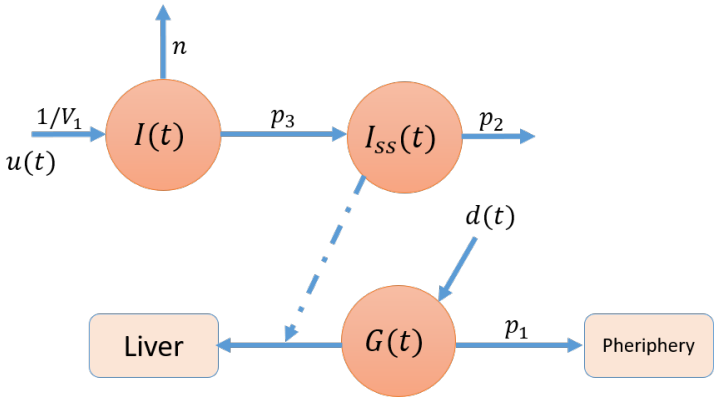

Figure 42. Schematic representation of Bergman's minimal model

The model formulated in [56], describes the carbohydrates catabolism to monosaccharide taking place during meal digestion, as well as intestinal absorption. The intravenous glucose injection, represented by a two-compartment chain with identical transfer rates $1/t_{max,g}$, is given by:

$$d(t) = \frac{D_g A_g t e^{-t/t_{max,g}}}{V_g t_{max,g}^2} \tag{5.49}$$

where D_g [g] is the proportion of carbohydrates consumed, A_g is the carbohydrate bioavailability, $t_{max,g}$ [min] the time-of-maximum presence rate of glucose in the available glucose compartment and V_g [L/Kg] is the partition volume of the available compartment (glucose distribution space).

Motivated by these simple glucose-insulin models, other approaches were proposed. Recently, in [99] the following linear parameter- variant (LPV) model from the subcutaneous insulin delivery $(pmol/min)$ to the subcutaneous glucose discrepancy (mg/dl) is presented:

$$G_j(s) = k_j \frac{(s+z)\, e^{-15s}}{(s+p_1)\,(s+p_2)\,(s+p_3)} \tag{5.50}$$

where $z = 0.1501$, $p_2 = 0.0138$ [min^{-1}], $p_3 = 0.0143$ [$min^{-2}/(pmol/L)$] and the dominant pole p_1 [min^{-1}] is a variant parameter as a function of glucose. When considering the inter-patient variability, the model was adjusted by means of the 1800 rule, obtaining a personalized gain k indicated by k_j [mg/dL].

5.3.2. Feedforward control design

Considering that the linear system (5.50) is controllable, its flat output, f, is given by:

$$f(s) = \frac{e^{-15s} u(s)}{(s+\bar{p}_1)\,(s+p_2)\,(s+p_3)} \tag{5.51}$$

Therefore, the plasma glucose is determined by the flat output by means of the following expression:

$$\hat{G}(t) = \bar{k}\left(\dot{f}(t) + z f(t)\right) \tag{5.52}$$

where $\bar{k}$ and $\bar{p}_1$ are parameters of average model of adult patients in the UVA/Padova simulator.

$$f^{(3)} = u_d - (p_1+p_2+p_3)\,\ddot{f} - (p_1p_3+p_1p_2+p_2p_3)\,\dot{f} - p_1p_2p_3 f \tag{5.53}$$

with $u_d(t)$ the input signal delayed, i.e. $u_d = u(t-15)$.

Letting $\xi(t) = -(p_1+p_2+p_3)\,\ddot{f} - (p_1p_3+p_1p_2+p_2p_3)\,\dot{f} - p_1p_2p_3 f$, the original problem is reduced to one defined on a simpler system, said to be in perturbed Brunovsky's canonical form:

$$f^{(3)} = u_d + \xi(t) \tag{5.54}$$

$\xi(t)$ is the disturbance signal that includes the depreciated dynamics and the effect of glucose ingestion.

A state extended observer or GPI observer (5.55) is designed for the system (5.54), which provides simultaneous estimations of the phase variables associated with the flat output f and of the disturbance $\xi(t)$:

$$\begin{aligned} \dot{f}_0 &= f_1 + \lambda_3(f - f_0) \\ \dot{f}_1 &= f_2 + \lambda_2(f - f_0), \\ \dot{f}_2 &= u_d + z_1 + \lambda_1(f - f_0) \\ \dot{z}_1 &= \lambda_0(f - f_0) \end{aligned} \tag{5.55}$$

where f_0 is the estimation of the flat output f, f_1 and f_2 are the first and second derivatives of f_0 and $z_1 = \hat{\xi}(t)$ is the disturbance estimation. To guarantee an establishment time close to 5 minutes of the estimation error, the observer gain parameters in equations (4.12) to (4.15) were set as: $T = 1.25$ [min], $\alpha_0 = 1$ and $\alpha_1 = 8$. As a result, the estimation error characteristic polynomial is defined by $p_{obs}(s) = s^4 + 349.6s^3 + 15280s^2 + 97780s + 78230 = 0$.

Based on equations (5.52) and (5.55) the derivative of glucose can be estimated by means of the following expression:

$$\hat{\dot{G}}(t) = \bar{k}\left[f_2 + (\lambda_2 + z\lambda_3)(f - f_0) + zf_1\right] \tag{5.56}$$

5.3.3. Feedback control design

Automatic regulation of blood glucose levels has competitive control objectives such as fast response for meal perturbations and CGM noise immunity. Since these commitments are very difficult to achieve with LTI controllers, multiple control structures have been proposed. In this work, a unique control scheme to regulate glucose in multiple adult patients with type 1 diabetes is presented. In order to validate the robust design methodology, the UVA/Padova simulator is used, which was included in the first simulator accepted by the U.S. Food and Drug Administration as a substitute to animal trials for preclinical testing of insulin therapies for T1D patients [67, 68].

For the robust controller design, the Smith predictor and observer parameters in Fig. 43 are set for the average adult model of the UVA/Padova. By considering high uncertainty and intra-patient parametric variation the quantitative feedback theory is used to satisfy the desired performance specifications. If the feedback control scheme of Fig. 28 and equation (4.21) are considered, the equivalent plant with uncertainty (that contains the predictor, observer, the model of the glucose metabolic process in the patient, the CGM sensor and the insulin pump) is obtained.

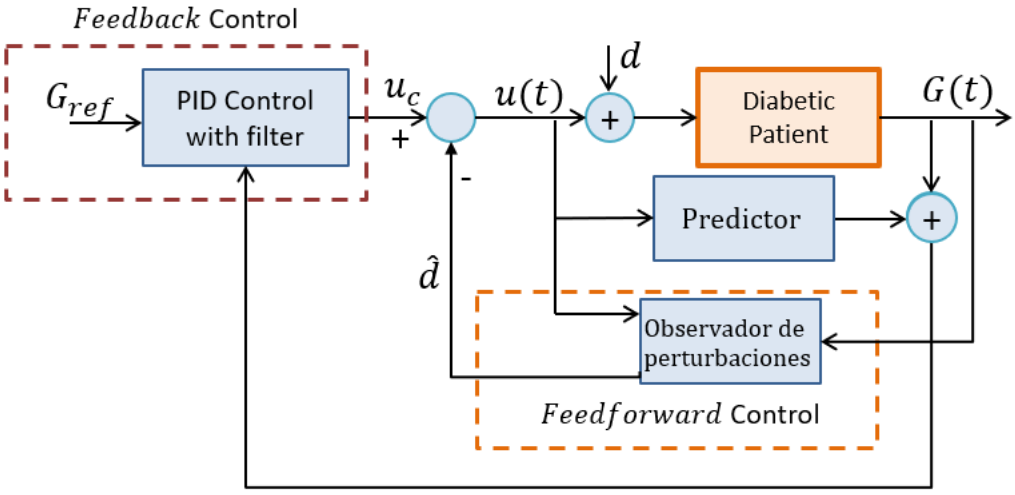

Figure 43. Block diagram of the robust control approach for closed-loop Artificial Pancreas

Definition of robustness specifications

As a frequency-domain methodology, QFT works with a vector of frequencies of interest. Based on the families of equivalent-plants generated from the definition of the parametric uncertainty and by inspection of the Bode diagram, the following vector of working frequencies is defined: $w = [0.0003, 0.04, 0.4, 1]$. For the glucose regulation system an adequate glucose level in the patient in the presence of strong disturbances due to food intake is required. Considering the benefits of the disturbance observer, robust stability specifications and reference tracking can be defined for the feedback controller design.

In order to obtain a phase margin around $30.5°$ a $\delta_U = 1.9$ is set in the robust stability specification in eq. (4.30). For blood glucose response to meal the following references tracking specifications have been considered:

$$\begin{aligned} T_U(s) &= \frac{7.744 * 10^{-5}(10s+1)}{s^2 + 0.0264s + 4.84 * 10^{-4}} \\ T_L(s) &= \frac{0.16}{(40s+1)(50s+1)(60s+1)} \end{aligned} \tag{5.57}$$

These frequency specifications correspond to a closed loop time constant between 65 and 95 minutes.

The controller design by loop-shaping is carried out on the Nichols chart. The bilinear transformation, z-domain to the w'-domain and vice versa, is used in order

to accomplish the QFT design for discrete control system design in the w'-domain. If the simulations satisfy the desired performance specification, then due to the bilinear transformation, the z-domain controller $K(z)$ is obtained [55]. However, the non-minimum phase (n.m.p.) characteristic of a w'-domain plant transfer function requires an all-pass-filter to apply the QFT technique. When it has a small practical sampling period a *pseudocontinuous*-time (PCT) representation of a sampled-data system can be used.

Fig. 44 shows the QFT bounds and the loop shaping of $K(s)$ for the obtained PTC system. It is done by adding poles and zeros until the nominal loop lies near its bounds. The proposed PID controller appropriately meets all the bounds and the discrete transfer function is given by the following expression:

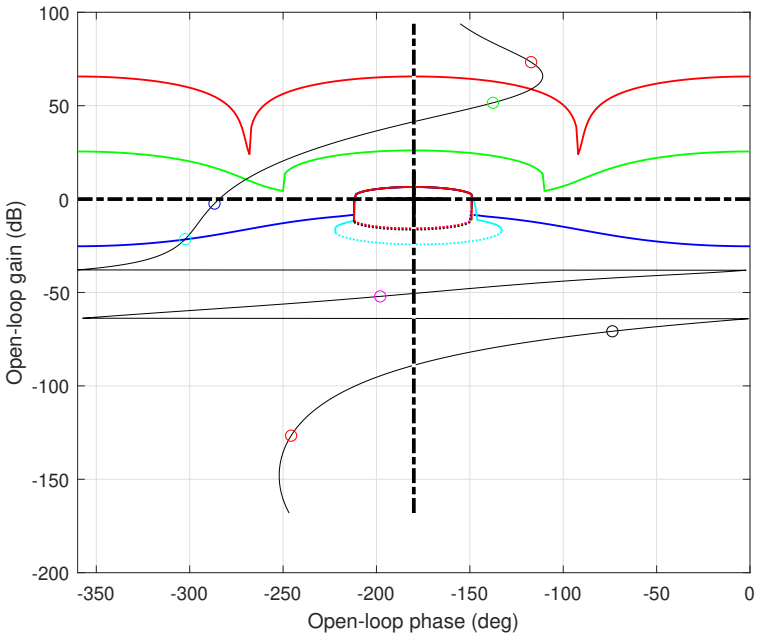

Figure 44. QFT-bounds and $K(s)$ design-loop-shaping

$$K(z) = K_p + K_i T_s \frac{1}{z-1} + K_d \frac{N}{1 + N\frac{T_s}{2}\frac{z+1}{z-1}} \tag{5.58}$$

where $K_p = -0.01767$, $K_i = -6.9872 * 10^{-5}$, $K_d = -1.1067$, $N = 1.13024$ and $T_s = 5$ [min].

Taking into account the controller $K(z)$ defined in equation (5.58), the reference tracking specifications presented in (4.32), and the equivalent plant model presented in (4.21), a prefilter $F(z)$ assures that all the input/output function $FKP_{eq}/(1 + KP_{eq})$ are inside the band defined by the limits $T_U(\omega)$ and $T_L(\omega)$. The prefilter is shown in (5.59), and the input/output functions and limits in Fig. 45.

$$F(z) = \frac{7.63z + 7.278}{z^2 - 1.859z + 0.8681} 10^{-4} \tag{5.59}$$

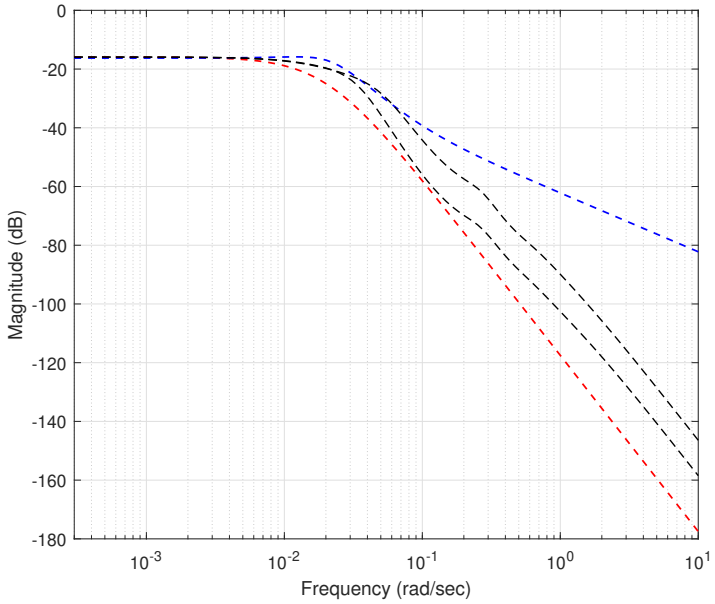

Figure 45. Prefilter for reference tracking specification.

Anti-windup mechanism

To overcome the limitations of simple LTI controllers, the inclusion of a non-linear scheme is proposed, as shown in Fig. 46. The structure consists of an anti-windup stage with an inner-loop around the integral part for the actuator saturation. Also two switches are added to control insulin infusion and avoid hypoglycemic events. The first switch allows the suspension of insulin when glucose values are lower than basal glucose, i.e. $\Delta G = G(t) - G_b < 0$. The second switch is used to limit the insulin application provided by the controller only when there is a positive derivative in the measured or estimated glucose. This ensures that the pump only delivers insulin when there is an increase in glucose due to meal intake, otherwise the infusion will be suspended.

5.3.4. Numerical validations and analysis

The analysis of the closed-loop stability in the frequency domain is shown in Fig. 47. The dashed line is the stability specification δ_U defined in equation (4.30). The solid line represents the worst case of all the possible functions $KP_{eq}/(1 + KP_{eq})$ at

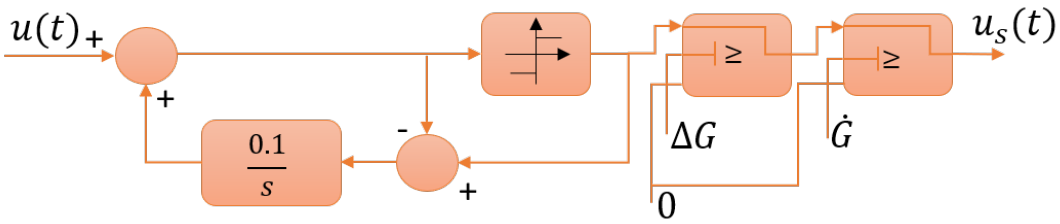

Figure 46. Nonlinear dynamic control structure

each frequency due to the model uncertainty. The control system meets the stability specification (the solid line is below the dashed line δ_U) for all the plants within the uncertainty.

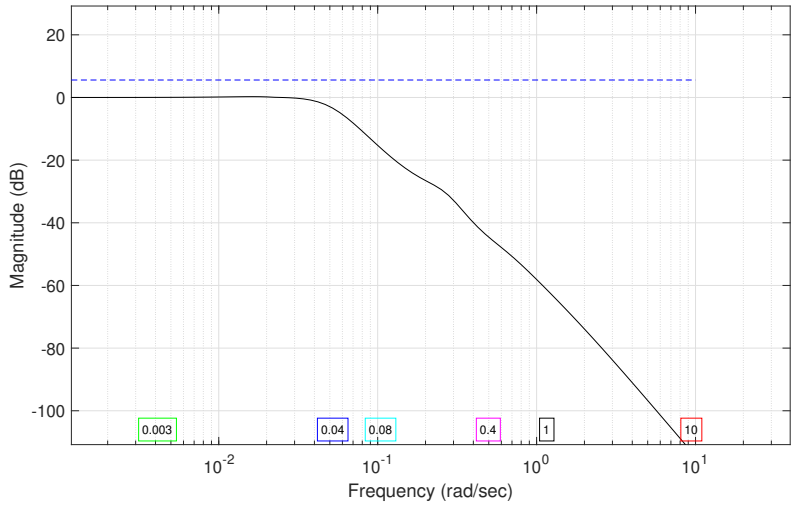

Figure 47. Stability analysis, frequency domain: δ_U specification (dashed line), and worst case of $KP_{eq}/(1+KP_{eq})$ within the uncertain plants at each frequency (solid line).

Test 1: Three meals

Prior to the clinical trial, the algorithm must be meticulously tested *in silico*. In this researcher, some results are shown considering the following points: *i*) the complete *in silico* adult cohort of the 10 subject FDA accepted UVA/Padova simulator, a CGM as sensor, and a CSII pump; *ii*) all meals contain 90 g of carbohydrates; *iii*) The first meal that is shown in simulation for each *in silico* subject is dinner.

Fig. 48 shows the results of blood glucose for the 10 adult patients. It can be validated that in none of the cases there are hypoglycemia levels.

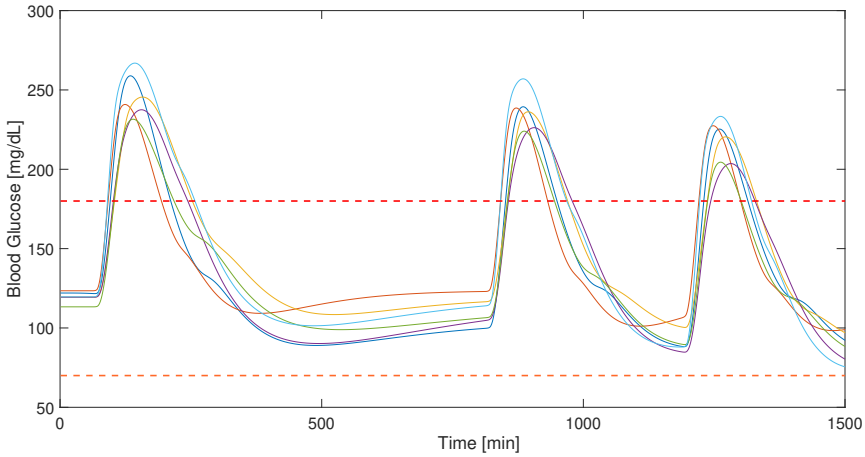

Figure 48. Proposed predictive.observer-based control using UVA/Padova simulator

Test 2: Two protocols

A second way to validate the robust controller designed for the complete cutting of patients was using two meal protocols presented in [26]. In Protocol #1 a high quantity of meal is considered, while protocol #2 presents fasting bands.

In this trial, the fasting phase of each patient is considered at the beginning of the simulation. In addition, a postprandial period (PP) and one night (N) are defined as the time interval of 5 hours following the start of a meal, and the period from midnight to 7:00 a.m., respectively [26]. Response times for the ten patients to both protocols are depicted in Fig. 49. It can be seen that the designed predictive feedback-feedforward controller does not show hypoglycemia levels in any of the cases.

5.3.5. Conclusions

In this section, a robust control strategy for the artificial pancreas problem for a set of adult patients was presented. A linearized model with uncertainty is used for designing a linear state controller using loop-shaping, joint to a feedforward controller based on GPI observer that simultaneously estimates states and disturbances. A safety stage is added to regulate the amount of insulin once the blood glucose concentration begins to decrease. This fact avoids low late postprandial levels and hypoglycemic events and enables a safer closed-loop control. The most significant advantage of this glucose regulation structure is that it does not require an individualized design of the controller for each patient, but rather a single controller is obtained for the set of adult patients. *In silico* results showed exemplary behavior in all patients in different trial tests.

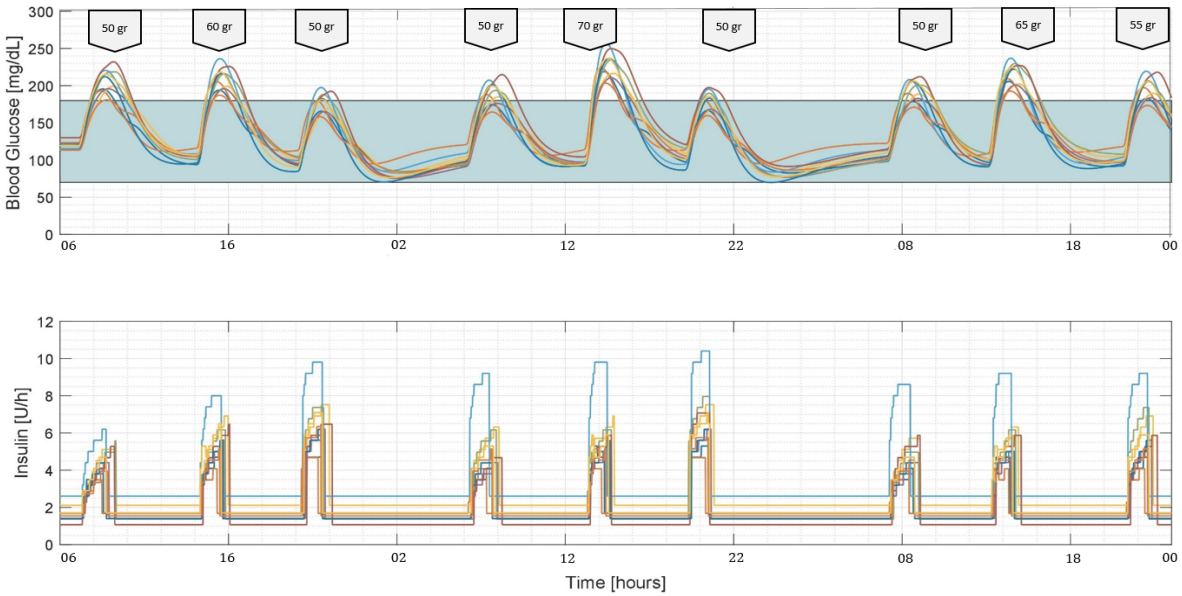

(a) Protocol 1

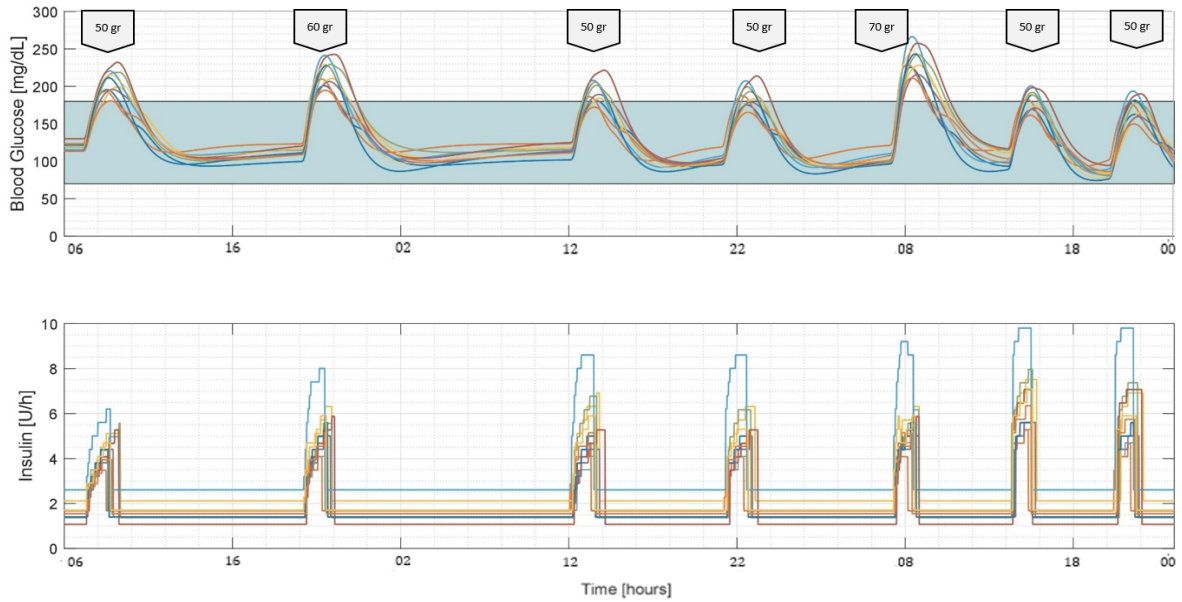

(b) Protocol 2

Figure 49. Closed-loop responses for all the *in silico* adults (complete UVA/Padova simulator) to protocol#1 and to protocol#2.

6. EXPERIMENTAL VALIDATION

This chapter validates the experimental implementation of the control scheme proposed in this doctoral thesis in a full-scale Raceway photobioreactor. For the description of this experimental case, all the information published by the author in [21] has been taken. Experimental validation required the use of MATLAB software.

6.1. Experimental Case: Raceway Photobioreactor

Since the 50's, the study of raceway-type photobioreactors has grown profoundly intending to present industrial-scale solutions for the microalgae culture. Due to its scalability and ease of cultivation, it is considered the most suitable production technology for the industrial of microalgae culture. Furthermore, this type of photobioreactor is preferred due to its low initial investment, simple operation, and low maintenance costs, compared to tubular-type photobioreactors [123]. This fact allows the use of raceway photobioreactors for the production of biofuels from microalgae biomass.

In this process, in addition to solar irradiance and temperature, pH can be considered the most important variable that influences the photosynthesis process in a photobioreactor. The CO_2 modifies the pH value since it changes the acidity of the microalgae growth medium. Thus, different control schemes are present to manipulate this variable to regulate the pH level. Basic on-off controllers usually regulate the pH conditions due to their simplicity and the lack of dynamic models. On the other hand, PID and feedforward controllers have shown effective results in reducing the influence of disturbances (i.e., radiation) on the pH tracking [30, 33]. Other control structures with beneficial results in photobioreactors are the predictive control [14, 32, 129], event-based approach [88, 89] and model-free control [120].

This section describes a robust output feedback scheme, based on two-degrees-of-freedom proportional-integral (PI) control and GPI observer for the active disturbances rejection in a Raceway type photobioreactor. This novel scheme approximately determines the non-linearities and exogenous and endogenous perturbations, using the GPI observers, which include internal models represented by polynomials in time and whose updating is automatic, allowing approximations arbitrarily close to the perturbations unknown. Unlike state feedback control based only on GPI observers, the inclusion of a 2-DOF proportional-integral controller guarantees the robust-

ness of the closed-loop control system using only the maximum sensitivity as the design parameter.

6.2. Microalgal bioreactor: Operating principle

A Raceway reactor is a continuous flow system made up of a recirculation channel, usually about 0.3 m deep. Nutritious fertilizer is added into these channels, and the crop is agitated with a paddle wheel. Although different types of open reactors have been put into operation during the last decades, the most widely used photobioreactors include large shallow ponds, tanks, circular ponds and ponds with channels [127].

The photobioreactor used in this research is placed at the Estación Experimental Las Palmerillas in Almeria (Spain). It has a total surface area of 100m^2, and two 50m channels, joined by U-shaped curves (see Fig. 50). The entire reactor is made of white 3mm thick fiberglass and operates at a constant depth of 0.2m to ensure desired performance, and taking into account power consumption issues, provides a capacity of 20 m^3 of medium (Fig. 50). The fluid circulates through a marine plywood paddle-wheel, with eight paddles with 1.2m diameter, activated by an electric motor with gear reduction and speed control using a frequency inverter [88].

The photobioreactor can be separated into three fundamental parts: paddlewheel, channels and sump. Consequently, three pH-T and dissolved oxygen probes (5083 T and 5120, Crison, Barcelona, Spain) were placed at the end of each of these sections, connected to transmitters (MM44, Crison, Barcelona, Spain). On a scheduled basis, air or CO2 is supplied to the bottom of the sump using a diffuser to control dissolved oxygen and pH of the culture. The gas flow into the photobioreactor is measured with a mass flow sensor (PFM 725S-F01-F, SMC, Tokyo, Japan) [31].

6.3. Dynamic model of photobioreactor

The average irradiance strongly influences the growth rate of the microalgae (I_{av}) received by the cells [1]. This variable is modeled as a function of the biomass density (C_b), the total incident radiation on the reactor surface (I_o), the light decrease of the biomass (K_a) and the light path or culture depth (h) [46]. By considering the variation of the amount of biomass with time, *t*, and the location along the reactor, *x*, the average irradiance in any region of the photobioreactor could be computed using the following equation:

$$I_{av}(t,x) = \frac{I_0(t)}{K_a C_b(t,x)h}\left(1 - e^{(-K_a C_b(t,x)h)}\right) \tag{6.1}$$

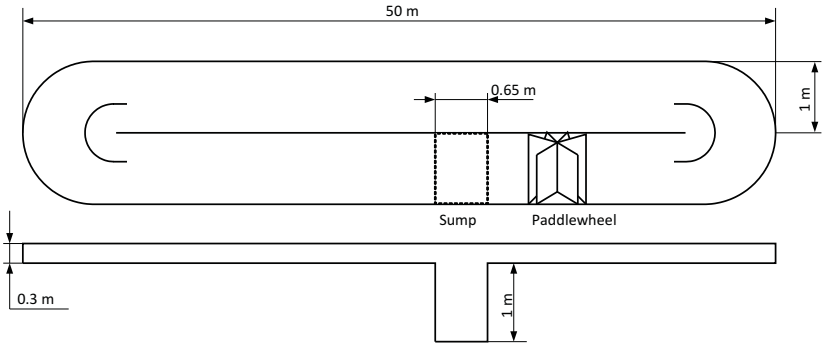

(a) Top and side views of the photobioreactor

(b) Experimental facilities

Figure 50. Raceway Photobioreactor

The photosynthesis ratio (P_{O_2}), described as the oxygen composition rate per biomass mass unit, could be calculated as a function of dissolved oxygen concentration $[O_2]$, average irradiance and pH into the culture, by the subsequent equation:

$$P_{O_2}(t,x) = (1-\alpha_s)\,\frac{P_{O_{2,max}} I_{av}(t,x)^n}{K_i e^{I_{av}(t,x)m} + I_{av}(t,x)^n}\cdot$$
$$\left(1-\left(\frac{[0_2](t,x)}{K_{O_2}}\right)^z\right)\left(B_1 e^{\frac{-C_1}{pH(t,x)}} - B_2 e^{\frac{-C_2}{pH(t,x)}}\right) - \alpha_s R_{O_2} \tag{6.2}$$

where $P_{O_{2,max}}$ is the upper limit of the photosynthesis rate of microalgae under optimal conditions, R_{O_2} is a dissolved oxygen release coefficient, *n* is the exponent of the average radiation function, K_i, m and z are form coefficients and K_{O_2} is the oxygen inhibition constant. As the shadow influences the rate of photosynthesis, it is

described by a dispersed factor α_s in each cross-sectional surface. For the pH effect on the photosynthesis rate, C_1 and C_2 are the activation energies of the Arrhenius model, and B_1 and B_2 are the preexponential components [28].

Additionally, the carbon dioxide uptake, P_{CO_2}, could be described as a one-to-one molar proportion between oxygen and carbon dioxide [96], from a basic equation of photosynthesis, as follows:

$$P_{CO_2}(t,x) = -P_{O_2}(t,x) \tag{6.3}$$

Additionally, by regarding an average value of oxygen coefficient yield, Y_{b/O_2}, the resulting biomass could be calculated by the following equation:

$$P_b(t,x) = Y_{b/O_2} P_{O_2}(t,x) \tag{6.4}$$

The injection of CO_2 directly influences the pH, changing the acidity of the microalgae culture. To guarantee a high rate of photosynthesis, the optimal pH is between 7.0 and 9.0, with no significant photosynthesis rate variation being measured in this range. Considering this fact, it is feasible to implement a control law to keep the pH around 7.7 employing CO_2 injections to change its value [89].

Linear model for control design

To propose a control law, this study uses a perturbed linear model at the operating point. As is well known, the pH of the culture is highly dependent on the supply of CO_2 and solar radiation. The CO_2 injected contributes to the generation of carbonic acid and causes a decrease in the pH of the culture. Besides, in the presence of irradiance, the microalgae carry out photosynthesis, a process in which the culture absorbs CO_2 and produces O_2, thereby causing a gradual increase in pH. However, the rise of solar radiation produces variations in the rate of photosynthesis, causing an expansion of the pH rate [88].

The process dynamics could be depicted by a simplified linear model considering the following statements:

- The process control variable is the pH of the culture.
- The opening of the flue gas injection valve is the manipulated variable.
- The solar irradiation is the primordial perturbation of the system.

The following expression represents the linear model describing the pH level as a function of the irradiance and the CO_2 injection input around a operation point [88]:

$$pH(s) = \frac{k}{\tau s + 1} e^{-\lambda s} u(s) + \frac{k_r}{\tau_r s + 1} I(s) \tag{6.5}$$

where pH is the pH level of the culture, u is the amount of CO_2 injected or control signal, and I is the solar radiation. $k = -0.228\ [pH]$, $\tau = 158.5\ [min]$ and $\lambda = 2.98\ [min]$ are the gain, time constant and delay of the transfer function from CO_2 to pH, and $k_r = 0.0007\ [pH]$ and $\tau_r = 1903\ [min]$ are the gain and time constant of the transfer function from irradiation to pH. Figure 51 shows two examples of the model validation obtained around the operating point of the system and with respect to a unit step input signal. Notice that a fit greater than 80 % is obtained in both cases.

6.4. GPI observer design

Taking into account that the time delay of the transfer function from CO_2 to pH is much smaller than the time constant of the system, equation (6.5) can be approximated by the perturbed first order equation defined as:

$$\dot{y} = ku(t) + \xi(t) \tag{6.6}$$

In order to estimate the disturbance, the following GPI observer is defined:

$$\begin{aligned} \dot{\hat{y}} &= ku(t) + z_1 + \lambda_3(y - \hat{y}) \\ \dot{z}_1 &= z_2 + \lambda_2(y - \hat{y}) \\ \dot{z}_2 &= z_3 + \lambda_1(y - \hat{y}) \\ \dot{z}_3 &= \lambda_0(y - \hat{y}) \end{aligned} \tag{6.7}$$

where $z_1 = \hat{\xi}(t)$ is the estimated external perturbation (joint effect of the solar radiation and the non-modelled dynamics).

By selecting the coefficients λ_i, it is possible to obtain the estimation error characteristic polynomial defined by:

$$p_{obs}(s) = s^4 + \lambda_3 s^3 + \lambda_2 s^2 + \lambda_1 s + \lambda_0 = 0 \tag{6.8}$$

The coefficients $\lambda_0 ... \lambda_3$ are calculated using the methodology in [64] described in the previous section.

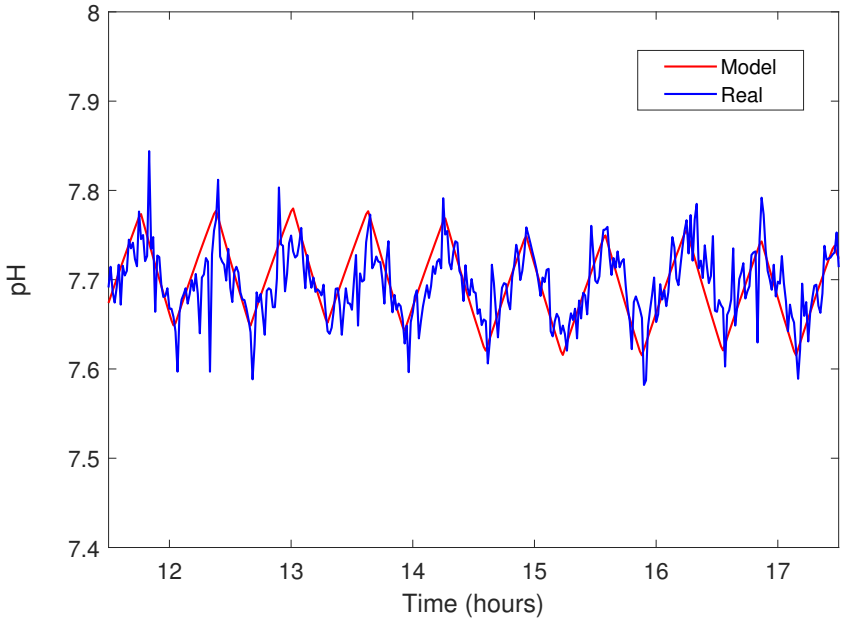

(a) Validation around the operating point

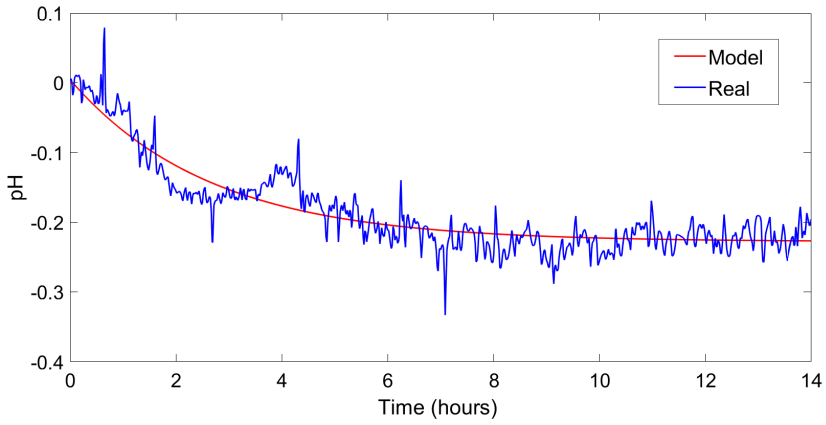

(b) Step response validation

Figure 51. Model validation examples

6.5. Feedback controller design

In Figure 52 the control system that includes disturbance observer implemented in this work is illustrated. $P_{eq}(s)$ is the equivalent plant of both plant and observer.

If a linear model without parametric uncertainty is considered, the equivalent plant model corresponds to the model of the plant without observer [23]. In this case $P_{eq}(s) = P(s)$, where $P(s)$ is the transfer function from the amount of CO_2 injected to pH level of the culture, defined in (6.5). This allows the observer's design to be done

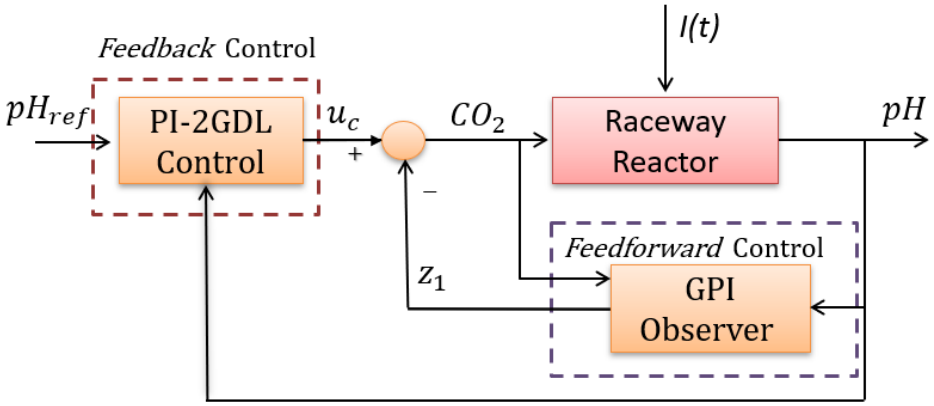

Figure 52. Two-degrees-of-freedom closed-loop control system

independent of the tuning of the controller parameters.

Using the process model gain, k, the time constant, τ, and the transformation $\hat{s} = \tau s$, the transfer function from the variation of CO_2 to the *pH* could be presented in a normalized form as follows:

$$P_{eq}(\hat{s}) = P(\hat{s}) = \frac{1}{\hat{s}+1} e^{-\tau_L \hat{s}} \tag{6.9}$$

where $\tau_L = \lambda/\tau$ is the time delay of the normalized model

The control law for the normalized process is given by:

$$u_c(\hat{s}) = \hat{k}_p \left[\beta r(\hat{s}) - y(\hat{s}) + \frac{1}{\hat{\tau}_i \hat{s}} (r(\hat{s}) - y(\hat{s})) \right] \tag{6.10}$$

where,

$$K_p = \frac{\hat{k}_p}{k}, T_i = \hat{\tau}_i \tau \tag{6.11}$$

Solving the optimization problem (4.50), the resulting normalized controller parameters can be expressed by the expressions (6.12), (6.13) and (6.14) as functions of the controlled process normalized model (6.9) and the target robustness level [3]:

$$\hat{k}_p = \frac{a_0 + a_1 \tau_L}{a_2 + a_3 \tau_L + a_4 \tau_L^2 + a_5 \tau_L^3} \tag{6.12}$$

$$\hat{\tau}_i = \frac{b_0 + b_1 \tau_L}{b_2 + b_3 \tau_L + b_4 \tau_L^2 + b_5 \tau_L^3 + b_6 \tau_L^4} \tag{6.13}$$

$$\beta = c_0 + c_1 \tau_L + c_2 \tau_L^2 + c_3 \tau_L^3 \tag{6.14}$$

The coefficients a_i,b_j y c_k are a function of the maximum sensitivity specified in the optimization problem.

6.6. Experimental results and discussions

This section shows the simulation and experimental results using the presented GPI observer coupled with the 2DOF Proportional Integral controller to regulate pH in raceway photobioreactors. The first step is concentrate on pH process modeling to obtain the dynamical response to input variables. A linearized model around the operating point was used for controller design purposes.

In this research, the photobioreactor was programmed to utilize flue gases, as shown in Figure 53. The distribution was adjusted by a solenoid ON/OFF valve, which is switched automatically using a consistent control algorithm. Regardless of the control structure, the solenoid valve is operated with the PWM (Pulse Width Modulation) technique, so that the control signal is transformed into a pulse train of variable width [88]. This actuator limits the volumetric flow rate of CO_2 between 0 to 5 L/min.

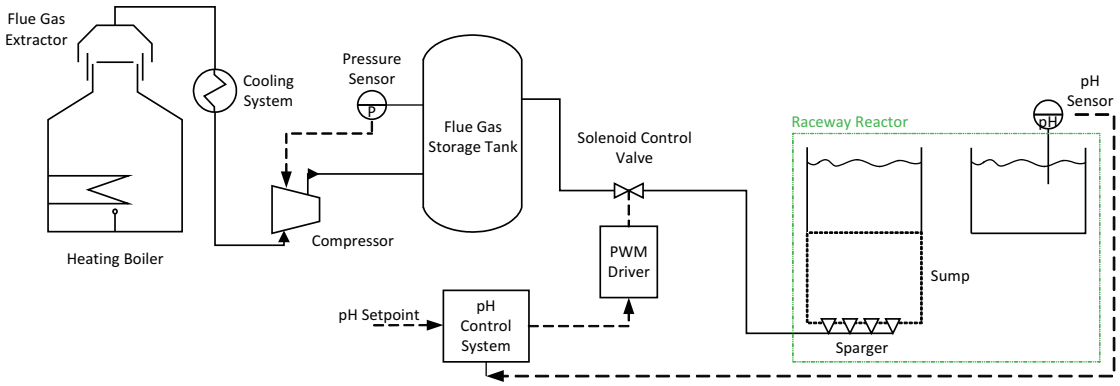

Figure 53. Control system of pH

The robust controller was experimentally validated at real conditions on a raceway photobioreactor in a 7-day period in Almería (Spain) in winter 2017 (on December 20 and 21, 2017 and January 12 to 16, 2018). During this stage the microalgae culture system was exhibited to different solar irradiance profiles, thus the proposed Linear Active Disturbance Rejection Control (LADRC) approach was adequately evaluated.

In order to obtain a phase margin greater than 42° and a minimum gain margin of 1.71dB (this is a robustness given by $M_s = 1.4$), the constants of equations (6.12), (6.13) and (6.14) were selected as shown in Table 9 [3]. The proposed control law, which combines the active disturbance rejection approach with the robust two-degree freedom PI control, was defined by the following equation:

$$u(s) = K_p \left[\beta r(s) - y(s) + \frac{1}{T_i s} e(s) \right] - \frac{1}{k} z_1 \tag{6.15}$$

Table 9. Robust tuning coefficients

j	a_j	b_j	c_j
0	0.7253	-0.1606	0.5049
1	0.6505	47.67	0.8330
2	0.0023	4.166	-0.1034
3	2.143	30.23	0
4	1	7.973	- - -
5	0	-4.738	- - -
6	- - -	1	- - -

Therefore, to guarantee a time constant approximately 25 times lower than the process time constant the observer gain parameters for the observation error were set as: $T = 6$ [min], $\alpha_0 = 4$, $\alpha_1 = 4$ and $m = 3$. Therefore the estimation error characteristic polynomial is defined by $p_{obs}(s) = s^4 + 9.105s^3 + 20.72s^2 + 13.82s + 2.303 = 0$. Although the dynamics of the observer can be made faster, the constraints of the actuators must be considered to avoid saturation. The robust controller was started using a 1-min sampling time.

Figure 54 shows experimental results for 7 days with profiles of sunny and cloudy environment and a pH set-point fixed on 7.7. CO_2 injection is not authorized during the night since microalgae carry out the respiration process absorbing oxygen and generating CO_2. In this case, the control signal is deactivated and the reference and the output are superimposed. However, this is not a problem since the pH level depends on the solar irradiation (no present in this part of the day), which influences the rate of photosynthesis.

In order to validate the performance of the controller, two specific experimentation days were selected (See Fig. 55). The sixth day corresponds to a sunny day, without significant changes in solar irradiance. The LADRC scheme guarantees a suitable set-point tracking, mitigating the perturbations induced by the solar radiation profiles and variations in the pH due to the environment's carbon value (acting as a non-measurable perturbation). The GPI observer considers the linear model of the system and predicts measurable and unmeasurable disturbance using a radically new perspective in state estimation, based on differential algebra. The 2DOF proportional-integral controller ensures the robustness level for pH control purposes using the maximum sensitivity as specification.

The first experimental day was very cloudy, but despite the energetic disturbances associated with the appearance of clouds that suddenly generate abrupt changes in

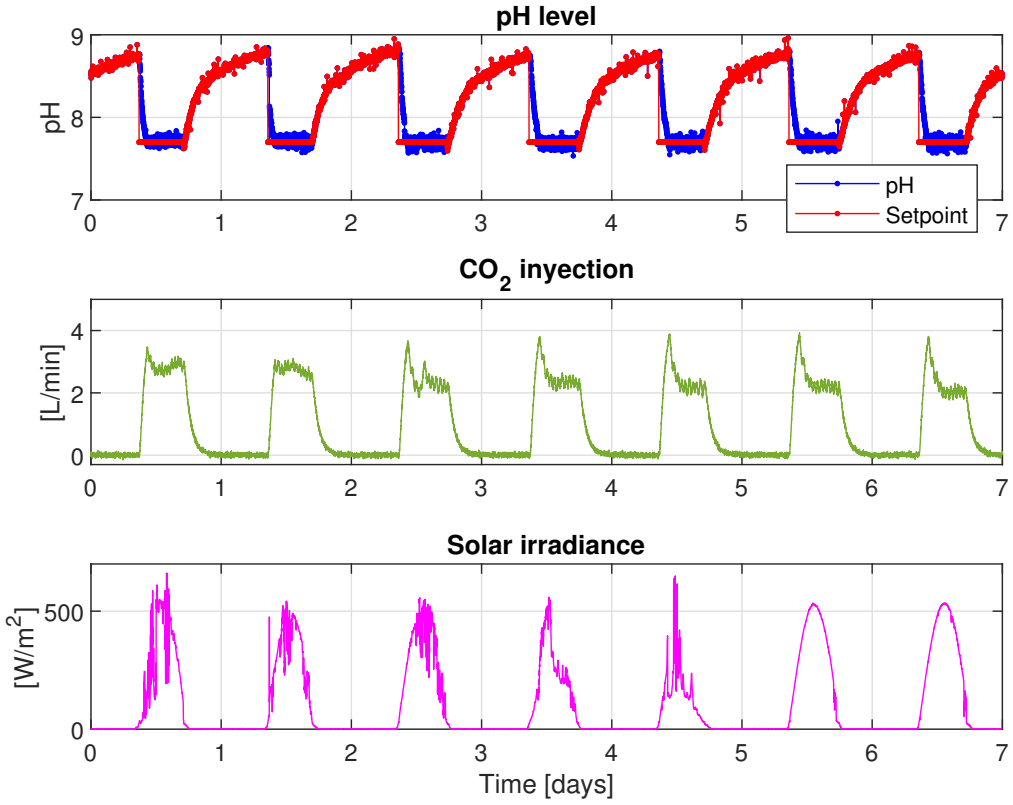

Figure 54. Experimental results of the robust LADRC for seven days

solar radiation, the robust controller performed well. Based on the experimental results, it could conclude that the controller can significantly mitigate the perturbance effect. This fact is due to the GPI observer estimates the disturbance and the unknown dynamics of the control system, and suppresses its effect by complementing the control law with a cancellation effort. In all cases, the CO_2 injection is maintained in the range of work of the valve (0 to 5 L/min), i.e., at no time were impulsive peaks due to the performance of the high gain disturbances observer.

On the other hand, to contrast the operation of the suggested controller with a controller commonly used in microalgae production, simulation results are shown in Figure 56. For this purpose, a PI controller coupled to a feedforward disturbance compensator is tuned. The simulations were executed using the non-linear model of the photobioreactor implemented and developed in the simulator described in [31]. The irradiance values used in the simulation correspond to measurements taken at the Las Palmerillas experimental station during a sunny day and a cloudy day.

The PI feedback controller was tuning in accordance with the SIMC (Skogestad Internal Model Control) design rule [113], resulting parameters $K_p = -5.69$

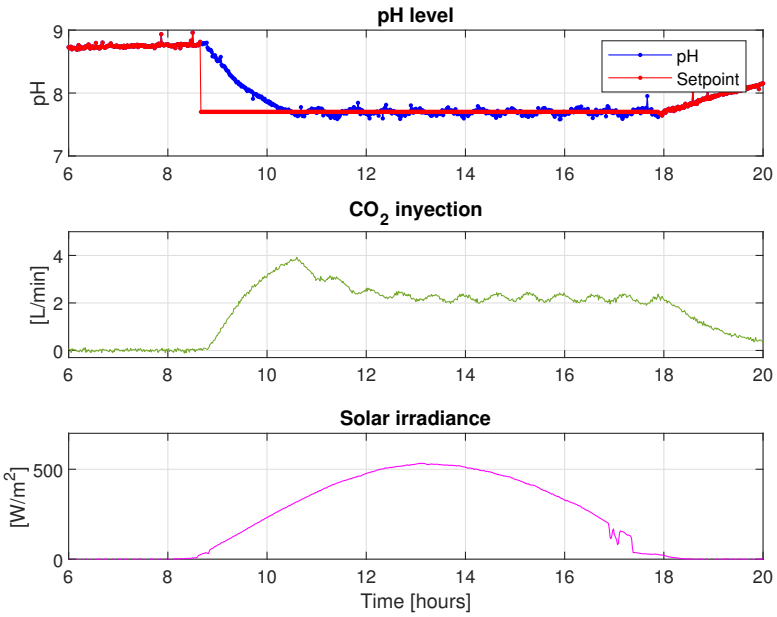

(a) Sixth day: sunny day

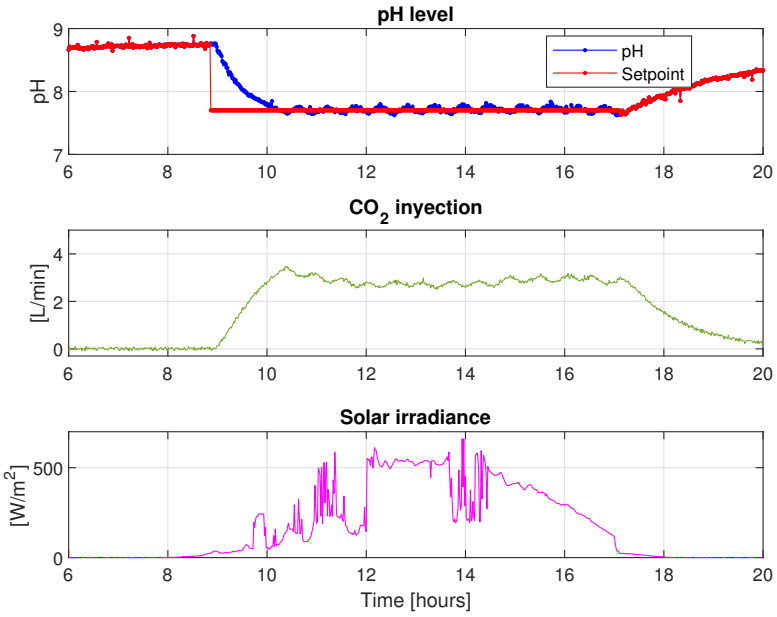

(b) First day: cloudy day

Figure 55. Robust LADRC details for first and sixth day

and $T_i = 232.4$ min. An anti-windup [6] was added to handled with the control signal saturation. For this purpose, a time constant $T_t = 116$ min has been tuned

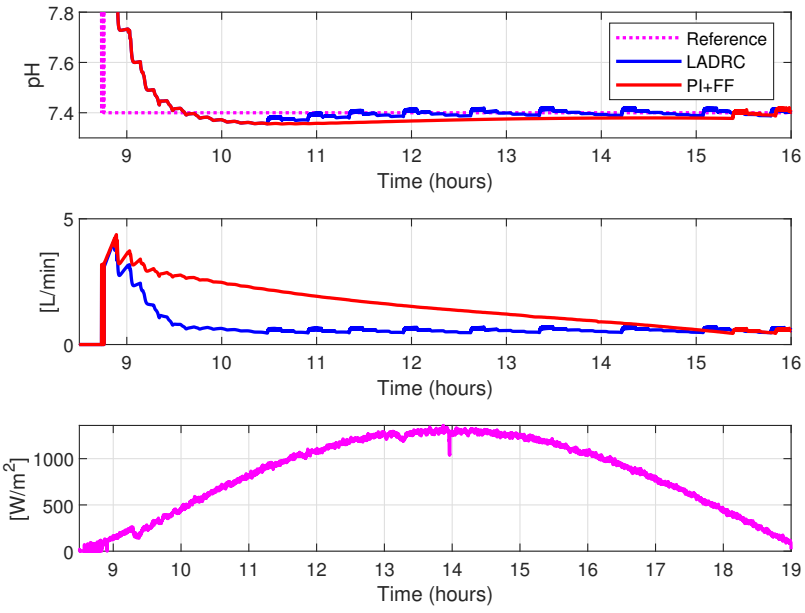

(a) Simulation on sunny day

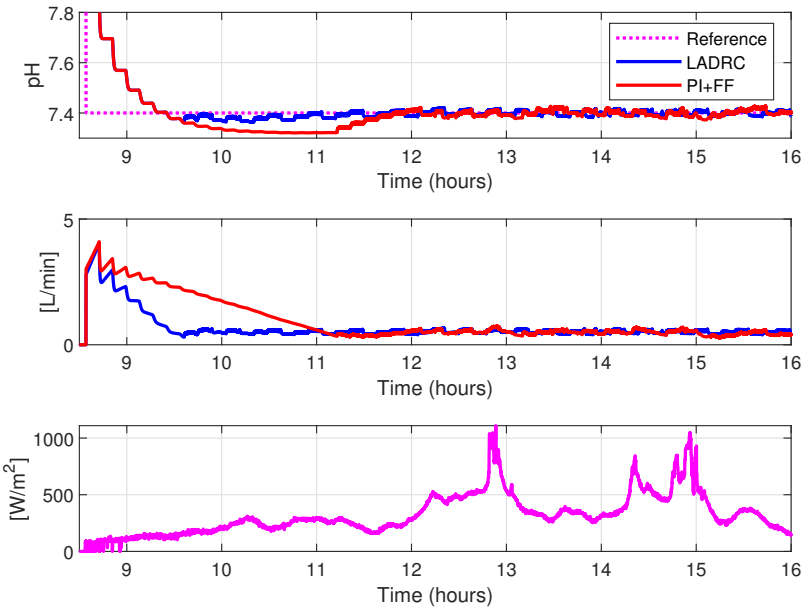

(b) Simulation on cloudy day

Figure 56. A comparative between PI+FF and LADRC

to reset the integrator. The feedforward disturbance compensation was obtained using the metodology presented in [87], obtaining the following transfer function: $C_{ff}(s) = -(0.0412s + 6.69 * 10^{-4})/(123.4s + 1.86)$, where the non-realizable part was neglected due to the time-delay reversal problem. All controllers have been executed with sampling time $T_s = 1$ min.

Both validated control schemes can fix the pH level close to its reference (Figure 56). Nevertheless, the configurations using the GPI observer provides greater quickness and precision. While the PI+Feedforward controller guarantees an establishment time of 185.9 min for the cloudy day and 397.7 min for the sunny day, the LADRC scheme guarantees establishment times of 71.2 and 129.5 min, respectively.

Table 10. Performance indexes for feedforward PI controller and LADRC scheme for a sunny day and a cloudy day.

2*Control scheme	Cloudy			Sunny		
	IAE	IAU	CSE	IAE	IAU	CSE
PI+CFF	262.96	5553	3.80	252.12	9175.7	7.24
LADRC	197.55	4065	4.58	172.95	4975.7	7.14

In addition, Table 10 shows three performance indices for the two controllers: the Integrated Absolute Error (IAE), the Integrated Absolute Control signal (IAC) and the Control System Effort (CSE). These indices were calculated using the following expressions:

$$\begin{aligned} IAE &= \int_0^\infty |e(t)|dt \\ IAC &= \int_0^\infty |u(t)|dt \\ CSE &= ||\Delta u(t)|| \end{aligned} \tag{6.16}$$

The IAE index indicates that the best precision, for the two days inspected, is achieved with the LADRC scheme. Besides, the LADRC structure delivers the lowest IAU value, being the most efficient in the use of control resources. The increased accuracy of that control scheme based on GPI observers is achieved at the cost of higher control signal variability, shown by the CSE index, where LADRC provides the highest value. However, based on the results obtained in the performance indexes, the LADRC uses the least amount of combustion gases of all the configurations tested, being the most efficient in terms of energy consumption.

On the other hand, the amount of uncertainty can be reduced through active disturbance rejection, implemented on an inner loop to produce a well-behaved plant,

which is then regulated by the robust PI controller in the outer loop. Figure 57 shows the bode plot of the plant transfer function assuming parametric uncertainty for K and T of 50 $\%$ around the operation point, and it also shows the plant bode diagram with GPI observer. It is observed that the effect of the parametric uncertainty is considerably reduced by adding a disturbance observer, which allows to obtain greater robustness in terms of the photobioreactor model parameter variations.

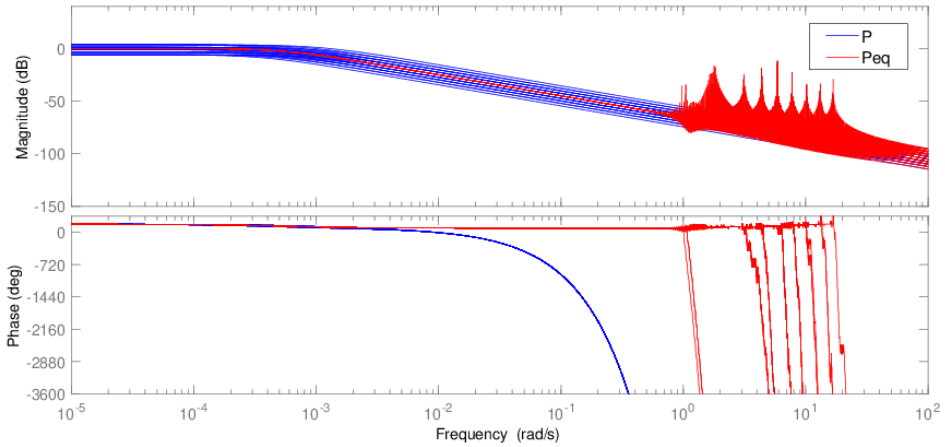

Figure 57. Bode plot of the Plant $P(s)$ and equivalent plant with observer $P_{eq}(s)$

Despite the notorious high-frequency peaks present in the equivalent plant with observer magnitude bode diagram, it is essential to note that the standard robust performance specifications, reference tracking, and disturbances rejection, are required at lower frequencies. However, if there are problems in the rejection of the sensors' noise, the disturbance observer can be redesigned.

6.7. Conclusions

In this section, the GPI observer's evaluation, coupled with a robust tuning of the 2DOF PI controller, was presented. The study was carried out by means an experimental validation, where a pH control challenge in a raceway photobioreactor was examined. The results demonstrate that the novel robust control scheme provides a positive influence on the studied process, even in the presence of modeling and perturbance prediction errors. The experimental results for seven days with different irradiance profiles show that the pH value was maintained around the setpoint, and it can be inferred that the compensator can attenuate the perturbation influence for both cloudy and sunny days. This fact can be achieved since the GPI observer estimates the disturbance and unknown dynamics of the control system and suppresses its effect by complementing the control law with a cancellation effort. The inclusion

of 2DOF proportional-integral dealt with the performance/robustness trade-off using the required closed-loop control system robustness in terms of maximum sensitivity. The uncertainty could be considerably reduced by using an active disturbance rejection implemented on the inner loop in order to produce a well-behaved plant, which was then regulated by the robust PI controller in the outer loop.

To compare the performance of the proposed controller with a controller commonly used in microalgae production, a PI controller coupled to a feedforward disturbance compensator was tuned. Although the simulations indicated that both control schemes mitigated the disturbances' effect, the configurations using the GPI observer obtained more exceptional quickness and precision. Besides, the performance indices evaluated indicate that the LADRC used the least amount of combustion gases of all the configurations tested, being the most efficient in terms of energy consumption.

7. CONCLUSIONS

Many problems or characteristics that affect the performance of dynamic systems must be considered during the controller design process. Taking into account all the existing challenges in a control system is a difficult task and could be regarded as a significant problem in the controller design. In this dissertation, a robust scheme approach is proposes taking into account some of the essential open control problems presented in various dynamic systems, such as parametric uncertainty, time delays, and external disturbances. Therefore, the main contribution of this thesis is the study of the open control problems mentioned to obtain robust controllers that effectively improve the dynamics of systems with these problems.

The control approach combines robust feedback law and feedforward control. The robust feedback controller is designed for tracking and stabilization of uncertain plants. The inclusion of a 2DOF scheme allows dealing with the performance/robustness trade-off using the required closed-loop control system specifications. Thus, the use of feedback techniques of two degrees of freedom, such as QFT and robust tuning method for 2DoF Proportional-integral controllers proved to be a useful tool for robustness in systems with parametric uncertainty and external disturbances. To overcome the fundamental limitations of linear controllers, the use of reset mechanisms in the design of feedback controllers is encouraged in this dissertation. It was observed that the addition of this element is favorable because it guarantees speed (bandwidth) and phase margin (robustness) in the control system without compromising both specifications.

In order to mitigate the effect of disturbances, this dissertation presents generalized proportional integral (GPI) observers in the feedforward scheme as a useful tool for active disturbances rejection. Due to that selection of these parameters is not easy, this dissertation proposes the use of a methodology to suitably mitigate the typical peaking phenomenon in the design of high gain observers by the pole assignment method. It was shown that the addition of the disturbance observer significantly reduces the effect of parametric uncertainty in the model, which improves the robustness of the control system and facilitates the design of the feedback controller.

A. CODES PROGRAM

This appendix presents the programs used in the numerical validations and in the experimental implementation.

A.1. One-state Refrigeration Cycle

Figure 58. Block diagram of the refrigeration cycle

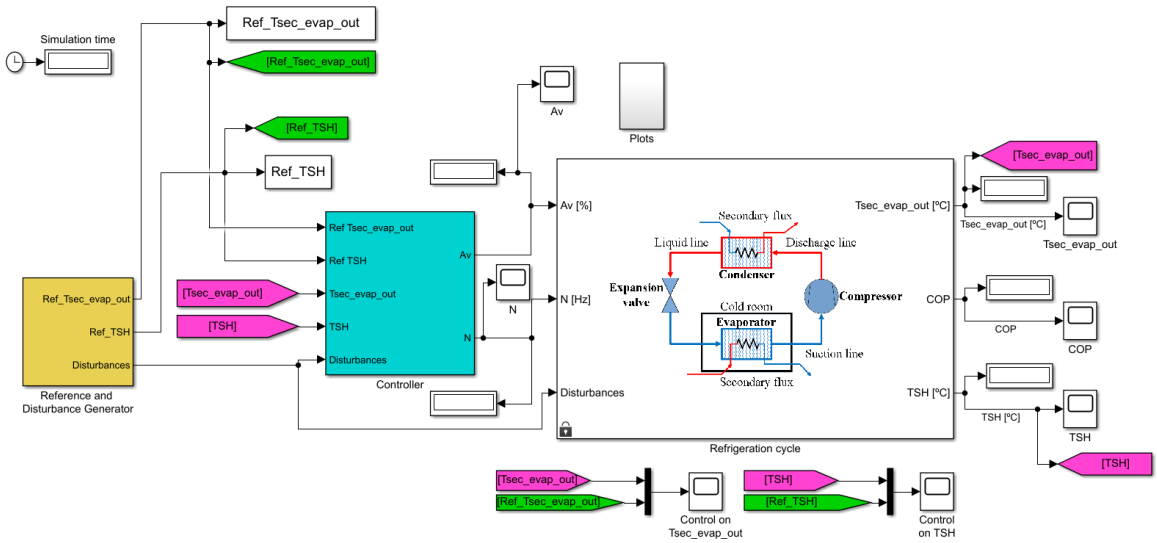

In order to operate the controller, the following observer parameters must be activated:

```
%Parámetros del observador para n=2, m=2
a0=4;a1=4;T=6;
a2=0.5*a1*(sin(2*pi/4)+sin(pi/4))/sin(2*pi/4);
a3=0.5*a1*(sin(3*pi/4)+sin(pi/4))/sin(3*pi/4);
L4=T^4*a0/(a3*a2^2*a1^3);L3=T^3*a0/(a2*a1^2);
L0=a0/L4;L1=a0*T/L4;L2=T^2/(a1*L4);
```

A.2. Offshore Wind Turbine

A.3. Glucose Control in Type 1 Diabetes

A.4. Raceway Photobioreactor

```
%%%%%%%%%%%%%%%%%%%%%%%%%%%%%%%%%%%%%%%%%%%%
%Control PH usando PI-2GDL y observador
%%%%%%%%%%%%%%%%%%%%%%%%%%%%%%%%%%%%%%%%%%%%

if exist('t_last_pH','var')==0
    t_last_pH=clock;
end

if exist('active','var')==0
    active=1;
end

if exist('xobs_1','var')==0
    xobs_1=[0;0;0;0];
end

if exist('ek_1','var')==0
    ek_1=0;
end

if exist('inte_1','var')==0
    inte_1=0;
end

if etime(clock,t_last_pH)>=60 %Esto es para tener tiempos de
control distintos de tiempo de muestreo del SCRIPT
   t_last_pH=clock;

   if exist('pH_old','var')==1
      pH_old(1:9)=pH_old(2:10);
      pH_old(10)=pH3;
   else
       pH_old(1:10)=pH3;
   end

   pH_filtrada=(sum(pH_old))/10;

   %Controlador PI-2GDL

   phref=7.7;
   OD2_max=180;

beta=0.5205;Kp=-3.9174;Ti=1020.6;k=-1;ts=1;
k3=9.105;k2=20.72;k1=13.82;k0=2.303;
Ao=[-k3,1,0,0;-k2,0,1,0;-k1,0,0,1;-k0,0,0,0];
Bo=[1,k3-1;0,k2;0,k1;0,k0];
Co=[0,-1,0,0];Do=[1,0];
[G,H]=c2d(Ao,Bo,ts);

ek = phref - pH_filtrada;
inte=inte_1+ts*(ek+ek_1)/2*Kp/Ti;
us=Kp*(beta*phref - pH_filtrada)+inte;%Señal de control PI-2GDL
```

```
u=[us;-ek/k];
xobs=G*xobs_1+H*u;

%/*actualizacion de senales*/
ut=us-xobs(2);%Señal de control total
inte_1=inte;
ek_1=ek;
xobs_1=xobs;
out1=ek;
out2=xobs(1);
out3=xobs(2);
out4=us;

if pH_filtrada > 8.0
        active=1;
        inte_1=0;
        xobs_1=0;
        if pH_filtrada > phref && Rad > 15
            VCO2=100;
        else
            if pH_filtrada <phref
                VCO2=0;
            end
        end
        VAireRW1=0;

    elseif pH_filtrada < phref && OD2 > OD2_max
        active=0;
        VCO2=0;
        VAireRW1=5;

    else
        switch(active)
            case 0
                VCO2=0;
                VAireRW1=5;
            case 1
                if pH_filtrada > phref && Rad > 15
                     VCO2=ut*100;
                     VCO2=0.5*VCO2+50;
                     VAireRW1=5;
                else
                    if pH_filtrada <phref
                        VCO2=0;
                        VAireRW1=0;
                    end
                end
        end
end
end
```

Figure 59. Block diagram of the controller

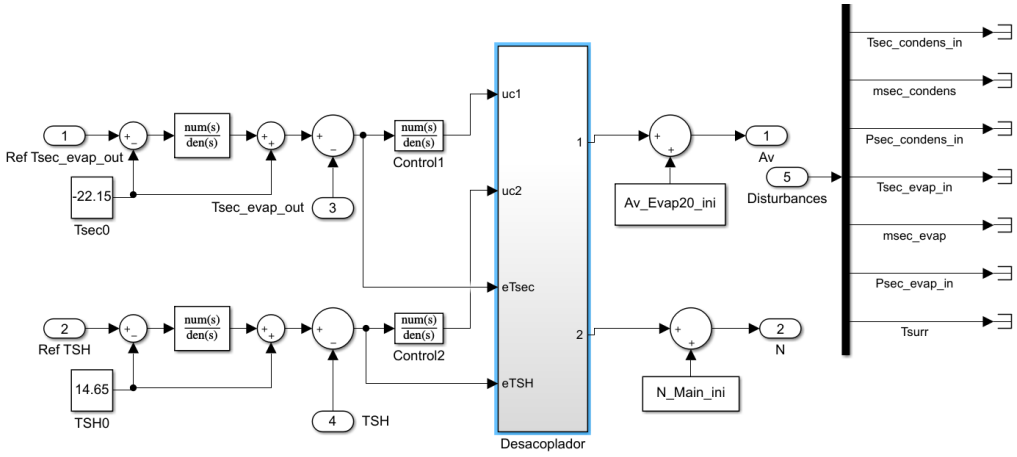

Figure 60. Block diagram of wind turbine control

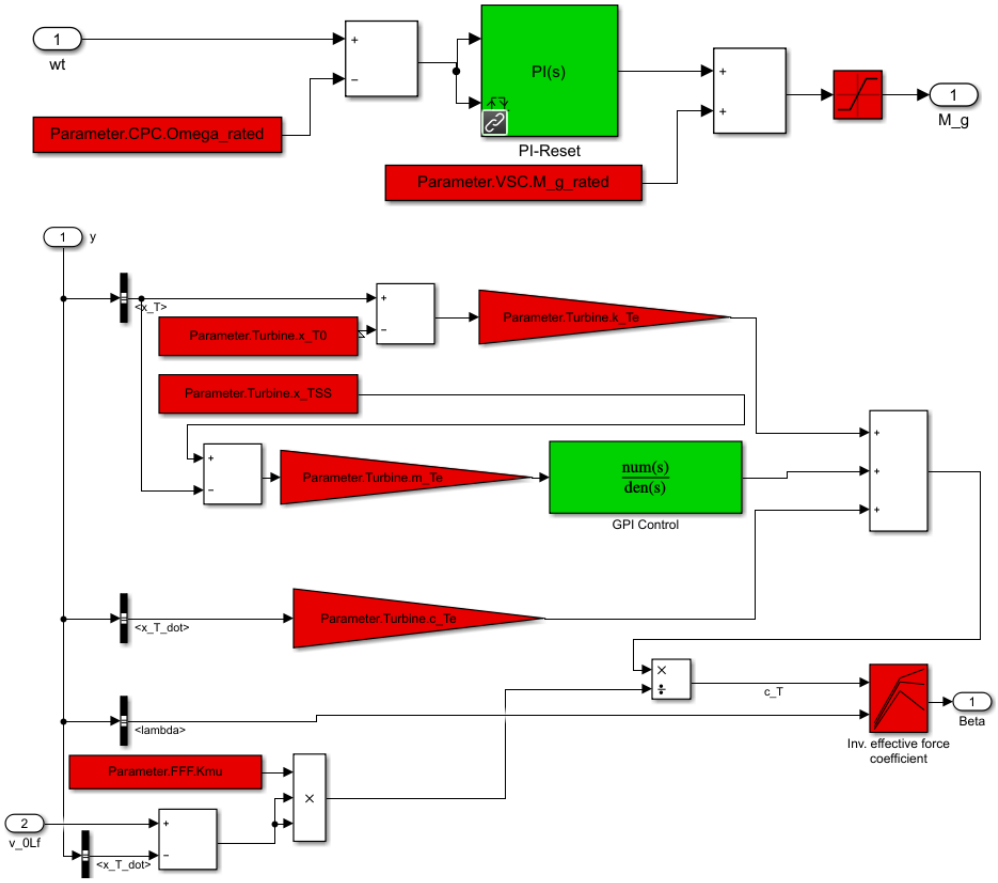

Figure 61. Block diagram of glucose system

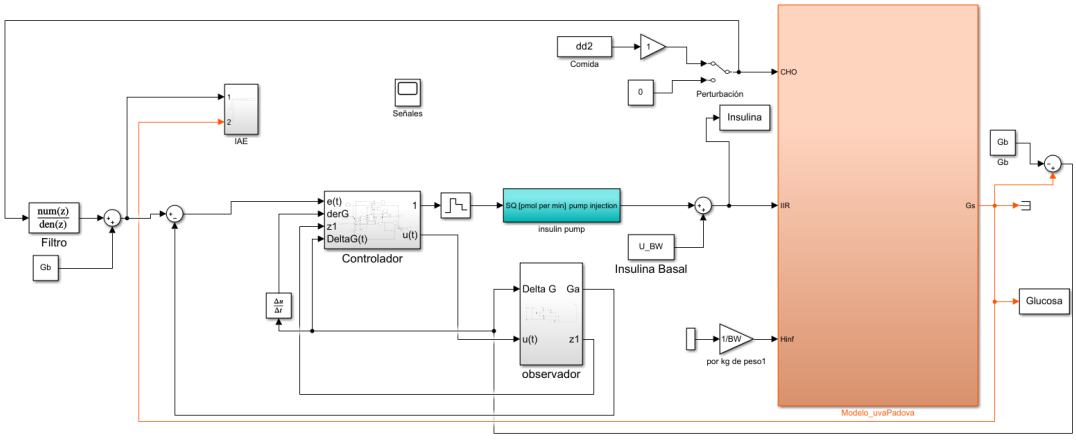

Figure 62. Block diagram of Raceway fotobioreactor

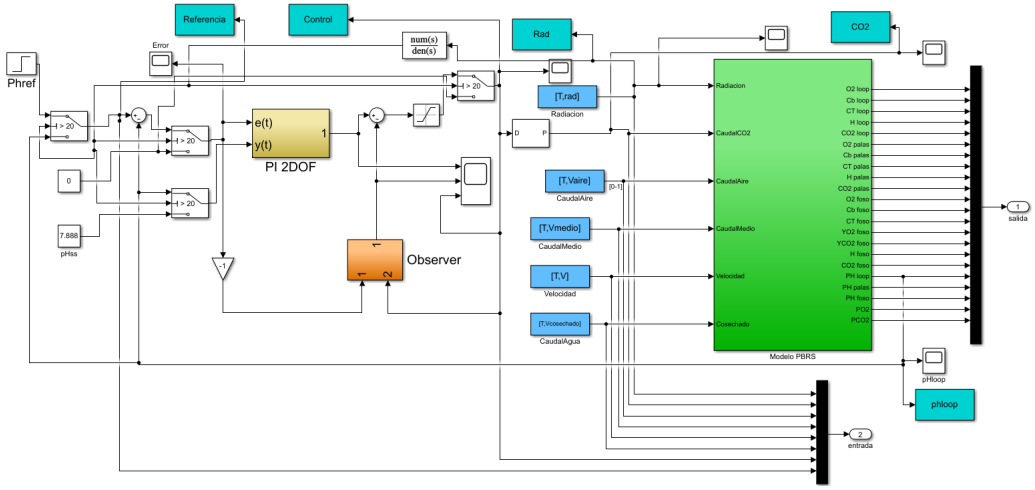

BIBLIOGRAPHY

Acién Fernández, F., García Camacho, F., Sánchez Pérez, J., Fernandez Sevilla, J., and Molina Grima, E. (1997). A model for light distribution and average solar irradiance inside outdoor tubular photobioreactors for the microalgal mass culture. *Biotechnology and bioengineering*, 55(5):701–714.

Alfaro, V. M. and Vilanova, R. (2012). Model-reference robust tuning of 2-DOF PI controllers for first-and second-order plus dead-time controlled processes. *Journal of Process Control*, 22(2):359–374.

Alfaro, V. M. and Vilanova, R. (2016). *Model-reference robust tuning of PID controllers*. Springer.

Alfaya, J. A., Bejarano, G., Ortega, M. G., and Rubio, F. R. (2015). Controllability analysis and robust control of a one-stage refrigeration system. *European Journal of Control*, 26:53–62.

Artstein, Z. (1982). Linear systems with delayed controls: A reduction. *IEEE Transactions on Automatic control*, 27(4):869–879.

Astrom, K. J. (2005). Advanced pid control. *ISA-The Instrumentation, Systems, and Automation Society*.

Åström, K. J. and Hägglund, T. (2009). *Control PID avanzado*. Pearson, Madrid.

Athanasius, G. and Zhu, J. (2009). Design of robust controller for wind turbines. In *Emerging Trends in Engineering and Technology (ICETET), 2009 2nd International Conference on*, pages 7–12. IEEE.

Baños, A. and Barreiro, A. (2011). *Reset control systems*. Springer Science & Business Media.

Barreiro, A. and Baños, A. (2012). Sistemas de control basados en reset. *Revista Iberoamericana de Automática e Informática Industrial RIAI*, 9(4):329–346.

Bejarano, G., Alfaya, J. A., Ortega, M. G., and Rubio, F. R. (2015). Multivariable analysis and h control of a one-stage refrigeration cycle. *Applied Thermal Engineering*, 91:1156–1167.

Bejarano, G., Alfaya, J. A., Ortega, M. G., and Vargas, M. (2017). On the difficulty of globally optimally controlling refrigeration systems. *Applied Thermal Engineering*, 111:1143–1157.

Bejarano, G., Alfaya, J. A., Rodríguez, D., Morilla, F., and Ortega, M. G. (2018). Benchmark for pid control of refrigeration systems based on vapour compression. *IFAC-PapersOnLine*, 51(4):497–502.

Berenguel, M., Rodríguez, F., Acién, F., and García, J. (2004). Model predictive control of ph in tubular photobioreactors. *Journal of Process Control*, 14(4):377–387.

Bergman, R. N., Phillips, L. S., and Cobelli, C. (1981). Physiologic evaluation of factors controlling glucose tolerance in man: measurement of insulin sensitivity and beta-cell glucose sensitivity from the response to intravenous glucose. *The Journal of clinical investigation*, 68(6):1456–1467.

Bordons, C. and Camacho, E. (2007). *Model predictive control*. Springer Verlag London Limited.

Boumhidi, J., Farhane, N., and Boumhidi, I. (2013). Neural network sliding mode controller for a variable speed wind turbine el-mahjoub boufounas. *Control and Intelligent Systems*, 41(4).

Bozorg, M. and Termeh, F. (2011). Domains of pid controller coefficients which guarantee stability and performance for lti time-delay systems. *Automatica*, 47(9):2122–2125.

Carreño-Zagarra, J. (2014). Control robusto de la dinámica de un robot manipulador, considerando incertidumbre paramétrica. Master's thesis, Universidad Industrial de Santander.

Carreño-Zagarra, J., Villamizar, R., Moreno, J., and Guzmán, J. (2019a). Predictive active disturbance rejection control for insulin infusion in patients with t1dm. *IFAC-PapersOnLine*, 52(17):105–110.

Carreño-Zagarra, J. J., Guzmán, J. L., Moreno, J. C., and Villamizar, R. (2019b). Linear active disturbance rejection control for a raceway photobioreactor. *Control Engineering Practice*, 85:271–279.

Carreño-Zagarra, J. J. and Vilamizar, R. (2018). Nonlinear robust control of offshore wind turbines based on flat filtering and reset compensation. In *2018 IEEE 14th International Conference on Control and Automation (ICCA)*, pages 1186–1191. IEEE.

Carreño-Zagarra, J. J., Villamizar, R., Moreno, J. C., and Guzmán, J. L. (2018). Active disturbance rejection and pid control of a one-stage refrigeration cycle. *IFAC-PapersOnLine*, 51(4):444–449.

Chait, Y. and Yaniv, O. (1993). Multi-input/single-output computer-aided control design using the quantitative feedback theory. *International Journal of Robust and Nonlinear Control*, 3(1):47–54.

Chen, W.-H., Yang, J., Guo, L., and Li, S. (2016). Disturbance-observer-based control and related methods—an overview. *IEEE Transactions on Industrial Electronics*, 63(2):1083–1095.

Colmegna, P. H., Sanchez-Pena, R. S., Gondhalekar, R., Dassau, E., and Doyle, F. J. (2015). Switched lpv glucose control in type 1 diabetes. *IEEE Transactions on Biomedical Engineering*, 63(6):1192–1200.

Commission, I. E. et al. (2005). Iec 61400-1: Wind turbines part 1: Design requirements. *International Electrotechnical Commission*.

Costache, T., Fernández, F. G. A., Morales, M., Fernández-Sevilla, J., Stamatin, I., and Molina, E. (2013). Comprehensive model of microalgae photosynthesis rate as a function of culture conditions in photobioreactors. *Applied microbiology and biotechnology*, 97(17):7627–7637.

Diekmann, O., Van Gils, S. A., Lunel, S. M., and Walther, H.-O. (2012). *Delay equations: functional-, complex-, and nonlinear analysis*, volume 110. Springer Science & Business Media.

Fernández, I. (2014). *Modelling and control strategies for the microalgal production in industrial photobioreactors*. PhD thesis, University of Almería.

Fernández, I., Acién, F., Guzmán, J., Berenguel, M., and Mendoza, J. (2016a). Dynamic model of an industrial raceway reactor for microalgae production. *Algal Research*, 17:67–78.

Fernández, I., Berenguel, M., Guzmán, J. L., Acién, F. G., de Andrade, G. A., and Pagano, D. J. (2016b). Hierarchical control for microalgae biomass production in photobiorreactors. *Control Engineering Practice*, 54:246–255.

Fernández, I., Peña, J., Guzman, J. L., Berenguel, M., and Acién, F. G. (2010). Modelling and control issues of ph in tubular photobioreactors. *IFAC Proceedings Volumes*, 43(6):186–191.

Fliess, M., Lévine, J., Martin, P., and Rouchon, P. (1995). Flatness and defect of non-linear systems: introductory theory and examples. *International journal of control*, 61(6):1327–1361.

Fliess, M., Marquez, R., Delaleau, E., and Sira-Ramírez, H. (2002). Correcteurs proportionnels-intégraux généralisés. *ESAIM: Control, Optimisation and Calculus of Variations*, 7:23–41.

Freeman, J. and Balas, M. (1999). An investigation of variable speed horizontal-axis wind turbines using direct model-reference adaptive control. In *Proc. 18th ASME Wind Energy Symp*, pages 66–76.

Fridman, E., Fridman, L., and Shustin, E. (2000). Steady modes in relay control systems with time delay and periodic disturbances. *Journal of Dynamic Systems, Measurement, and Control*, 122(4):732–737.

Furutani, E. and Araki, M. (1998). Robust stability of state-predictive and smith control systems for plants with a pure delay. *International Journal of Robust and Nonlinear Control: IFAC-Affiliated Journal*, 8(10):907–919.

Gahinet, P. and Apkarian, P. (1994). A linear matrix inequality approach to h control. *International journal of robust and nonlinear control*, 4(4):421–448.

Gao, J. and Budman*, H. M. (2004). Reducing conservatism in the design of a robust gain-scheduled controller for non-linear chemical processes. *International Journal of Control*, 77(11):1050–1061.

Garcia-Sanz, M. (2017). *Robust control engineering: practical QFT solutions*. CRC Press.

Garcia-Sanz, M. and Guillen, J. (1999). Smith predictor for uncertain systems in the qft framework. In *Progress in system and robot analysis and control design*, pages 239–250. Springer.

Garcıa-Sanz, M., Guillén, J., and Ibarrola, J. (2001). Robust controller design for uncertain systems with variable time delay. *Control Engineering Practice*, 9(9):961–972.

Garcia-Sanz, M. and Houpis, C. H. (2012). *Wind energy systems: control engineering design*. CRC press.

Gouaisbaut, F., Dambrine, M., and Richard, J.-P. (2002). Robust control of delay systems: a sliding mode control design via lmi. *Systems & control letters*, 46(4):219–230.

Grima, E. M., Sevilla, J. F., Pérez, J. S., and Camacho, F. G. (1996). A study on simultaneous photolimitation and photoinhibition in dense microalgal cultures taking into account incident and averaged irradiances. *Journal of Biotechnology*, 45(1):59–69.

Gu, D.-W., Petkov, P., and Konstantinov, M. M. (2005). *Robust control design with MATLAB®*. Springer Science & Business Media.

Haddad, W. M., Chellaboina, V., and Hayakawa, T. (2001). Robust adaptive control for nonlinear uncertain systems. In *Proceedings of the 40th IEEE Conference on Decision and Control (Cat. No. 01CH37228)*, volume 2, pages 1615–1620. IEEE.

Hale, J. K. and Lunel, S. M. V. (2013). *Introduction to functional differential equations*, volume 99. Springer Science & Business Media.

Han, J. (2009). From pid to active disturbance rejection control. *IEEE transactions on Industrial Electronics*, 56(3):900–906.

Hinrichsen, D. and Pritchard, A. J. (2011). *Mathematical systems theory I: modelling, state space analysis, stability and robustness*, volume 48. Springer Science & Business Media.

Hohenbichler, N. (2009). All stabilizing pid controllers for time delay systems. *Automatica*, 45(11):2678–2684.

Horowitz, I. (1982). Quantitative feedback theory. In *IEE Proceedings D (Control Theory and Applications)*, volume 129, pages 215–226. IET.

Houpis, C. H., Rasmussen, S. J., and Garcia-Sanz, M. (2018). *Quantitative feedback theory: fundamentals and applications*. CRC press.

Houpis, C. S. and Rasmussen, S. J. (1999). Quantitative feedback theory: Fundamentals and applications.

Hovorka, R., Canonico, V., Chassin, L. J., Haueter, U., Massi-Benedetti, M., Federici, M. O., Pieber, T. R., Schaller, H. C., Schaupp, L., Vering, T., et al. (2004). Nonlinear model predictive control of glucose concentration in subjects with type 1 diabetes. *Physiological measurement*, 25(4):905.

Huang, C. and Sira-Ramírez, H. (2015). Flatness-based active disturbance rejection control for linear systems with unknown time-varying coefficients. *International Journal of Control*, 88(12):2578–2587.

Ioannou, P. A. and Sun, J. (2012). *Robust adaptive control*. Courier Corporation.

Jahangeer, K., Tay, A. A., and Islam, M. R. (2011). Numerical investigation of transfer coefficients of an evaporatively-cooled condenser. *Applied Thermal Engineering*, 31(10):1655–1663.

Jain, A., Schildbach, G., Fagiano, L., and Morari, M. (2015). On the design and tuning of linear model predictive control for wind turbines. *Renewable Energy*, 80:664–673.

Jena, D. and Rajendran, S. (2015). A review of estimation of effective wind speed based control of wind turbines. *Renewable and Sustainable Energy Reviews*, 43:1046–1062.

Jonkman, J., Butterfield, S., Musial, W., and Scott, G. (2009). Definition of a 5-mw reference wind turbine for offshore system development. Technical report, National Renewable Energy Laboratory (NREL), Golden, CO.

Keel, L., Kim, Y., and Bhattacharyya, S. (2008). Ch. 6 transient response control via characteristic ratio assignment. In *Lecture note of the 17th IFAC World Congress Tutorial Workshop: Advances in Three Term Control, Seoul*.

Kim, Y. C., Keel, L. H., and Bhattacharyya, S. P. (2003). Transient response control via characteristic ratio assignment. *IEEE Transactions on Automatic Control*, 48(12):2238–2244.

Kim, Y. C. and Wu, J. (2012). Damping characteristics of the k-polynomial. In *Control, Automation and Systems (ICCAS), 2012 12th International Conference on*, pages 1842–1847.

Kolmanovskii, V., Niculescu, S.-I., and Gu, K. (1999). Delay effects on stability: A survey. In *Decision and Control, 1999. Proceedings of the 38th IEEE Conference on*, volume 2, pages 1993–1998. IEEE.

Kovatchev, B., Breton, M., Dalla Man, C., and Cobelli, C. (2008). In silico model and computer simulation environment approximating the human glucose/insulin utilization. *Food and Drug Administration Master File MAF*, 1521:338–346.

Kovatchev, B. P., Breton, M., Dalla Man, C., and Cobelli, C. (2009). In silico preclinical trials: a proof of concept in closed-loop control of type 1 diabetes.

Lavretsky, E. and Wise, K. A. (2013). Robust adaptive control. In *Robust and adaptive control*, pages 317–353. Springer.

Li, B. and Alleyne, A. G. (2010). A dynamic model of a vapor compression cycle with shut-down and start-up operations. *International Journal of refrigeration*, 33(3):538–552.

Li, H., Shi, K., and McLaren, P. (2005). Neural-network-based sensorless maximum wind energy capture with compensated power coefficient. *IEEE transactions on industry applications*, 41(6):1548–1556.

Li, S., Yang, J., Chen, W.-H., and Chen, X. (2014). *Disturbance observer-based control: methods and applications*. CRC press.

Manitius, A. and Olbrot, A. (1979). Finite spectrum assignment problem for systems with delays. *IEEE transactions on Automatic Control*, 24(4):541–552.

Matuš, R. (2008). *Robust Control of Systems with Parametric Uncertainty: An Algebraic Approach*. Tomas Bata University in Zlín.

Michiels, W. and Niculescu, S.-I. (2007). *Stability and stabilization of time-delay systems: an eigenvalue-based approach*. SIAM.

Moradi, H. and Vossoughi, G. (2015). Robust control of the variable speed wind turbines in the presence of uncertainties: A comparison between h and pid controllers. *Energy*, 90:1508–1521.

Niculescu, S.-I. (2001). *Delay effects on stability: a robust control approach*, volume 269. Springer Science & Business Media.

Normey-Rico, J. E. and Camacho, E. F. (2007). Control of dead-time processes. *Time (minutes) Time (minutes)*.

Normey-Rico, J. E. and Camacho, E. F. (2008). Dead-time compensators: A survey. *Control engineering practice*, 16(4):407–428.

Olgac, N. and Cavdaroglu, M. E. (2011). Full-state feedback controller design with "delay scheduling" for cart-and-pendulum dynamics. *Mechatronics*, 21(1):38–47.

Olgac, N., Ergenc, A. F., and Sipahi, R. (2005). "delay scheduling": a new concept for stabilization in multiple delay systems. *Journal of Vibration and Control*, 11(9):1159–1172.

Olgac, N., Sipahi, R., and Ergenc, A. F. (2007). 'delay scheduling', an unconventional use of time delay for trajectory tracking. *Mechatronics*, 17(4-5):199–206.

Oliveira, V. A., Cossi, L. V., Teixeira, M. C., and Silva, A. M. (2009). Synthesis of pid controllers for a class of time delay systems. *Automatica*, 45(7):1778–1782.

Ortega, M. and Rubio, F. (2004). Systematic design of weighting matrices for the h mixed sensitivity problem. *Journal of Process Control*, 14(1):89–98.

Pao, L. Y. and Johnson, K. E. (2009). A tutorial on the dynamics and control of wind turbines and wind farms. In *American Control Conference, 2009. ACC'09.*, pages 2076–2089. IEEE.

Patek, S. D., Breton, M. D., Chen, Y., Solomon, C., and Kovatchev, B. (2007). Linear quadratic gaussian-based closed-loop control of type 1 diabetes.

Pawłowski, A., Guzmán, J. L., Berenguel, M., Acíen, F. G., and Dormido, S. (2018). Application of predictive feedforward compensator to microalgae production in a raceway reactor: A simulation study. *Energies*, 11(1):123.

Pawlowski, A., Mendoza, J. L., Guzmán, J. L., Berenguel, M., Acién, F., and Dormido, S. (2014). Effective utilization of flue gases in raceway reactor with event-based ph control for microalgae culture. *Bioresource technology*, 170:1–9.

Pawlowski, A., Mendoza, J. L., Guzmán, J. L., Berenguel, M., Acién, F. G., and Dormido, S. (2015). Selective ph and dissolved oxygen control strategy for a raceway reactor within an event-based approach. *Control Engineering Practice*, 44:209–218.

Perruquetti, W. and Barbot, J.-P. (2002). *Sliding mode control in engineering*. CRC press.

Ramírez, D. R. (2002). *Control predictivo mín-máx: análisis, caracterización y técnicas de implementación*. PhD thesis, Universidad de Sevilla.

Rasmussen, B. (2005). Dynamic modeling and advanced control of air conditioning and refrigeration systems.

Richard, J.-P., Gouaisbaut, F., and Perruquetti, W. (2001). Sliding mode control in the presence of delay. *Kybernetika*, 37(3):277–294.

Rocha, R. et al. (2003). A multivariable h/sub/spl infin//control for wind energy conversion system. In *Control Applications, 2003. CCA 2003. Proceedings of 2003 IEEE Conference on*, volume 1, pages 206–211. IEEE.

Roh, Y.-H. and Oh, J.-H. (1999). Sliding mode control with delay compensation for uncertain input-delay systems. In *Proceedings of the 1999 American Control Conference (Cat. No. 99CH36251)*, volume 1, pages 309–313. IEEE.

Rubio, F. C., Fernandez, F., Perez, J., Camacho, F. G., and Grima, E. M. (1999). Prediction of dissolved oxygen and carbon dioxide concentration profiles in tubular photobioreactors for microalgal culture. *Biotechnology and Bioengineering*, 62(1):71–86.

Rubio, F. R. and Sánchez, M. J. L. (1996). *Control adaptativo y robusto*, volume 9. Universidad de Sevilla.

Sala, A., Cuenca, Á., and Salt, J. (2009). A retunable pid multi-rate controller for a networked control system. *Information Sciences*, 179(14):2390–2402.

Sánchez-Peña, R., Colmegna, P., Grosembacher, L., Breton, M., De Battista, H., Garelli, F., Belloso, W., Campos-Nánez, E., Simonovich, V., Beruto, V., et al. (2017). Artificial pancreas: First clinical trials in argentina. *IFAC-PapersOnLine*, 50(1):7731–7736.

Sastry, S. and Bodson, M. (2011). *Adaptive control: stability, convergence and robustness*. Courier Corporation.

Schlipf, D. (2016). *Lidar-assisted control concepts for wind turbines*. PhD thesis.

Selvam, K., Kanev, S., van Wingerden, J. W., van Engelen, T., and Verhaegen, M. (2009). Feedback–feedforward individual pitch control for wind turbine load reduction. *International Journal of Robust and Nonlinear Control*, 19(1):72–91.

Sidi, M. J. (2001). *Design of Robust Control Systems: From classical to modern practical approaches*. Krieger Publishing Company.

Silva, G. J., Datta, A., and Bhattacharyya, S. P. (2007). *PID controllers for time-delay systems*. Springer Science & Business Media.

Simoes, M. G., Bose, B. K., and Spiegel, R. J. (1997). Fuzzy logic based intelligent control of a variable speed cage machine wind generation system. *IEEE transactions on power electronics*, 12(1):87–95.

Sipahi, R., Niculescu, S.-I., Abdallah, C. T., Michiels, W., and Gu, K. (2011). Stability and stabilization of systems with time delay. *IEEE Control Systems Magazine*, 31(1):38–65.

Sira-Ramírez, H. (2018). From flatness, gpi observers, gpi control and flat filters to observer-based adrc. *Control Theory and Technology*, 16(4):249–260.

Sira-Ramirez, H. and Agrawal, S. K. (2004a). *Differentially flat systems*. CRC Press.

Sira-Ramirez, H. and Agrawal, S. K. (2004b). *Differentially flat systems*. CRC Press.

Sira-Ramírez, H., Cortés-Romero, J., and Luviano-Juárez, A. (2011). Robust linear control of nonlinear flat systems. In *Robust Control, Theory and Applications*. InTech.

Sira-Ramirez, H., Luviano-Juárez, A., Ramírez-Neria, M., and Zurita-Bustamante, E. W. (2018). *Active disturbance rejection control of dynamic systems: a flatness based approach*. Butterworth-Heinemann.

Sira-ramírez, H. J., García-Rodríguez, C., Cortés-Romero, J., and Luviano-Juárez, A. (2014). *Algebraic identification and estimation methods in feedback control systems*. Wiley Online Library.

Skogestad, S. (2003). Simple analytic rules for model reduction and pid controller tuning. *Journal of process control*, 13(4):291–309.

Slotine, J.-J. E., Li, W., et al. (1991). *Applied nonlinear control*, volume 199. Prentice hall Englewood Cliffs, NJ.

Smith, O. J. (1957). Closed control of loop with dead time. *Chemical engineering progress*, 53:217–219.

Song, Y., Dhinakaran, B., and Bao, X. (2000). Variable speed control of wind turbines using nonlinear and adaptive algorithms. *Journal of Wind Engineering and Industrial Aerodynamics*, 85(3):293–308.

Sorribes, A. and Gil, G. (2011). *Sistemas dinámicos con retardos temporales*. PhD thesis, Tesis doctoral, UPV, Valencia, Espana.

Stépán, G. (1989). *Retarded dynamical systems: stability and characteristic functions*. Longman Scientific & Technical.

Takatsu, H., Itoh, T., and Araki, M. (1998). Future needs for the control theory in industries—report and topics of the control technology survey in japanese industry. *Journal of Process Control*, 8(5-6):369–374.

Tebbani, S., Titica, M., Join, C., Fliess, M., and Dumur, D. (2016). Model-based versus model-free control designs for improving microalgae growth in a closed photobioreactor: Some preliminary comparisons. In *Control and Automation (MED), 2016 24th Mediterranean Conference on*, pages 683–688. IEEE.

Van Kuik, G. and Peinke, J. (2016). *Long-term Research Challenges in Wind Energy-A Research Agenda by the European Academy of Wind Energy*, volume 6. Springer.

Wang, Y.-J. (2011). Graphical computation of gain and phase margin specifications-oriented robust pid controllers for uncertain systems with time-varying delay. *Journal of Process Control*, 21(4):475–488.

Weissman, J. and Goebel, R. (1987). Design and analysis of pond system for the purpose of producing fuels. final report. *Solar Energy Research Institute, Golden CO, SERI/STR*, pages 231–2840.

Wen, C., Zhou, J., Liu, Z., and Su, H. (2011). Robust adaptive control of uncertain nonlinear systems in the presence of input saturation and external disturbance. *IEEE Transactions on Automatic Control*, 56(7):1672–1678.

Wu, F., Zhang, X.-P., Ju, P., and Sterling, M. J. (2008). Decentralized nonlinear control of wind turbine with doubly fed induction generator. *IEEE Transactions on Power Systems*, 23(2):613–621.

Wu, Y., Gu, J., and Yu, X. (2002). Finite time sliding mode control for time delay systems. In *Proceedings of the 4th World Congress on Intelligent Control and Automation (Cat. No. 02EX527)*, volume 2, pages 872–877. IEEE.

Xu, L., Weathers, P. J., Xiong, X.-R., and Liu, C.-Z. (2009). Microalgal bioreactors: challenges and opportunities. *Engineering in Life Sciences*, 9(3):178–189.

Yang, X., Xu, L., Liu, Y., and Xu, D. (2007). Multivariable predictive functional control for doubly fed induction generator. In *Control and Automation, 2007. ICCA 2007. IEEE International Conference on*, pages 80–83. IEEE.

Yoo, S. J., Jeong, D. H., Kim, J. H., and Lee, J. M. (2016). Optimization of microalgal photobioreactor system using model predictive control with experimental validation. *Bioprocess and biosystems engineering*, 39(8):1235–1246.

Zhong, Q.-C. (2006). *Robust control of time-delay systems*. Springer Science & Business Media.

Zimmet, P., Alberti, K., and Shaw, J. (2001). Global and societal implications of the diabetes epidemic. *Nature*, 414(6865):782–787.